REPORT No. 94

WALL SHEAR-STRESS AND LAMINARISATION IN ACCELERATED TURBULENT COMPRESSIBLE BOUNDARY-LAYERS

by
JAMES LUDLOW NASH-WEBBER

April 1968

GAS TURBINE LABORATORY
MASSACHUSETTS INSTITUTE OF TECHNOLOGY
CAMBRIDGE, MASSACHUSETTS 02139

WALL SHEAR-STRESS AND LAMINARISATION IN ACCELERATED TURBULENT COMPRESSIBLE BOUNDARY-LAYERS

by

JAMES LUDLOW NASH-WEBBER

Under the Sponsorship of:

General Electric Company

Allison Division of General Motors Company

GAS TURBINE LABORATORY

REPORT No. 94

April 1968

MASSACHUSETTS INSTITUTE OF TECHNOLOGY

Cambridge, Massachusetts

Per ardua ad astra

Eheu, fugaces !

ABSTRACT

Turbulent-laminar transition in compressible, steeply-accelerated, adiabatic, turbulent boundary layers on a smooth wall was investigated experimentally in the ranges of Mach and Reynold's numbers typical of nozzles used in propulsive devices. Correlation of the present and previously published data suggests that the transition of such a shear layer may be predicted by consideration of its trajectory on a plane having an acceleration parameter K and a Reynold's number R_{δ_2} as coordinates. An ab initio design method has been developed, based on these findings, which will ensure laminar flow before and at the throat of a sufficiently small nozzle operating at sufficiently small total pressure. A new type of surface-pitot was developed and calibrated and used to measure wall shear stresses in both transitional and non-transitional flows. Decrease of wall shear-stress in laminarising flows was found.

General-purpose computer programs for data-reduction, surface-pitot calibration and interpretation and boundary layer development predictions were developed.

ACKNOWLEDGEMENTS

Being as it were the child of two of the Institute's families--the Aero & Astro Dept. Propulsion Group and the Gas Turbine Lab., I have many people to thank for their ever-available help in advancing my work. The pleasant working conditions within these groups provides a welcome degree of insulation from the insensate pressures of the Institute as a whole. Though it is perhaps invidious to single out anyone, I should like to thank most especially:

Professor Edward Taylor, whose outgoing personality and incisive insight into the problem made research a pleasure;

Professor Gordon Oates, who, as project supervisor always contrived to maintain a sense of humor and a degree of optimism despite all setbacks;

The other members of my Thesis Committee, for their time and trouble in setting me back on the straight and narrow at frequent intervals;

Thorwald Christensen, without whose skill and tireless efforts in the machine-shop and at a dozen other trades the experiment would have clanked to a halt;

John and Joan Moore for their valuable assistance with the machine calculations;

Lotti Gopalakrishnan, for typing and retyping the reports, often from my atrocious scrawl, and for feeding me coffee and cookies at frequent intervals; and

Bonnie, who saw the work through to the end, and was an ever-present help in time of trouble.

TABLE OF CONTENTS

LIST OF FIGURES

LIST OF TABLES

NOTATION

A, A_1 B, B_1 C	Constants used in skin friction fence calibration relations
a, b	Constants of skin friction law (See Appendix I)
c_f	Skin friction coefficient $(\tau_w / \frac{1}{2}\rho_\delta u_\delta^2)$
$\tilde{c}_f$	Walz' skin friction coefficient $(\tau_w / \rho_\delta u_\delta^2)$
$\tilde{c}_D$	Walz' shear work integral
d	Fence height
f_P, f_2, F F_R, F_L	Functions defined in Appendices I & II
H_{12}	Shape factor $\equiv (\delta_1)_u / (\delta_2)_u$
H_{12}^*	Shape factor $\equiv \delta_1 / \delta_2$
H_{32}	Shape factor $\equiv (\delta_3)_u / (\delta_2)_u$
H_{32}^*	Shape factor $\equiv \delta_3 / \delta_2$
K	Acceleration Parameter $\equiv \frac{\nu_w}{u_\delta^2} \cdot \frac{du_\delta}{dx}$
M	Mach Number
N, n	Empirical exponents used in Walz' theory (See III.C.1)
P	Pressure
ΔP	Pressure difference
R	Reynold's Number (general); Radius
R_{δ_2}	Reynold's Number based on momentum thickness $\frac{\rho_\delta U_\delta \delta_2}{\mu_w}$
r	Recovery factor
T	Temperature
T'	Sommer & Short reference temperature: $T_\delta \left[1 + .035\, M_\delta^2 + 0.45 \left(\frac{T_w}{T_\delta} - 1\right)\right]$

U, u	Velocities in the x direction
u_τ	Friction velocity $(\tau_w/\rho)^{\frac{1}{2}}$
v	Velocity in the y direction
x	Streamwise coördinate
y	Normal coördinate
z	Walz' normal coördinate

Greek letters

α	Skin friction function (See III.C.1 and III.B)
β	Dissipation function (See III.C.1)
γ	Ratio of specific heats c_p / c_v
δ	Conventional boundary layer thickness
δ_L	Boundary layer thickness defined by Launder (See III.B)
δ_1	Displacement thickness $\int_o^\delta (1 - \frac{\rho u}{\rho_\delta u_\delta})\, dy$
δ_2	Momentum thickness $\int_o^\delta \frac{\rho u}{\rho_\delta u_\delta} (1 - \frac{u}{u_\delta})\, dy$
δ_3	Energy thickness $\int_o^\delta \frac{\rho u}{\rho_\delta u_\delta} (1 - (\frac{u}{u_\delta})^2)\, dy$
δ_4	Density defect thickness $\frac{1}{2}\int_o^\delta \frac{\rho u}{\rho_\delta u_\delta} (\frac{\rho_\delta}{\rho} - 1)\, dy$
μ	Viscosity
ν	Kinematic viscosity
ϕ, ψ	Correction functions of Walz'[33] theory (See III.C.1)
ρ	Density
Θ	Heat transfer parameter
τ	Shear stress
λ	Heat conduction coefficient
ζ	Shape factor of Escudier[36] (See III.C.3)

Subscripts

o	Stagnation conditions
δ	Free-stream conditions
w	Wall conditions
e	Recovery conditions
u	Evaluated with constant fluid properties
δ_2	Based on momentum thickness
d	Based on fence height
E	Effective (in turbulent flow)

I. INTRODUCTION

A. Motivation and Background to the Problem

Fluid dynamicists of the more classical sort have spent much time and effort on trying to understand the behavior of boundary-layers in adverse pressure-gradients. Comparatively little effort has been devoted to the phenomena occuring in favorable pressure-gradient flows. Many propulsive devices, however, incorporate favorable pressure-gradient flows, and the continuing effort to push these to their limits of performance is currently rendering mandatory a much larger effort aimed at a better understanding of such flows. This study attempts to redress further the imbalance of research effort and, in particular, to advance our knowledge of the "relaminarisation" phenomenon.

The turbulent flow problem has been with us from the dawnings of fluid dynamics. Progress toward satisfactory enunciation of the problem, let alone elucidation, has been distressingly slow. In particular, when we come to examine the status of the turbulent shear flow problem, we find a wide divergence between the need of the designer of any sort of fluid-flow equipment for information and the ability of the theoretician to supply it. Since the problem will not go away, this has resulted in the formation of a large school of empiricists dedicated to the production of useable design data. The efforts of these workers are, nevertheless, greatly hampered by the inability of the available theory to point towards the correct design of experiments or greatly to help with the correlation of their results. It has accordingly been necessary to break the problem up into many smaller pieces, and these often indeed into several special cases before useful progress could be made.

On two such sub-problems,a great deal of work has been done. These are the laminar-turbulent transition problem and the equilibrium turbulent

boundary-layer problem. In these problems, for several special cases where the upstream history of the shear layer may be carefully controlled, "theory" and experiment have been notably at one. In particular, there have resulted the useful similarity laws of Clauser[1] and of Coles[2] for equilibrium and near-equilibrium shear flows, and several plausible transform theories to allow the extension of incompressible results to compressible flow have been proposed. Two major schools of thought on the subject of transforms are presided over by Coles[3] and Crocco[4], but their differences have yet to be resolved. Efforts at a general treatment of the turbulent shear-flow problem have appeard at intervals, most recently and notably those of Hawthorne[9] and Kutateladze and Leont'ev[10].

Several types of computational method for such flows have been developed, based on these ideas. These appear to enjoy success in direct ratio to the similarity between the problem to which they are applied and the data from which they were formulated. These methods will be treated in Section III of this report.

On the subject of turbulent shear flows which are very far from equilibrium, our ignorance is most profound. Nature has, however, decreed that such flows are to be found in many of our fluid-flow devices, which circumstance renders an attack on the problem highly desirable, though scarcely more tractable for all that. In particular, a new and important phenomenon has manifested itself in the special case of turbulent shear flows in a very strongly negative pressure gradient, such as can occur in certain duct flow devices, such as nozzles and turbine blades. This phenomenon is evidenced as a very considerable decrease in the macroscopic transport properties of the shear layer.

This has led to previously inexplicably low results in nozzle heat-transfer experiments such as those of Wilson and Pope[5] in 1954, who were

apparently the first to encounter the phenomenon, at least in the Western world: Papers by Deich et al [29, 30] refer to a first discovery, in 1948, in Russia, of the phenomenon, during study of trans- and supersonic flows past a sphere, and later encounters, in steam ejectors, in 1954.

It was widely speculated[6, 7, 8] that this most desirable (in general) phenomenon might be identified with the onset of a reverse transition from turbulent to laminar shear flow. Conclusive evidence of reverse transition was reported by Senoo[11] in 1957. He investigated the end-wall flow of a turbine nozzle cascade, finding that for the conditions of his experiment, the boundary layer, while demonstrably turbulent upstream of the throat, exhibited a laminar profile in and downstream of the throat. Little insight into the flow mechanisms involved could, however, be gained from this study.

During this period also, very large efforts in rocket-engine research were getting under way. Countless tests to measure combustion chamber and nozzle heat-transfer rates were run. Attempts to correlate and elucidate these results proved less than satisfactory. Indeed, the best known of these, the correlation of Bartz[12] could seldom be relied on to produce results for the peak heat flux accurate within a factor of two either way, even in those rare cases where the boundary-layer upstream of the nozzle was well determined. References 13 through 16 are representative of the heat transfer measurements reported in the literature.

To account for that residuum of grossly low heat transfer results which could not be prodded into the same pen with the majority, invocation of the notion of a turbulent-laminar reverse transition of the boundary-layer was sometimes attempted, on frankly intuitive grounds. In 1954, Preston[17] had suggested that there might be some minimum value of Reynolds number, R_{δ_2}, say 320, based on momentum thickness, below which a turbulent boundary layer could not exist. There might then perhaps be significant

effects if the sharply accelerated shear layer attained sufficiently small values of δ_2. Qualitative arguments could be brought to bear on the effect of the stretching of vortex filaments in the shear layer by the acceleration of the free-stream flow: namely that the scale of the turbulence should be shifted towards the small wave lengths, thus promoting molecular-viscous dissipation. It was not clear whether the required deficit of turbulent energy production vis à vis dissipation would require,in addition, a mechanism for suppressing turbulence production. The details of such a mechanism were also wanting. Indeed, stability theory of turbulent shear flows was, and remains, in that limbo reserved for interesting but unsolved problems.

A common feature of these studies was the complexity of the flows studied. There was no way to separate out the effects of wall-cooling, wall curvature, chemical reaction, compressibility, multiphase flow, free-stream turbulence, wall roughness or free-stream acceleration, each of which could be expected to have some effect on the phenomenon.

This dilemma was apparent to several workers. Amongst the first to attempt more concisely defined experiments were: Back and his co-workers at JPL; the group at Stanford, separately reported by Kline and co-workers and by Moretti and Kays; the group at United Aircraft Research Labs; and several groups in Russia. References 18 through 20 contain essentially the same material from JPL; 21, 22 and 23 refer to Stanford works which themselves list their precursors; 24, 25 and 26 are complementary, and cover the UAC work; and 29 reviews the Russian work. Most significantly for a better understanding of the mechanisms involved, Launder[27, 28] conducted detailed experiments in which all effects bar that of free-stream acceleration were effectively absent. It is worthwhile to review briefly the important conclusions to be drawn from the above studies.

The JPL workers ran tests on a 45°-15° conical-conical convergent-divergent nozzle through which a mixture of air and methanol combustion products at some 1500°R was passed, with stagnation pressures from 30 to 250 psia. The nozzle was water-cooled in annular segments, and the mean heat flux per segment measured calorimetrically. Typical free-stream/wall temperature-ratios were about 2. Thickness of the inlet boundary layer, which was measured, could be varied by changing the length of the nozzle approach section.

Compared with the best current laminar and turbulent boundary-layer heat-transfer theories in use in that laboratory, it was found that although experimental values and the turbulent prediction were in fair agreement at the higher stagnation pressures tested, there was a tendency in the lower stagnation pressure tests - i.e. the lower Reynold's number tests - for the experimental data to fall away from the turbulent prediction and approach the laminar one. Although the detailed conclusions of this study were subsequently disputed by O'Brien[24], the general and expected tendency for preferential laminarisation at the lower Reynolds numbers appeard to be confirmed.

No detailed boundary-layer measurements were taken down-stream of the nozzle entry, and there was no way to separate out conclusively the individual effects of wall-cooling and acceleration on the relaminarisation phenomenon.

The study at UAC Research Labs[24, 25, 26] was similar in concept, but here a two-dimensional test geometry rather similar to the one reported in the present study was used. Cryogenic cooling of the test section was used, giving large free-stream/wall temperature-ratios and some detailed boundary-layer measurements were taken. It was again found that relaminarisation occurred for flow Reynolds Numbers below some upper limit for each of a

series of nozzles having different values of an acceleration parameter, and that this reverse transition was promoted by increased wall cooling. Since this study was definitely hardware-oriented, the data were presented in terms of quantities like rocket thrust level and throat Reynolds numbers, which inevitably makes comparison with other data difficult in any quantitative way. Again, the effects of wall cooling and acceleration of the free stream were not separately discoverable.

Moretti and Kays[23] conducted an experiment in which both free-stream velocity and wall temperature could be varied continuously for a turbulent boundary layer having effectively constant fluid properties. They found clear evidence of relaminarisation for values of K, the free-stream acceleration parameter, greater than about 2.5×10^{-6}, with heat transfer reduced to levels anticipated for a laminar boundary layer. Significantly, there was no further reduction in heat transfer for values of K greater than 3.5×10^{-6}, from which it was concluded that turbulence production was completely suppressed in this regime. Since the free-stream/wall temperature-ratio was near unity for this study, one might conclude that the results observed were due primarily to the acceleration effect.

In a massive study of flows in water channels, Schraub[21] and Kline[22] and their many co-workers found that turbulence production appears to occur in "bursts" of a complex flow structure within what has traditionally been called the "laminar sublayer", and that the rate of bursting could be correlated (inversely) with the value of K, with complete suppression for $K > 3.5 \times 10^{-6}$. These studies have advanced enormously our understanding of the mechanism of turbulence production.

Deich and Lazarev[29] reported in 1964 on experiments run on three different test sections at the Moscow Power Engineering Institute: an axi-symmetric tunnel with a second throat, a two-dimensional tunnel with

a second throat and a tunnel with a skewed-axis nozzle and diffuser. For the first two, it was found that despite a high level of free-stream turbulence induced by a normal shock just downstream of the first throat, the acceleration imposed on the turbulent boundary layers approaching the second throat rendered them laminar, as detected both by total-head traverses and hot-wire measurements. More detailed shear layer measurements were made on the third test section, where relaminarisation was again found. It was found, moreover, that the onset of relaminarisation was marked always by a sharp decrease in momentum thickness not attributable to the effects of pressure gradient on a fully turbulent boundary layer.

This work is unfortunately reported in very sparse detail, making comparison with other work difficult. If one assumes, however, that the stagnation pressure was near one atmosphere for these tests, then K was over 4×10^{-6}, i.e. well within the limits required for relaminarisation as found in the present study and earlier work.

In 1963 and 1964 Launder[27, 28] made very detailed boundary-layer measurements in highly accelerated flows of an adiabatic turbulent boundary layer at very low Mach and Reynold's numbers ($M < 0.07$, $R_{\delta_2} < 1.2 \times 10^3$). He found that for $K > 2 \times 10^{-6}$ the boundary layer underwent a progressive reversion to a state almost indistinguishable from a laminar one in terms of mean velocity profile, shear stress, separation bahavior, mean energy balance and re-transition (to turbulent) behavior, while nevertheless retaining a marked turbulence signal. He found also that the onset of relaminarisation was marked by a large and unmistakable rise in the value of the shape-factor H_{12}, and was preceded by large departures of the mean profile from the logarithmic "law of the wall" universally valid for near-equilibrium turbulent boundary layers. This work is a striking confirmation of the entirely independent Russian results mentioned above.

From the velocity-profile oriented point of view, it appeared that the relaminarisation process in Launder's flows proceeded through the growth of the "laminar sublayer" within the turbulent shear layer until the latter was supplanted entirely. This finding is in no way invalidated by the discovery by Kline et al.[22] of the further details of the process, involving formation of an unsteady, bursting "streak" structure within the "laminar" flow. We might, however, in the light of these discoveries, do well to modify our conceptual model of a "laminar" sublayer, and simply note the existence of a region near the wall in which molecular viscosity dominates the flow.

There seems no reason to suppose a priori that the well-known Reynold's analogy between heat and momentum transfer should be valid for highly non-equilibrium turbulent flows like those treated above, and indeed, in 1963, Romanenko, Leont'ev and Oblivin[39] reported on experiments in which both heat transfer and shear stresses in a highly accelerated flow near $M = 0.5$ were measured, leading them to conclude that the Reynold's analogy should indeed be abandoned for such flows. Their shear measurements were taken with hot-wire equipment, and wall shear stress was inferred from the conservation relations for the shear layer in integral form. No great accuracy is to be expected from this procedure (see ref. 35), and their alternate method of finding the wall shear stress, essentially that of Clauser[1] seems equally suspect in view of the large departures from universality found by Launder and others for such shear layers.

B. Introduction to the Present Study

Given the above considerable body of knowledge about the relaminarisation phenomenon, it seemed desirable, when assessing the goals of the present study, to try to extend our knowledge into flow regimes typical of actual fluid machinery, as measured by such parameters as Mach and Reynold's numbers,

and to express the results in some form immediately useful for design purposes. It seemed clear that a necessary first step was the separation of the effects of free-stream acceleration and strong wall-cooling. This study treats the adiabatic-wall case. It also seemed desirable to measure as directly as possible wall shear stresses typical of highly non-equilibrium accelerating flows, this information being scanty or absent in all the reported work up to the time the project was initiated.

Recent work by Hopkins and Keener[31] and by Patel[32] gave reason to believe that some form of wall-pitot could be used for this purpose - see Section II.B.1. and Appendix I. The present study appears to incorporate the first published attempt to measure local wall shear-stress by a quasi-direct method in turbulent compressible boundary layers in extreme pressure gradients. The calibration procedure revealed a "universal" calibration for the essentially two-dimensional wall-pitot geometry chosen. This happy circumstance offers a new and useful technique for skin friction measurements in very thin boundary layers, with or without an imposed pressure gradient.

To facilitate both instrumentation and comparison with the major part of previously published data, a nominally two-dimensional experimental geometry was chosen. Provision was made for variation of the imposed pressure gradient, and for detailed shear-layer measurements. Unit Reynold's number could be varied through a 10:1 range. Section II.A treats the experimental facility.

Examination of velocity-profile development in a series of pressure gradients, taken in conjunction with the associated and confirmatory wall shear stress measurements allowed the delineation of the coupled effects of acceleration and characteristic Reynold's number. These results are presented in the form of a directly useful "laminarisation map" having

these parameters as coördinates.

Any given nozzle-wall shear-layer has a trajectory on such a diagram. Thus, if laminarisation is found to occur within some region of the diagram, entry of the trajectory corresponding to any actual or proposed device into such a region indicates the onset of laminarisation in that device. This process may, however, not be carried to completion if the boundary layer remains within the required ranges of K and R_{δ_2} for an insufficient flow length. These matters are treated in Section IV.

A computation scheme suitable for general turbulent and laminar two-dimensional and axi-symmetric compressible boundary-layer calculations was developed, based essentially on that of Walz[33, 34]. This scheme can be applied at the design stage of nozzle development, allowing rapid and reasonably accurate estimation of the onset and/or absence of any laminarising phenomena.

Further improvements in the prediction method were sought through incorporation of the recent, improved empirical relations of Fernholz[35] and of Escudier[36]. These various schemes were also extensively compared with data from the literature, covering both equilibrium and non-equilibrium cases in favorable and adverse pressure gradients.

A complete listing of the FORTRAN IV computer program associated with these schemes is given in Appendix V. Every effort has been made to facilitate the routine use of this program even by those totally unfamiliar with the details of the method.

Since the present study is for the adiabatic-wall case, and it has been found that wall cooling promotes reverse transition[37, 38], the suggested design procedure is essentially conservative except for cases where the fluid is cooler than the nozzle. It is qualitatively clear how

the "stability boundary" found in this study should move with positive or negative heat transfer, but quantitative information awaits much more experimental work.

C. The Method of Walz et al

1. A Brief Presentation of Theory

Building on earlier work, Walz[33, 34] produced, in 1965, an explicit-integral theory for calculation of compressible, turbulent or laminar, two-dimensional or axisymmetric boundary layers, with or without heat transfer. The main features of this method are summarised below, but the reader is urged to consult the original references for a full presentation.

The equations for momentum- and energy-conservation and continuity take the forms:

$$\rho u \frac{\partial u}{\partial x} + \rho v \frac{\partial u}{\partial y} = - \frac{dP}{dx} + \frac{\partial \tau}{\partial y} \tag{18}$$

$$c_p \left(\rho u \frac{\partial T}{\partial x} + \rho v \frac{\partial T}{\partial y}\right) = u \frac{dP}{dx} + \tau \frac{\partial u}{\partial y} + \frac{\partial}{\partial y} \left(\lambda_E \frac{\partial T}{\partial y}\right) \tag{19}$$

$$\frac{\partial(\rho u)}{\partial x} + \frac{\partial(\rho v)}{\partial y} = 0 \tag{20}$$

where $$\tau = \mu_E \frac{\partial u}{\partial y} \tag{21}$$

Weighting (18) by u^k and (20) by $(u^{k+1}/k+1)$ and integrating the sum in the interval $0 \leq y \leq \delta$ yields the relation

$$\frac{df_k}{dx} + f_k \left(2 + k + \frac{g_k}{f_k} - M_\delta^2\right) \frac{du_\delta/dx}{u_\delta} + e_k = 0 \tag{22}$$

where $$e_k = (k + 1) \int_o^\delta \left(\frac{u}{u_\delta}\right)^k \frac{\partial}{\partial y} \left(\frac{\tau}{\rho_\delta \, u_\delta^2}\right) dy \tag{23}$$

$$f_k = \int_o^\delta \frac{\rho u}{\rho_\delta u_\delta} \left(1 - \left(\frac{u}{u_\delta}\right)^{k+1}\right) dy \tag{24}$$

$$g_k = - (k + 1) \int_o^\delta \left[\frac{\rho u}{\rho_\delta \, u_\delta} - \left(\frac{u}{u_\delta}\right)^k\right] dy \tag{25}$$

k can be any arbitrary dimensionless number, but the particular choices of $k = 0$ and $k = 1$ are particularly interesting physically, resulting in the usual momentum integral equation and the kinetic-energy integral equation, with

$$g_o \equiv \delta_1, \; g_1 \equiv 2\delta_4, \; f_o \equiv \delta_2, \; f_1 \equiv \delta_3 \tag{26}$$

and

$$-e_o \equiv \frac{\tau_w}{\rho_\delta \, u_\delta^2} = \tilde{c}_f \tag{27}$$

$$e_1 \equiv \tilde{c}_D = \tilde{c}_f \int_o^1 \frac{\tau}{\tau_w} \, d\left(\frac{u}{u_\delta}\right) \tag{28}$$

These last two quantities, namely the skin friction coefficient $\tilde{c}_f$ and the shear work (or "dissipation") integral $\tilde{c}_D$ have been written with a tilde to emphasise that they are not the usual definitions, having exactly half the numerical value of the more conventional forms.

Walz also finds it useful to introduce the quantities $(\delta_1)_u$, $(\delta_2)_u$, $(\delta_3)_u$, $(\delta_4)_u$ where the subscript indicates that the integrals are to be performed with $\rho \equiv \rho_\delta$.

Shape factors H_{12}, H_{12}^*, H_{32}, H_{32}^* and H_{43}^* can now be defined:

$$H_{12} \equiv (\delta_1)_u/(\delta_2)_u \qquad H_{12}^* \equiv \delta_1/\delta_2$$

$$H_{32} \equiv (\delta_3)_u/(\delta_2)_u \qquad H_{32}^* \equiv \delta_3/\delta_2 \tag{29}$$

$$H_{43}^* \equiv \delta_4/\delta_3$$

A length parameter is also defined:

$$z \equiv \delta_2 \, R_{\delta_2}^{\,n} \tag{30}$$

Two auxiliary functions incorporating $\tilde{c}_f$ and $\tilde{c}_D$ may be introduced with advantage, viz.:

$$\tilde{c}_f \equiv \frac{\alpha}{R_{\delta_2}^{\,n}} \frac{\delta_2}{(\delta_2)_u} \qquad \tilde{c}_D \equiv \frac{\beta}{R_{\delta_2}^{\,N}} \frac{\delta_2}{(\delta_2)_u} \tag{31}$$

Finally, a heat-transfer parameter is required, viz.:

$$\theta \equiv \frac{T_e - T_w}{T_e - T_\delta} \tag{32}$$

where $$\frac{T_e}{T_\delta} = 1 + r \frac{\gamma - 1}{\gamma} M_\delta^2 \tag{33}$$

Putting (23) - (33) into (22) results in the integral relations for momentum and kinetic-energy conservation for compressible laminar and turbulent boundary layers with heat transfer in the form:

$$\frac{dz}{dx} + z \frac{du_\delta/dx}{u_\delta} \left(F_1 + n \frac{d\mu_w/dx}{du_\delta/dx} \frac{u_\delta}{\mu_w}\right) - F_2 = 0 \tag{34}$$

$$\frac{dH_{32}^*}{dx} + H_{32}^* \frac{du_\delta/dx}{u_\delta} \left(F_3 - \frac{F_4}{z}\right) = 0 \tag{35}$$

where $$F_1 \equiv (2 + n) + (1 + n) H_{12}^* - M_\delta^2 \tag{36}$$

$$F_2 \equiv (1 + n) \alpha \left(\delta_2/(\delta_2)_u\right) \tag{37}$$

$$F_3 \equiv 1 - H_{12}^* + 2 H_{43}^* \tag{38}$$

$$F_4 \equiv \frac{\delta_2}{(\delta_2)_u} \left(2\beta R_{\delta_2}^{n-N} - \alpha H_{32}^*\right) \tag{39}$$

It should also be noted that the shape factors are connected by the relations:

$$H_{12}^* = \frac{H_{12}}{\delta_2/(\delta_2)_u} + r \frac{\gamma-1}{2} M_\delta^2 \left(H_{32}^* - \theta\right) \tag{40}$$

$$H_{43}^* = r \frac{\gamma-1}{2} M_\delta^2 \frac{H_{32} - \theta}{H_{32}^*} \tag{41}$$

Up to this point, the development has involved no empirical approximations. For the solution of the coupled equations (34) and (35) we now require a hierarchy of empirical relations, summarised below. Only

chosen to impose the required pressure gradients on its boundary layer. These are shown in Figure 8.

For calibration of the skin friction fences, which required an accurately zero pressure gradient, a flexible 0.375" aluminum plate was opposed to the test plate. This was mounted on jackscrews to allow variation of its contour. The L.E. of this plate was again faired into the main contraction with a nose-piece. Considerable difficulty was initially experienced with highly non-uniform (in y) velocity distributions in the free-stream with the test section set up in this calibration configuration. This was a consequence of the 2:1 asymmetry of the second stage of the contraction. A first-order analysis of this potential flow problem due to Oates[52] indicated a method of determining that position of the leading-edge/nose-piece with respect to the test plate's nose-piece which would give minimum distortion of the free-stream velocity distribution near the entrance. This analysis is treated in Appendix III. Repositioning of the flexible plate L.E. yielded a distribution less than 1% from uniform at the first measuring station (x = 12").

Throughout this report, the origin of coördinates is the L.E. of the plastic test plate, which is also the location of the boundary layer trip. This was a 0.06" x 0.1" transverse slot in the surface. A more substantial roughness element or "spoiler" consisting of a 2" wide strip of 0.062" perforated steel plate, laid flat on the surface, could also be fitted at this point to provide an artificially thickened shear layer.

Nozzle-blocks A, B and C were chosen in their final forms with a view to obtaining interesting trajectories on a $K - R_{\delta_2}$ diagram, discussion of which is the main burden of Section IV of this report. Nozzle-block A is in fact one of the two blocks used to form the uniform Mach 2 flow which is

the usual business of the tunnel. Table 1 lists the important characteristics of the free-stream flows produced by these three test sections. See also figure 9.

Thirty-nine static pressure orifices (0.016") were distributed along the centerline of the plastic plate, with a variable spacing so as to allow accurate determination of gradients in the converging and throat regions of the test sections. These were connected to a bank of mercury manometers. In addition, for the zero pressure gradient operation required for calibration, seven downstream orifices, distributed over the whole instrumented length of the test section, were monitored for differential static pressure with respect to the L.E. tap, using inclined water manometers. This enabled the jackscrews to be adjusted so as to obtain a maximum deviation from constant static pressure of less than 0.05%.

Stagnation pressure for the isentropic part of the flow was measured with an 0.059" pitot probe in the free-stream at x = 14". Total temperature was monitored with a bare thermocouple in the settling section.

3. Probes, skin-friction fences and associated equipment

Total-pressure distribution in the shear layers could be measured at twelve statons along the test plate. Conventional flattened, sharp-edged total head probes were used for this purpose. Some of these are shown in Figure 2. Tip sizes varied from 0.007" x 0.025" to 0.017" x 0.042", the smallest size being used wherever practicable. These probes were mounted in remotely controlled and/or driven traversing rigs, as illustrated in Figure 3. These had traversing ranges of 1.3" and 2.2", using micrometer heads as the rotating elements. A miniature 10-turn helipot was driven off each head by a step-down pulley system. Acting as voltage-dividers, these supplied the X-channel signals for a pair of Moseley X-Y recorders.

Pitot-static differential pressure was fed in each case to one of a number of differential-pressure transducers, having ranges between 0 ± 0.2 psid to 0 ± 15 psid. These were mostly of the Statham unbonded strain-gauge type except for an Eico 0 ± 0.5 psid variable reluctance type. This latter was found to be unreliable below 0.1 psid and was consequently not used in this range. Three well-filtered, smoothed solid-state DC power-supplies of nominal 6, 10 and 28 V ratings were used to supply the references for the various transducers and helipots. These were supplied, in turn, off a 115 V. AC magnetic type line-voltage stabilizer. A twenty-minute warmup period proved adequate to ensure that reference-voltage variations over the course of some hours remained smaller than the test-equipment resolution. In no case did ripple exceed 0.1%.

The signals from the transducers were fed to the Y-channels of the X-Y recorders. Grounded, shielded cable was used for all connections. The transducers themselves were isolated from rapid temperature fluctuations and mechanical shock in specially-constructed enclosures, which served to maintain their operating components in the same orientation with respect to the gravity vector. This last precaution was found to be an absolute necessity for accurate work. A valved bypass system provided for accurate zeroing of each transducer/recorder pair immediately before each traverse in the actual electrical and ambient-pressure environment then existing.

One of the probe-traversing rigs was motorised, the motor speed being variable from 3 to 15 rpm through variable input DC voltage, supplied by a nominal 28 V DC power supply connected to line through a variable transformer.

The skin-friction sublayer-fence configuration chosen was that of Figure 6. This provides for a square-edged step in the surface many times

wider than its height, preceded by a minimally-sized round orifice designed to measure the pressure of the field immediately in front of the step. This geometry is only one of several possible. Some of the others are shown in Figure 7. Although the pressure difference created between this type of fence and a local static orifice is only about a third that of a double-sided geometry, the former was chosen as being easiest to make in the very small sizes required ($d < 0.002$" in some cases). There was also the problem of dust and oil-film contamination. Other workers have had considerable difficulty detecting contamination in the double-sided configuration, due to the presence of two similarly-sized tiny orifices. In the present geometry, the local static tap has 16 times the area of the fence orifice and is effectively always clear. This allows an easier determination of the onset of contamination.

The fences of each nominal size (d = .010", .007", .004" and .002") were milled en masse and rigorously cleaned and degreased after the drilling and deburring of the nominal 0.0039" orifices. Deburring was accomplished under high magnification.

The fences were mounted in a 4 x 7 array, with one fence of each of the four nominal sizes at each station. They were a light press-fit into reamed holes and were sealed on the underside with epoxy cement. After mounting, each fence-element L.E. was carefully blended into the plastic surface by hand scraping under magnification. Finally, the actual finished fence heights were measured to better than 0.0001" using a dial gauge and traverse. Figure 4 shows some of the fences mounted in the test plate. Precautions, not always entirely successful, were taken to exclude dust and oil from the test surface.

The fences, and the local static-pressure orifices at each of the seven x stations, were connected to a bank of 28 U-tube water manometers

except in cases where the large shear to be encountered necessitated the substitution of mercury instruments for certain fences. Since the total pressure differences to be measured were as little as 0.1% of the total dynamic head, and the tunnel ambient-pressure was usually considerably above or below atmospheric, great care had to be taken in sealing each of the several hundred tubing joints in the various pressure-measuring systems. "Glyptal"enamel was used for this purpose.

The theory of wall-pitots in general, and the single-sided skin-friction fence in particular is treated in Appendix I. The calibration and interpretation procedure used forms the burden of Section B.1 of this chapter.

It is believed that this constitutes the first reported use of this particular geometry for shear-stress measurements.

B. Calibration

1. Skin-Friction-Fence Calibration and Interpretation

The object of the calibration procedure used was to provide, for each individual fence, a unique relation between its readings, the local skin friction and any other pertinent parameters of the flow field. (See Appendix I)

A choice of "reference standard" for the calibration had to be made between three possibilities

a) skin-friction balance as used by Coles[2] and others[31,41],

b) Preston tube[40],

c) calculation.

Choice a) was rejected on the grounds of complexity, difficulty and expense. Considerable doubt as to the calibration of the Preston tube is still evident in the literature, with various investigations[40, 41, 42]

showing differences of up to 15% in their calibrations, whereas the recent work of Fernholz[35] on a correlation of skin-friction data in zero-pressure-gradient flows gave a law which correlated the available data within 5% for some 80% of the data and within 10% for the remainder. It was, therefore, decided to calibrate with reference to this correlation law, which is set out in Appendix VII. The fairly elaborate logic of the calibration may best be understood through reference to the block diagram of Figure 29.

For an adiabatic flow, the Fernholz law requires knowledge of the local values of R_{δ_2} and M_δ. The test section was operated in a zero-pressure-gradient flow, at fixed subsonic M_δ, at a series of Reynolds numbers. Boundary-layer total-head traverses were taken at a series of streamwise-distributed stations for each nominal Reynolds number increment. Thus the momentum-thickness distributions on the test wall could be measured, and the local skin friction computed. At the same time, readings were taken of the skin-friction-fence manometers. Since the density corrections required for evaluation of the experimental velocity profiles were small at the Mach number chosen ($M_\delta = 0.45$), no total-temperature traverses were thought necessary. Reliance was placed on the well-known relation of Van Driest[47] for the temperature profile of a turbulent boundary layer on an adiabatic flat plate, which gives $T = T\,(T_w, M_\delta, \bar{u}/u_\delta)$. This is set out in Appendix VIII.

A machine integration procedure was used to evaluate the experimental profiles for the integral thicknesses δ_1, δ_2, δ_3, $(\delta_1)_u$, $(\delta_2)_u$, $(\delta_3)_u$ and for the shape factors H_{12}, H_{32}, H^*_{12}, H^*_{32}. This is set out in Appendix IX.

Finally, the measured results and the computed c_f were plotted against each other in a suitable non-dimensional form for each fence. The method of non-dimensionalisation chosen was that of Hopkins and Keener[31], which

provides the necessary corrections for effects of compressibility. Since their procedure had proved to work well for both Preston tubes and Stanton tubes, there seemed little reason to doubt that it would prove equally reliable for the generically similar skin-friction fence. The details of this procedure are described in Appendix I.

Examination of the reduced calibration data, showed that for each individual fence, the data could be well fitted by a law of the form

$$\log(F_R) = A + B \log (F_L) + C [\log(F_L)]^2 \qquad (1)$$

where C is a very small coefficient. This was not unexpected, since the results for a Preston tube are similar[40], but the fidelity of the data to the above law was nevertheless comforting. Furthermore, it was found that all the data of all the fences could be fitted remarkably well by the linear part of the same law, viz.:

$$\log (F_R) = A_1 + B_1 \log (F_L) \qquad (2)$$

Figure 31 shows all 532 measured data points on the same plot, and the best-fit line for form (2) through them, while Figure 32 shows the results for a typical individual fence. All the curve-fitting was done by machine using standard techniques[46].

This whole data reduction procedure was combined into a single computer program which is listed in Appendix II, and whose logic is, in part, the subject of Figure 30.

Since curve-fitting routines are essentially "mindless" affairs, the precaution was taken of getting a machine plot (Calcomp) of the two- and three-term calibration curves, equation (1),for each fence,together with all the data points for that fence. This allowed an evaluation of which curves

could reasonably be extrapolated outside the ranges of shear covered in the calibration runs. See figures 31 and 32. In those few cases where fence readings showed marked scatter, it was decided to use the "universal" calibration (equation (2)) instead. The "universal" calibration constants found were:

$$A_1 = -0.18668 \text{ and } B_1 = 0.74325 \tag{3}$$

To review, we now had a relation for each fence, and a "universal" one for all fences, of the form:

$$c_f = c_f\,(\Delta P,\ P_\delta,\ M_\delta,\ T_\delta) \tag{4}$$

or, since isentropic flow may be assumed,

$$c_f = c_f\,(\Delta P,\ P_w,\ P_o,\ T_o) \tag{5}$$

in terms of experimentally measured quantities. These relations were obtained at a fixed Mach number and in zero pressure gradient.

Thus, to interpret the readings of a given fence at some other Mach number, only a simple inversion of the procedure of Hopkins and Keener was required, but to complete the interpretation, a correction had to be made for the effects on the readings of any pressure gradient present.

We have, up to now, no entirely successful analytical description of the viscous flow over a step, with or without an axial pressure gradient, despite several valiant attempts, most notably by Gadd[44], Thom[45], Trilling and Häkkinen[42], Taylor[51] and Patel[32].

The simple first-order correction procedure described by Patel did, however, show that we might expect such corrections to be reasonably small - less than 25% - even in the most severe pressure gradients we proposed to investigate. In contrast, Preston tube corrections can be over 60%. With

this in mind, therefore, a somewhat extended form of Patel's analysis was completed, taking into account non-uniformity of fluid properties, and using a rather more realistic, but still inexact, prescription for the effect of the oncoming non-uniform (in y) momentum flux on the readings of the device. This is set out in Appendix I.

It should be recognised that the solution of this problem involves the solution of the full two-dimensional Navier-Stokes equations for a compressible fluid, with mixed boundary conditions, a task which is currently considerably beyond the state of the art. Even the attempt by Gadd[44] on the purely incompressible laminar Couette flow over a small step proved of limited applicability. There is certainly room for work on a better correction procedure - either theoretical or experimental - than that used here. Given such an improved procedure, the data of this study could easily be reworked to incorporate it.

The assumption is made that the effects of compressibility and of pressure gradient are only weakly coupled. This will be true for any boundary layer whose laminar sublayer has sensibly constant (in y) fluid properties, especially density. For flows up to at least Mach 2, this assumption will not be seriously in error to at least the order of accuracy implied by the pressure-gradient-effects correction-analysis.

It will be seen from Figure 30, which treats the logic of the interpretation procedure, that such a decoupling is in fact assumed, since in each cycle of the iteration procedure described in Appendix I, the raw reading is corrected before reference to the calibration equation.

The exponent in the relation

$$\Delta P = a\tau^{b} \qquad (6)$$

required by the correction analysis to account for effects of unit Reynold's

number variation was obtained by a best-fit to all the calibration data. A value of 1.31 proved to fit all but 10% of the data to better than 5%.

The computer program for the iterative interpretation procedure described above, detailed in Appendix I and whose logic forms the subject of Figure 30 is listed in Appendix II. In addition to the RHS quantities of equations (1, 2), the program also requires a value, in each case for the relative pressure gradient, $\frac{d(P/P_o)}{dx}$, obtained from some such diagram as Figure 8. The constants A, B and C for each fence and A_1, B_1 are punched onto cards as part of the output of the calibration program. These cards then form part of the data set of the interpretation program.

Examination of the output of the program for a given run reveals at once whether any of the four fences at each x station were partially blocked by dust or oil, through a clearly spurious low value of c_f by comparison with its neighbors. A choice can also be made between the calibration curves to be used in the event - such as at very low absolute values of shear - that extrapolation beyond the calibrated range is needed. In any event, the differences over which this somewhat subjective "weighting" had to be exercised seldom amounted to as much as 10%. Manometer-reading errors at very low absolute shears ($\Delta P < 2$ mm water) were the largest single source of random error, though the effects of dust and oil in putting certain fences completely out of commission for individual runs were certainly more prevalent at these low densities. It is thus not surprising to find that experimental scatter of c_f values is most marked at the lowest-density tunnel-operating conditions.

2. Linearity Checks of Transducers and Recorders

At several intervals during the course of the experiments, linearity checks were performed on the transducers and recorders used. A manometer

was used as the reference standard. Care was taken to ensure that the same transducer-recorder pairing was maintained for all subsequent tests.

It was found that each pair was commendably linear throughout its whole nominal range, except very close to zero pressure difference. The Statham transducers were superior to the Eico in this respect.

The linearity of response of the traverse-reporting potentiometers and recorder channels was also checked at intervals. Provided that due care was taken to allow sufficient warmup time for the line-voltage stabilisation device, power supplies and recorder D.C. amplifiers, no deviation from linearity, within the resolution capability of the recorder, was ever found.

Exclusive of the above caveat, the Moseley recorders were found to be astonishingly drift-free over a period of hours, and are to be highly recommended.

C. Experimental Procedure

For each nozzle profile to be tested, the tunnel was run at a series of standard conditions on P_o, T_o and back-pressure, as nearly as possible. Local static pressures were measured, allowing establishment of local free-stream quantities, and, by numerical differentiation, all pressure-gradient-dependent quantities such as K. Assumption of a recovery factor of 0.88 (see e.g. Ref. 34) allowed determination of local fluid properties at the surface. The pressure-ratio data were smoothed before being put into the various computational schemes discussed in the next chapter.

Total-head traverses could be taken two at a time, using the two traversing rigs, for each standard operating condition, provided that the probes were not so placed as to cause mutual interference. In each case, the scale factors on the X-Y recorders were adjusted so as to yield the largest trace that would fit onto the 8-1/2" x 11" plotting sheets. The traversing

rigs were driven sufficiently slowly that there was negligible "lag" or "hysteresis" in the plotting procedure.

The data of these traces were then converted to digital form, using variable y spacing to improve accuracy in regions of large u^2 variation, and punched onto cards for machine computation of the various integral parameters required for this study. The program used is written-up and listed in Appendix IX. Since total-temperature measurements were not attempted in the shear layers, density corrections are supplied through the relation of Van Driest[47]. (See Appendix VIII.) This applies, strictly speaking, only to the zero-pressure-gradient case, but, since the highest Mach number encountered for a traverse was only about 0.8, the density corrections are small, and the final effect on the integral parameters even further attenuated.

To further the general utility of the program, provision has been made for insertion of u and T data if required. The perennial problem of how to approximate the effect of the first element of such a digitised list is also treated in Appendix IX.

As a check, δ_2 and δ_3 were plotted versus P_o for each x, for each nozzle as the data-taking proceeded. In this way faulty data could be culled and the required runs repeated. In cases where there appears to be no reason to favor or discard some data that conflicts with other data obtained under nominally the same conditions, all the conflicting data elements are listed or plotted elsewhere in this report. To resolve doubts, resort was sometimes had to "fill-in" runs at intermediate values of P_o.

The values chosen for the parameters required to initiate the prediction programs were the means of several sets of profile data at the particular upstream point chosen. The points chosen were at nearly zero pressure gradient for all runs.

The skin-friction-fence manometers were read at each standard operating condition, for each run. The values quoted in Tables 2 - 5 are weighted means of several runs, except when the data appeared to group around two or more values. This occurrence probably indicated an incipient problem with contamination, but in such cases, both values are listed, since there seems little valid means to choose between them. Interpretation of the readings required machine computation by the procedure listed in Appendix II.

The tunnel had to be shut down and the test-section doors removed for each change of probe stations. This procedure was unavoidably laborious and resulted in large accumulations of tunnel time for a relatively small amount of data.

In determining the set of "standard" conditions to be run for each nozzle, a quick check of the actual pressure field was made for each nozzle, and a starting profile measured. This enabled a prediction of the likely trajectories for the shear layer on a $K - R_{\delta_2}$ plot, assuming fully turbulent behavior. In this way, the range of P_o likely to bracket the appearance of laminarisation could be estimated, and much unnecessary data-gathering avoided.

III. THEORETICAL PROGRAM

A. Brief Survey of Computational Methods

There exists a vast multitude of computational methods for the incompressible turbulent two-dimensional boundary-layer. There exist also a few theories for compressible boundary layers, usually based on some adaptation of an incompressible theory. Fortunately, several excellent reviews of computation methods [36, 48, 49] have appeared recently, which offer some guidance in the maze. There is no point in paraphrasing these here except insofar as the special needs of this study dictate.

In his admirably clear scheme for classifying such theories, Spalding [49] distinguishes between:

(i) "Complete" theories, which aim to solve, by numerical means, more-or-less exactly the partial differential equations of conservation of mass, momentum, energy, etc., using as additional input empirical information about local quantities in the shear-layer such as effective viscosity, effective Prandtl number, etc. Patankar & Spalding [53] and Mellor & Gibson [55] have recently produced improved theories of this type.

(ii) "Parametric Integral" theories, in which profile relations containing several free parameters are assumed to hold good at each longitudinal station. The partial differential equations are then multiplied by each of a set of weighting functions of the dependent and/or independent variables and integrated across the layer, yielding a set of ordinary differential equations having the streamwise coördinate as the independent variable and the free paramenters as the dependent variables, which appear linearly. These then require a matrix inversion for isolation, followed by numerical integration of the resultant set of first-

order equations, yielding finally the free paramenters as algebraic functions of the streamwise coördinate. From these, any desired property of the solution may be exhibited - to the accuracy to which that property may be described by the number and nature of the parameters involved.

(iii) "Explicit Integral" theories, in which the partial differential equations, weighted in some manner, are integrated over the shear layer as a first step, yielding ordinary differential equations in "integral parameters" such as $\delta_1, \delta_2, \delta_3$, etc. with the streamwise coördinate as the independent variable. These are then subject to relatively quick and simple numerical solution procedures. These methods differ chiefly in the weighting functions used, the number and nature of the conservation laws invoked and the auxiliary relations used to relate explicitly the various integral parameters one to another.

One has to agree with Spalding that the approach of type (i) offers much hope of eventual relief from the woes of trying to relate an ever larger hierarchy of empirical correlations as we attempt to compute ever more more complex flows. However, the empirical input required for use of any type (i) method in the present case of a compressible boundary layer which may or may not undergo laminarisation appears utterly lacking at this juncture. The inputs required for types (ii) and (iii) computation are more easily obtained from commonly measured quantities. To this end, a representative method of each of these latter types will be examined further.

The method of Moses [50] and Launder [28] represents an early attempt to apply a parametric integral method to the problem of an incompressible laminarising flow. Further work on this method is treated in Section B.

The method of Walz [33, 34] of type (iii) purports to compute all cases of laminar or turbulent, compressible or incompressible, two-

dimensional or axisymmetric boundary layers, with or without heat-transfer, and as such is probably unique in its field. It seemed worthwhile, for the ends of this study, to make a considerable effert to develop a readily useable and foolproof machine-computation procedure incorporating this overall method, and to explore some of its limitations, especially in highly non-equilibrium compressible shear-flows. The relatively transparent nature of the auxiliary relations used in type (iii) methods offers perhaps the best hope, at the present state of the art, of ascertaining the modifications required for prediction of such flows. Section C deals further with this phase of the study.

None of the above methods can be invoked without a more-or-less precise knowlege of the properties of the shear layer at the starting point. Given an error in the specification of the starting conditions, there is a uniform tendency for the prediction to diverge from experiment in adverse, and to approach it in favorable pressure-gradients (usually). Type (ii) methods appear particularly susceptible to this starting problem.

B. The Method of Moses and Launder

In 1964 Moses[50] proposed a parametric integral theory for calculation of turbulent incompressible boundary layers. This corresponds precisely with the type (ii) scheme outlined above, where the momentum integral equation is the chief conservation relation invoked. A parametric description of the local velocity profile of the form

$$\frac{u}{u_\delta} = 1 + \alpha \log \frac{y}{\delta} + \beta\left(1 - 3\left(\frac{y}{\delta}\right)^2 + 2\left(\frac{y}{\delta}\right)^3\right) \qquad (7)$$

is used, where α,β are the parameters, which are related to other variables of the problem by the relations

$$\alpha = \frac{1}{\kappa} \left(\frac{c_f}{2}\right)^{1/2} \tag{8}$$

$$\beta = \alpha(\log (\alpha R_\delta) + 1.1237) - 1 \tag{9}$$

κ is the familiar constant from the Coles[2] universal velocity profile:

$$\frac{u}{u_\tau} = \frac{1}{\kappa} \log \left(\frac{y\, u_\tau}{\nu}\right) + B + \frac{\pi}{\kappa} \omega\left(\frac{y}{\delta}\right) \tag{10}$$

Since two parameters are invoked, two conservation relations are required. This is accomplished by causing the momentum integral equation to be separately satisfied over two strips, each of height $\delta/2$. This requires empirical specification of the effective viscosity and turbulent normal stress at the join .

With the procedure outlined in part A supra, the net result is a pair of simultaneous, first-order, ordinary differential equations in α and β of the form

$$\frac{d\delta}{dx} = F_1 (\alpha, \beta, \delta, u_\delta) \tag{11}$$

$$\frac{d\alpha}{dx} = F_2 (\alpha, \beta, \delta, u_\delta) \tag{12}$$

which can be solved by the familiar Runge-Kutta numerical procedure, given starting values of δ, α and u_δ at some x. Further details of the procedure are given in the cited reference.

The author has strong objections to the use of the quantity δ in either experimental or theoretical work of any sort. This quantity is extremely ill-defined, particularly for boundary layers having a large value of the shape factor H_{32}. In particular, its use as a normalizing quantity either for presenting experimental data or for computational purposes is fundamentally unsound, though staggeringly widespread, nevertheless.

Launder[28] subsequently modified this computational method in an effort to calculate the development of an incompressible turbulent boundary layer undergoing turbulent-laminar transition. The shear layer was again considered in two strips, characterised as a "viscous inner layer" and a "shear free outer layer", but the position of the boundary between the strips was allowed to vary. This boundary was at height δ_L. A parametric representation of velocity profiles in the form

$$\begin{aligned} \frac{u}{u_\delta} &= \alpha \left[(2-\beta)\left(\frac{y}{\delta_L}\right) + (\beta - 1)\left(\frac{y}{\delta_L}\right)\right] && 0 \leq \frac{u}{u_\delta} \leq \alpha \\ \frac{u}{u_\delta} &= \left(\frac{y}{\delta}\right)^\beta && \alpha \leq \frac{u}{u_\delta} \leq 1 \end{aligned} \tag{13}$$

was used, where $\alpha \equiv (u/u_{\delta_L})$. In addition, a Reynold's number was introduced as an explicit third parameter, defined as

$$R_{\delta_L} \equiv \frac{u_\delta \, \delta_L}{\nu} \tag{14}$$

This required another conservation equation, and conservation of mass within the shear layer was invoked. The net result was a set of three o.d.e.'s of form

$$\frac{d\alpha}{dx} = F_1 \left(\alpha, \beta, R_{\delta_L}, u_\delta, \frac{du_\delta}{dx}\right) \tag{15}$$

$$\frac{d\beta}{dx} = F_2 \left(\alpha, \beta, R_{\delta_L}, u_\delta, \frac{du_\delta}{dx}\right) \tag{16}$$

$$\frac{dR_{\delta_L}}{dx} = F_3 \left(\alpha, \beta, R_{\delta_L}, u_\delta, \frac{du_\delta}{dx}\right) \tag{17}$$

These are again solvable by the Runge-Kutta technique, given starting values of α, β and R_{δ_L}. It should be noticed that the parameter α is

connected to the wall shear-stress in the same way in the Launder and Moses formulations.

In order to obtain predictions of the data of his experiment, Launder required resort to a non-systematic specification of both the shear stress at the join between the strips and also the specification of that point (in x) from which the calculation should be initiated.

Additional criticisms of this calculation method also arise, from the point of view of ab initio calculation, as, e.g., in basic design: α, β and δ_L are not easily estimable or empirically well-known. Also, the assumption of mass-conservation within the shear layer seems physically unrealistic and manifestly raises some question as to the identity of the outer part of the shear layer vis-à-vis the free stream.

During the early phase of the present study, an attempt was made to overcome these objections through a more systematic formulation, and specification of an entrainment condition, à la Head[61], in place of the mass-conservation relation. Attention was also given to a parametric representation of the density profile of this sort of shear layer in a compressible flow, with a view to obtaining a parametric integral prédiction method for compressible relaminarising flows. This effort proved fruitless, due to the almost complete lack of experimental data and an inability to systemise the choice of initial conditions sufficiently well for an ab initio calculation, and was, therefore, abandoned.

Given a very considerable experimental effort over a period of some years, it may well be possible to generate sufficient data to permit the formulation of a sound parametric integral theory for the compressible case. This data would almost certainly, however, provide the required input for a "complete" theory of the type (i) discussed in section A. This latter approach is, in the end, likely to prove the most generally useful.

C. The Method of Walz et al

1. A Brief Presentation of Theory

Building on earlier work, Walz[33, 34] produced, in 1965, an explicit-integral theory for calculation of compressible, turbulent or laminar, two-dimensional or axisymmetric boundary layers, with or without heat transfer. The main features of this method are summarised below, but the reader is urged to consult the original references for a full presentation.

The equations for momentum- and energy-conservation and continuity take the forms:

$$\rho u \frac{\partial u}{\partial x} + \rho v \frac{\partial u}{\partial y} = - \frac{dP}{dx} + \frac{\partial \tau}{\partial y} \tag{18}$$

$$c_p \left(\rho u \frac{\partial T}{\partial x} + \rho v \frac{\partial T}{\partial y}\right) = u \frac{dP}{dx} + \tau \frac{\partial u}{\partial y} + \frac{\partial}{\partial y} \left(\lambda_E \frac{\partial T}{\partial y}\right) \tag{19}$$

$$\frac{\partial(\rho u)}{\partial x} + \frac{\partial(\rho v)}{\partial y} = 0 \tag{20}$$

where $$\tau = \mu_E \frac{\partial u}{\partial y} \tag{21}$$

Weighting (18) by u^k and (20) by $(u^{k+1}/k+1)$ and integrating the sum in the interval $0 \leq y \leq \delta$ yields the relation

$$\frac{df_k}{dx} + f_k \left(2 + k + \frac{g_k}{f_k} - M_\delta^2\right) \frac{du_\delta/dx}{u_\delta} + e_k = 0 \tag{22}$$

where $$e_k = (k + 1) \int_o^\delta \left(\frac{u}{u_\delta}\right)^k \frac{\partial}{\partial y} \left(\frac{\tau}{\rho_\delta \, u_\delta^2}\right) dy \tag{23}$$

$$f_k = \int_o^\delta \frac{\rho u}{\rho_\delta u_\delta} \left(1 - \left(\frac{u}{u_\delta}\right)^{k+1}\right) dy \tag{24}$$

$$g_k = - (k + 1) \int_o^\delta \left[\frac{\rho u}{\rho_\delta \, u_\delta} - \left(\frac{u}{u_\delta}\right)^k\right] dy \tag{25}$$

k can be any arbitrary dimensionless number, but the particular choices of $k = 0$ and $k = 1$ are particularly interesting physically, resulting in the usual momentum integral equation and the kinetic-energy integral equation, with

$$g_o \equiv \delta_1, \; g_1 \equiv 2\delta_4, \; f_o \equiv \delta_2, \; f_1 \equiv \delta_3 \tag{26}$$

and

$$-e_o \equiv \frac{\tau_w}{\rho_\delta \, u_\delta^2} = \tilde{c}_f \tag{27}$$

$$e_1 \equiv \tilde{c}_D = \tilde{c}_f \int_o^1 \frac{\tau}{\tau_w} \, d\left(\frac{u}{u_\delta}\right) \tag{28}$$

These last two quantities, namely the skin friction coefficient $\tilde{c}_f$ and the shear work (or "dissipation") integral $\tilde{c}_D$ have been written with a tilde to emphasise that they are not the usual definitions, having exactly half the numerical value of the more conventional forms.

Walz also finds it useful to introduce the quantities $(\delta_1)_u$, $(\delta_2)_u$, $(\delta_3)_u$, $(\delta_4)_u$ where the subscript indicates that the integrals are to be performed with $\rho \equiv \rho_\delta$.

Shape factors H_{12}, H_{12}^*, H_{32}, H_{32}^* and H_{43}^* can now be defined:

$$H_{12} \equiv (\delta_1)_u/(\delta_2)_u \qquad H_{12}^* \equiv \delta_1/\delta_2$$

$$H_{32} \equiv (\delta_3)_u/(\delta_2)_u \qquad H_{32}^* \equiv \delta_3/\delta_2 \tag{29}$$

$$H_{43}^* \equiv \delta_4/\delta_3$$

A length parameter is also defined:

$$z \equiv \delta_2 \, R_{\delta_2}^{\,n} \tag{30}$$

Two auxiliary functions incorporating $\tilde{c}_f$ and $\tilde{c}_D$ may be introduced with advantage, viz.:

$$\tilde{c}_f \equiv \frac{\alpha}{R_{\delta_2}^{\,n}} \frac{\delta_2}{(\delta_2)_u} \qquad \tilde{c}_D \equiv \frac{\beta}{R_{\delta_2}^{\,N}} \frac{\delta_2}{(\delta_2)_u} \tag{31}$$

Finally, a heat-transfer parameter is required, viz.:

$$\theta \equiv \frac{T_e - T_w}{T_e - T_\delta} \tag{32}$$

where $$\frac{T_e}{T_\delta} = 1 + r \frac{\gamma - 1}{\gamma} M_\delta^2 \tag{33}$$

Putting (23) - (33) into (22) results in the integral relations for momentum and kinetic-energy conservation for compressible laminar and turbulent boundary layers with heat transfer in the form:

$$\frac{dz}{dx} + z \frac{du_\delta/dx}{u_\delta} \left(F_1 + n \frac{d\mu_w/dx}{du_\delta/dx} \frac{u_\delta}{\mu_w}\right) - F_2 = 0 \tag{34}$$

$$\frac{dH_{32}^*}{dx} + H_{32}^* \frac{du_\delta/dx}{u_\delta} \left(F_3 - \frac{F_4}{z}\right) = 0 \tag{35}$$

where $$F_1 \equiv (2 + n) + (1 + n) H_{12}^* - M_\delta^2 \tag{36}$$

$$F_2 \equiv (1 + n) \alpha \left(\delta_2/(\delta_2)_u\right) \tag{37}$$

$$F_3 \equiv 1 - H_{12}^* + 2 H_{43}^* \tag{38}$$

$$F_4 \equiv \frac{\delta_2}{(\delta_2)_u} \left(2\beta R_{\delta_2}^{n-N} - \alpha H_{32}^*\right) \tag{39}$$

It should also be noted that the shape factors are connected by the relations:

$$H_{12}^* = \frac{H_{12}}{\delta_2/(\delta_2)_u} + r \frac{\gamma-1}{2} M_\delta^2 \left(H_{32}^* - \theta\right) \tag{40}$$

$$H_{43}^* = r \frac{\gamma-1}{2} M_\delta^2 \frac{H_{32} - \theta}{H_{32}^*} \tag{41}$$

Up to this point, the development has involved no empirical approximations. For the solution of the coupled equations (34) and (35) we now require a hierarchy of empirical relations, summarised below. Only

those for a turbulent boundary layer are given, those for the laminar case being similar in nature:

$$(\delta_2/(\delta_2)_u) \approx [1 + r\,\frac{\gamma-1}{2}\,M_\delta^2\,(H_{32}^* - \theta)\,(2 - H_{32})\phi] \tag{42}$$

$$H_{32}^* \approx H_{32}\,[1 + (2 - H_{32})\psi] \tag{43}$$

where $$\phi \approx 1 - 0.0719\,M_\delta + 0.00419\,M_\delta^2 \tag{44}$$

and $$\psi \approx 0.0114\,M_\delta\,(2 - \theta)^{0.8} \tag{45}$$

Also,

$$H_{12} \approx 1 + 1.48\,(2 - H_{32}) + 104\,(2 - H_{32})^{6.7} \tag{46}$$

$$\alpha \approx 0.0566\,H_{32} - 0.0842 \tag{47}$$

$$\beta \approx 0.0056 \tag{48}$$

$$n \approx 0.268 \tag{49}$$

$$N \approx 0.168 \tag{50}$$

$$r \approx 0.88 \tag{51}$$

The functions ψ and ϕ are seen to be correction functions for compressibility and heat-transfer effects, and are claimed to be useful up to $M_\delta = 5$.

2. Computational Scheme

Mean values of F_j $(j = 1, 4)$ may be defined over finite $\Delta x \equiv |x_i - x_{i-1}|$:

$$\overline{F}_j \equiv \frac{1}{2}\,(F_{j,i-1} + F_{j,i}) \tag{52}$$

The coupled differential equations (34), (35) may be put into axisymmetric form by the Mangler[58] coördinate transformation, and can then be written in the finite-difference form:

$$\frac{z_i}{z_{i-1}} \left(\frac{R_i}{R_{i-1}}\right)^{1+n} = B_z \, \bar{F}_2 \frac{\Delta x}{z_{i-1}} \left(\frac{1 + (R_i/R_{i-1})^{n+1}}{2}\right) \tag{53}$$

$$\frac{(H_{32}^*)_i}{(H_{32}^*)_{i-1}} = A_H + B_H \, \bar{F}_4 \frac{\Delta x}{(H_{32}^*)_{i-1}} \left(\frac{2}{z_{i-1} + z_i}\right) \tag{54}$$

where

$$A_z \equiv \left[\frac{(u_\delta)_{i-1}}{(u_\delta)_i}\right]^{\bar{F}_1} \qquad A_H \equiv \left[\frac{(u_\delta)_{i-1}}{(u_\delta)_i}\right]^{\bar{F}_3} \tag{55}$$

$$B_z \equiv \frac{1 - A_z \, (u_\delta)_{i-1}/(u_\delta)_i}{(1 + \bar{F}_1)(1 - (u_\delta)_{i-1}/(u_\delta)_i)} \tag{56}$$

$$B_H \equiv \frac{1 - A_H \, (u_\delta)_{i-1}/(u_\delta)_i}{(1 + \bar{F}_3)(1 - (u_\delta)_{i-1}/(u_\delta)_i)}$$

and R is the cross-sectional radius. For the two-dimensional case, $R_i \equiv 1$ for all i.

This development assumes that the "universal" functions F_j are in fact linearisable, an assumption which fails significantly only very near to a separation point.

There are several conceivable ways of "marching-out" the coupled equations (53) and (54) by computation involving iterative steps. Only one of these, to be described below, proves to be unconditionally stable for all cases short of separation.

The following quantities are necessary and sufficient input for a calculation:

(i) Initial conditions on: x, u_δ, $(\delta_2)_u$, $(\delta_3)_u$

(ii) The quantities $P_{i=1}$, T_o, Δx

(iii) The velocity field, in the form of a table of u_δ vs. x (or (P_δ/P_o) vs. x)

(iv) In the case of heat transfer, a table of T_w vs. x

(v) In the axisymmetric case, a table of R vs. x

This information, in conjunction with the hierarchy of exact and empirical relations (38) - (51) and their antecedents allows the following stepwise procedure:

(i) Find $(H_{32}^*)_{i=1}$

(ii) Estimate $(H_{32}^*)_{i=2}$

(iii) Thus find all coefficients of (53) and (54)

(iv) Hence obtain a first estimate of $z_{i=2}$

(v) Put these estimates of $(H_{32}^*)_{i=2}$ and $z_{i=2}$ into RHS of (54)

(vi) Hence obtain revised estimate of $(H_{32}^*)_{i=2}$

(vii) Compare the latest and penultimate estimated values of $(H_{32}^*)_{i=2}$. If the difference exceeds some predetermined value, iterate, by returning to step (iii) with the latest estimate of $(H_{32}^*)_{i=2}$.

(viii) After sufficiently close convergence of successive estimates of $(H_{32}^*)_{i=2}$ the step is complete, and steps (ii) through (vii) are repeated, with iteration as required, to find $(H_{32}^*)_{i=3}$ and so forth.

For best accuracy, the largest allowable value of Δx is that for which $\Delta u_\delta < 0.015\ u_\delta$ in the worst case. Convergence to $\left|(H_{32}^*)_i^{(m)} - (H_{32}^*)_i^{(m-1)}\right| \leq 0.00001$ typically requires less than 4 iterations, except at very close approach to a separation point. (m is the order of the iteration step.) This accuracy is barely within the single-precision resolution capability of a computer, and oscillations of amplitude less than 0.0001 can occasionally arise. In such a case the convergence criterion may be relaxed an order of

magnitude without serious effect on the overall accuracy of the calculation.

Appendix V contains a FORTRAN IV program to carry out this calculation for all the cases for which it is useful, and specific instructions for use of the program. The program has been written in such a way as to facilitate its use even by those totally unfamiliar with the method. The step size is found automatically, and the convergence criterion is reset as required. Every effort has been made to ensure that numerical "disasters" are forecast by the program as the calculation proceeds, and the appropriate messages printed-out before the case is terminated and the next case started. However, the unexpected can still happen, expecially if erroneous data is supplied, so that provision has also been made for a "debug" printout in which the major quantities of each subroutine are printed-out at each iteration or step, as well as much other information. This facility should not be invoked lightly, as the paper output is staggering.

Since H_{32} is the chief auxiliary quantity of the calculation, it was decided to specify $(\delta_2)_u$ and $(\delta_3)_u$ as the input required at the start of the calculation rather than δ_2 and δ_3. The $(\ )_u$ quantities are easily obtained if the starting velocity profile is available, while δ_2 and δ_3 require also that the density profile be available. In the event that only the numerical values of δ_2 and δ_3 are known, the auxiliary relations (42) - (45) may be invoked for $(\delta_2)_u$ and $(\delta_3)_u$. In the event that only $(\delta_2)_u$ (or δ_2) and H_{12} (or H_{12}^*) are known, H_{32} may be estimated by means of (40) and (46). The calculation method is naturally sensitive to poor estimates of H_{32}, but tends to be self-correcting after a number of steps, especially in zero or favorable pressure gradients.

It should be noted that the scheme adopted calculates the local values of M_δ through an isentropic-flow assumption. If the case in question

involves such a large heat addition to the flow that the isentropic assumption is seriously in error, a minor reprogramming, involving the use of M_δ as an additional input quantity will be required.

3. New Relations of Fernholz and Escudier

Fernholz[35] has recently produced alternate empirical formulations of the skin-friction, dissipation and shape-factor relations for a compressible turbulent boundary layer on a flat plate. These may be used in place of the Walz relations in the following way:

Replace eqn. (43) with:

$$H_{32}^* = 1.80 + 0.0072\, M_\delta \tag{58}$$

Replace (46) with

$$H_{12} = \left(1 - \left(\frac{c_1}{2}\right)^{1/2}\right) \left(7.506 - 0.202 \log_{10} \left(R_{\delta_2}\, \sigma^*\right)\right) \tag{59}$$

where $$c_1 = \frac{0.01015}{(R_{\delta_2}\sigma^*)^{0.15}} + \frac{0.786}{R_{\delta_2}\sigma^*} \tag{60}$$

and $$\sigma^* = \left(\frac{(\delta_2)_u}{\delta_2}\right)^{0.7} \tag{61}$$

where $$\frac{(\delta_2)_u}{\delta_2} = \left[H_{12}^* - r\,\frac{\gamma-1}{2}\, M_\delta^2\, (H_{32}^* - \theta)\right] / H_{12} \tag{62}$$

where $$H_{12}^* = H_{12} = 0.4\, M_\delta^2\, f_2(\theta) \tag{63}$$

The function $f_2(\theta)$ is unity for the adiabatic case.

We also obtain the skin friction coefficient

$$c_f = r_1 \left[\frac{0.01015}{R_{\delta_2}^{0.15}} \left(\frac{(\delta_2)_u}{\delta_2}\right)^{0.595} + \frac{0.786}{R_{\delta_2}}\right] \tag{64}$$

where $$r_1 = 1 + r\,\frac{\gamma-1}{2}\, M_\delta^2\, (1 - \theta) \tag{65}$$

thus we can replace (47) by

$$\alpha = \frac{1}{2} c_f \frac{(\delta_2)_u}{\delta_2} R_{\delta_2}^{0.268} \tag{66}$$

The dissipation coefficient β now becomes

$$\beta = \frac{1}{4} c_f H_{32}^{*} R_{\delta_2}^{0.268} \frac{(\delta_2)_u}{\delta_2} \tag{67}$$

in place of eqn. (48).

These relations have also been programmed into an alternate subroutine ("HANS") and are thus available for use as explained in Appendix V.

New relations, not restricted to zero pressure-gradient, are also available from Escudier[36], and take the following forms:

Eqn. (46) is to be replaced by:

$$H_{12} = 1.55 \left[0.0971 + (0.009428 - 3.1 (1.431 - H_{32})^{1/2})\right]^{-1} \tag{68}$$

Eqn. (47)is to be replaced by:

$$\alpha = S_s R_{\delta_2}^{0.268} \frac{(\delta_2)_u}{\delta_2} \tag{69}$$

where $$S_s = [0.243 \zeta^2 + 0.0376 \zeta - 0.00106 + 0.0914 \zeta^2/(1 + \frac{65}{\zeta})]/L^2 \tag{70}$$

where $$\zeta = \frac{2}{3} H_{32} - 1 + [\frac{2}{3} H_{32} (\frac{2}{3} H_{32} - 1)]^{1/2} \tag{71}$$

and $$L = \ell n \left[\frac{3.389 R_{\delta_2} \zeta}{(1 - \zeta)(1 + 2 \zeta)}\right] \tag{72}$$

Eqn. (48) is to be replaced by:

$$\beta = \bar{S} R_{\delta_2}^{0.268} \frac{(\delta_2)_u}{\delta_2} \tag{73}$$

where $$\bar{S} = (2 \zeta + 1) S_s/3 + T_q \tag{74}$$

where

$$T_q = \begin{cases} 0.00565\ (1 - \zeta)^{2.715} & \text{for } \zeta < 1 \\ 0.01\ (\zeta - 1)^3 & \text{for } \zeta > 1 \end{cases} \qquad (75)$$

These relations are also available in the alternate subroutine "MARCEL" and may be implemented according to the instructions of Appendix V. It should be noted that these relations are also useful for cases where the velocity profile shows an internal maximum, including the extreme case of a wall jet. Since the formulation is for the incompressible case, the required compressibility and heat transfer corrections are put in by the usual Walz relations.

4. Comparisons with Existing Data

The predictions of the Walz method were compared with adverse pressure-gradient data of Moses[50] and Goldberg[62] for both separating and non-separating cases, with zero pressure-gradient data of Smith & Walker[63], and with severe favorable pressure-gradient data of Launder[28], in addition to the data of the present study. The new relations of Escudier were also used for each test case, and the relations of Fernholz also used for a prediction of the zero pressure-gradient case. The results of the test cases based on previous data appear in Figures 11 - 13, while the data of the present study is treated in Figures 14 - 25.

Appendix VI details the sources of the particular data chosen, and lists any assumptions required to initiate the computations.

Looking first at the adverse pressure-gradient data of Figure 11 we note that both the Walz and Escudier relations predict early separation for the steep adverse, followed by relaxing, pressure-gradient of Moses # 5 while in the similar case of Goldberg # 3, the Walz relations result in an early

separation prediction. The Escudier relations show an under-prediction of shape-factor development. The Escudier relations give a more accurate prediction of δ_2 development in each case. For the less severe, non-separating case of Moses # 6, there is little to choose between the methods, for δ_2 prediction, but the Escudier relations for shape-factor again prove superior. The same findings hold good for the similar, but separating case of Goldberg # 6.

Figure 12 shows a conclusively laminarising case of Launder. Prediction of R_{δ_2}, up to the turbulent-laminar transition, is good for both sets of relations, with those of Escudier slightly superior. Thereafter the data lies grossly below the prediction. The shape factor prediction is decidedly poor, especially after transition, with the Walz relations proving superior.

Precisely the same behavior in very steep negative pressure-gradients was found when the Walz method was applied to the prediction of the flows of the present study. The uniform tendency of laminarising flows to depart from predictions based on correlations of normal turbulent boundary layer behavior in these two ways is crucial to the further development of this report, and will be discussed at length in the next chapter.

If one wishes to decide on a "best" method between the three relations offered by Walz, Fernholz and Escudier, the flat-plate data represented by Figure 13 proves singularly frustrating: For δ_2 calculation, there is little to choose between Walz and Fernholz, while the prediction of Escudier is definitely somewhat off. The same is true of the c_f prediction, with the Fernholz relations showing a slight initial superiority. For the shape-factor calculation, however, the Escudier relation corrects itself most rapidly, while the other two methods both predict high values of H_{12}^*.

The general conclusions, based on a comparison of all the predictions with their corresponding data, seem to be that δ_2 is well predicted, with the relations of Walz proving slightly better, most especially in favorable pressure-gradients. H_{12}^* is, however, relatively poorly predicted, with the Escudier relations clearly superior in zero and adverse pressure-gradients, and the Walz relations superior in favorable pressure-gradients. A high prediction of δ_2 development, and a low prediction of H_{12}^* development are consequent upon the appearance of turbulent-laminar transition in the physical flow.

IV. PRESENTATION AND DISCUSSION OF RESULTS

A. Location of Turbulent-Laminar Transition Points

Previous work on laminarisation[27, 28, 29] indicated that the onset of laminarisation in a turbulent boundary layer is marked by a sharp decrease of the momentum thickness below that to be expected for a "normal" turbulent boundary layer. This showed clearly in the work of Launder[27, 28], who presented his results in the form of H_{12} vs. x diagrams. At the low velocities with which that study was concerned, H_{12} and H_{12}^* (see definition in Chapter III, Section C) are virtually identical. The Russian work[29] was, by contrast, carried out in the high-subsonic regime, in the converging section of a two-throat tunnel, downstream of a normal shock standing at the exit of the first converging-diverging nozzle. This identification of the turbulent-laminar transition points was confirmed by hot-wire measurements in each of the studies cited.

A difficulty arises, however, if one wishes to apply a shape-factor criterion to the high-subsonic or transonic free-stream velocity regimes, where the fluid properties change rapidly. In particular, the rapidly decreasing density in that part of the shear layer closest to the wall causes a strong rise in the value of H_{12}^* for $M_\delta > 0.7$, as is evident from examination of the definition of this parameter, viz:

$$H_{12}^* \equiv \frac{\int_o^\delta \left(1 - \frac{\rho u}{\rho_\delta u_\delta}\right) dy}{\int_o^\delta \frac{\rho u}{\rho_\delta u_\delta}\left(1 - \frac{u}{u_\delta}\right) dy}$$

Thus, if one proposes to use a change in the value of H_{12}^* as an indicator of the onset of laminarisation in this regime, it is necessary to observe a

rise superimposed on another rise. This is likely to degrade further the inherently poor precision of identification due to the finite spacing of measuring stations. Following, however, a suggestion of Fernholz[56], we might seek to observe the behavior of the parameter H_{12}, which depends only on the geometrical shape of the velocity profiles, and disregards the weighting effect of the density ratios. A sharp rise from the reasonably constant values exhibited by this quantity for non-laminarising boundary layers would signal with greater precision the point of onset of an unusual phenomenon. As will be detailed below, it was in fact found that any sharp rises in H_{12} were coincident both with marked increases in the rate of change of H_{12}^* and also with marked decreases in the measured skin-friction. It is thus not unreasonable to infer that a sharp rise in the value of H_{12} for a turbulent compressible boundary layer is also indicative of turbulent-laminar transition.

Three nozzle profiles (Figure 8) were used in the present study, producing the free-stream flows detailed in Figure 9 and Table 1. In addition, a fourth case was created by placing a spoiler just upstream of the trip for a series of runs with nozzle C. This was in an effort to increase the range of R_{δ_2} studied with this nozzle. The spoiler was the largest that would still allow the relaxation of the shear layer to a state indistinguishable from a normal flat-plate boundary layer before the onset of acceleration.

Tables 2 - 5 and Figures 14 - 25 present the measured values of c_f, H_{12}^*, H_{12}, H_{32} and R_{δ_2} as functions of longitudinal coördinate x and stagnation pressure P_o. Since the test sections were in each case operated in the supersonic throat mode, changes in stagnation conditions should simply be regarded as giving rise to different characteristic densities. The

spread of stagnation temperatures was only some 15°R, thus changes in μ between the various "standard conditions" are small.

The qualitative behavior of H_{12}^* and H_{12} as functions of x and P_o, as illustrated in Figures 18 - 21 was rather similar for each of the four cases. Only one case need, therefore, be discussed in detail, e.g., nozzle A:

Beyond $x \geqslant 30"$, the H_{12}^* data appears to divide into two groups, that for $P_o = 5$ and 10"Hg. abs. diverging from that of $P_o = 15$ and 20 and from the prediction. Beyond x = 32.8", the data for $P_o = 15$ also rises sharply. The behavior for H_{12} is similar, but more marked, especially since the majority of the data and the predictions show an almost constant value of H_{12} with both x and P_o except for the behavior of the errant few.

Turning now to the behavior of δ_2 itself, we note from Figure 22 that while for $P_o = 20$, δ_2 has risen, at x = 35", slightly above the minimum value encountered, (following the sense of the prediction) the trend in the other three cases is for a continued strong decrease. As has been discussed in Chapter III, the general agreement between measurement and calculation is comparatively good, except in this particular range of x and P_o values.

The skin-friction measurements for nozzle A (Figure 14) appear to confirm the trends noted above: At the most upstream measuring station (x = 19"), the trend of c_f values with increase of unit Reynold's number (i.e. increase of P_o) is in line with the conventional experience with zero-pressure-gradient boundary layers, i.e. c_f decreases with increased Reynolds number. However, as the expansion proceeds, the behavior changes in a surprising way, viz: By x = 41", c_f for $P_o = 20$ has risen steadily to roughly double the initial value; for $P_o = 15$, c_f reaches a plateau at about x = 35", and is less than that of $P_o = 20$ at x = 41", the final

measuring station; for P_o = 10, there is a maximum around x = 30", followed by a steady fall, while the P_o = 5 data set follows the same trend, but peaks earlier and decreases very much more rapidly thereafter. The end result is that by the final measuring station, the order of c_f values with Reynold's number has been inverted, c_f now increasing with unit Reynold's number.

Given the above behavior of H_{12}^*, H_{12}, δ_2 and c_f with x and P_o, and remembering that K is an almost linear function of P_o at any x, it seems not unresonable to interpret the data in the following way:

(i) the P_o = 5 boundary layer entered turbulent-laminar transition at 28" < x < 30", with immediate anomalous reduction of δ_2 and c_f,

(ii) the P_o = 10 layer similarly entered transition at 29" < x < 32",

(iii) the P_o = 15 layer entered transition for x > 32", with little change in c_f from the entering value,

(iv) the P_o = 20 layer did not enter transition at all.

In an entirely similar way, transition points can be located for the other three cases. Nozzle B, for example, would be declared to have the P_o = 5 data showing transition at about x = 37", while the P_o = 10 data shows a rather "hesitant" transition at about x = 39". The P_o = 20 data behaves in an unexceptionally turbulent manner.

B. Shear-Layer Trajectories in the K - R_{δ_2} Plane

At this stage in our knowledge of laminarising turbulent boundary layers, it would be distinctly unwise to assert that we could list all the important parameters of the problem and thus perform a definitive dimensional analysis, vide Taylor[57]. The following quantities, however, have proven experimentally to influence the onset and course of the turbulent-

laminar transition phenomenon in the adiabatic-wall case: u_δ, δ_2, μ_w, ρ_w, ρ_δ, du_δ/dx.

Clearly this list is neither exhaustive nor unique, and the reference conditions are arbitrary. We can, however, construct the following two dimensionless groups:

$$K \equiv \left(\frac{\mu_w}{\rho_w u_\delta}\frac{du_\delta}{dx}\right) \quad \text{and} \quad R_{\delta_2} \equiv \left(\frac{\rho_\delta u_\delta \delta_2}{\mu_w}\right)$$

The significance of the group K has been remarked upon by Rotta[60], Mellor[59] and Launder[28] and several others in their consideration of incompressible flows. Since it is the ratio of pressure and shear forces acting on that limiting region of the shear layer at the wall, the only additional specification that has to be made for the compressible case is that fluid properties be evaluated at wall conditions, as has been indicated.

Examination of the literature reveals a surprising lack of uniformity in the definition of momentum thickness Reynold's number for compressible boundary layers, even on an adiabatic wall. Some authors use ρ_w in the numerator or μ_δ in the denominator. The form cited above seems, however, to be the most logical for the needs of this problem when considered thus: We wish to express the ratio of the inertial forces to the viscous forces which exist in that part of the shear layer nearest to the wall. Since we do not know with precision any other characteristic momentum, we choose that of the free stream, and so, for consistency, the density term is to be evaluated at free-stream conditions. The viscosity term should be evaluated at those well-defined conditions most closely approximating those of the near-wall layer. This indicates the choice of T_w as the suitable temperature for evaluation of μ.

An important point to notice about K and R_{δ_2} is that while they share several variables, K contains only variables pertaining to the free-stream, the only boundary-layer parameter, δ_2, being contained in R_{δ_2}. With an eye to achieving rational design procedures for nozzle flows, we might, therefore, seek to understand the laminarising phenomenon in terms of the behavior of these two quantities. It will now be shown that this approach is largely successful, rendering more intelligible the data of this investigation and the other detailed laminarisation data published up to now.

We come first to the concept of a "trajectory" of the shear-layer in the K - R_{δ_2} plane. This is simply obtained by a cross-plot of the data of, for example, Figures 9 and 22, for each discrete value of P_o and with x as the cursory polar coördinate. This way of presenting the data appears to be particularly useful in describing the "history" of a compressible shear layer in a rapidly expanding flow. The local density appears in both the force-ratios K and R_{δ_2}, but in an opposite sense. The mere fact of its rapid change makes separate evaluation of acceleration and Reynold's number effects extremely difficult at best. The cross-plotting technique offers, however, a way of assessing the coupled effects.

Figure 26 shows some typical shear-layer trajectories encountered in this and former studies. Since there exist no shockless flows having a discontinuous first spatial derivative of velocity, all trajectories must enter the diagram from the abscissa if considered far enough upstream. (It might be noted, in passing, that the negative K part of the plane is not unpopulated, and that the negative R_{δ_2} part of the plane contains the interesting wall-jets treated by Escudier[36].) It is an interesting exercise to try to visualize the flow required to produce an arbitrary trajectory. It quickly becomes clear that the upper right part of the positive-positive

quadrant is difficult of approach, requiring ever larger flow devices operating at ever lower characteristic densities, once the practical limits of (du /dx) have been realised. These latter are set by the tendency of a converging flow to accommodate a rapid change in area ratio through formation of an extended separation zone:

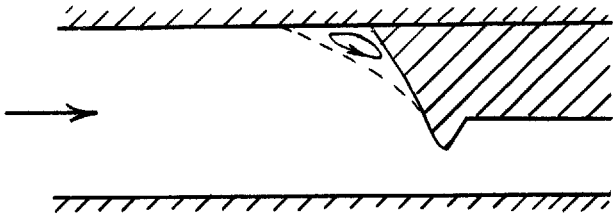

Nozzle B of this study exhibited clearly such a separated zone.

Since x is a cursory parameter for each trajectory, we can readily mark on each trajectory that point at which turbulent-laminar transition, if any, is detected. Figure 27 shows the result of such an operation for each of the four cases of this study. It will be observed that the trajectories for each case form a clearly evolutionary "family", though the fundamental shapes involved are hardly intuitively obvious. Open symbols mark transition points as determined by the methods described in Section A. Solid symbols denote that last transition point encountered in each hierarchy of increasing values of P_o (or equivalently, unit Reynold's number). The solid symbols may thus be regarded as defining the least favorable condition for each case that will in fact lead to transition in the converging portion of the duct. Such points will be called "boundary-points" for purposes of further discussion.

Taken as a group, the trajectories of Figure 27 strongly suggest the existence of a region of the $K - R_{\delta_2}$ plane which is uniquely susceptable to the relaminarisation phenomenon. Figure 28 shows the happy result of combining all the available data, including also that other published data which can be reworked into the required form, namely that of Launder[28] and

Wilson[6]. The observations of Kline et al[22] and the tentative recommendation of Launder have also been indicated for their respective ranges of R_{δ_2}. One observes that the data populates a region to the upper left of a line of boundary points. A line has been fitted through the available points and christened the "transition boundary". A suggested design procedure invoking the properties of this boundary and its associated regions is treated next.

C. Recommended Design Procedure for Laminar-Throat Supersonic Nozzles

1. Adiabatic Wall

The presentation and discussion up to this point admits of the following statements:

(i) There exists a parameter K which is a function of flow-device geometry and upstream conditions alone.

(ii) The development of the quantity R_{δ_2} may be adequately calculated up to the point of turbulent-laminar transition by several methods, one of which is that due to Walz[33, 34].

(iii) Beyond such a transition point, the value predicted for R_{δ_2} is too large.

(iv) There exists a region of the K - R_{δ_2} plane outside of which turbulent-laminar transition has not been observed.

(v) Sustained entry of a shear-layer trajectory into this region results in turbulent-laminar transition.

On the basis of the available evidence, it is difficult to be more precise about the units in which "sustained entry" is to be measured. As a very tentative number, however, it would seem that residence over the boundary for $\Delta x > 20\ \bar{\delta}_2$ is likely to ensure laminarisation of the shear layer. It should be noted in this regard that the effect is not a discontinuity in any sense. The effect of K on the supression of turbulence

production is monotonic in $0 \lesssim K \lesssim 3.5 \times 10^{-6}$ (Kline[22]), and the effects on departure of the velocity profiles from the logarithmic law of the wall are similarly continuous, with effects being clear long before the jump in H_{12} (Launder[27, 28]). The position of the recommended transition-boundary is simply a consequence of the transition marker chosen. No difficulty need, however, arise providing due care is taken to maintain a consistent approach to the question of prediction.

In the light of these observations, therefore, the following steps taken at the basic design stage of an adiabatic-wall nozzle seem likely to ensure an effectively laminar flow in the shear layer at the throat or before:

(a) Using conventional potential-flow theory, compute the near-wall free-stream flow, and obtain, in particular $K = K(x)$ for each nozzle profile of interest.

(b) Estimate as accurately as possible, from the known flow conditions upstream of the nozzle, those properties of the boundary layer necessary to initiate a computation from a point near to the entrance of the nozzle. Any calculation scheme capable of reasonably accurate prediction of $R_{\delta_2} = R_{\delta_2}(x)$ may be used. The method of Walz discussed in Chapter III is one such method.

(c) Plot K vs. R_{δ_2} trajectories for each nozzle and shear-layer combination of interest and observe the relation of these to the transition boundary of Figure 28. At this point it should be clear which of the design parameters need be changed to ensure a sustained entry of a trajectory into the laminarising region. Ensure that the value of x at which this occurs is as far upstream of the throat as possible. Note that the predicted value of δ_2 is likely to be too high after the boundary has been crossed.

NB. It may well be impossible to secure a turbulent-laminar transition in subsonic flow for large, high-density devices.

2. More General Cases

Our detailed, quantitative information is essentially limited to the case treated above, viz. the flow of non-reacting, semi-perfect gases in the shear layer on smooth adiabatic walls, with reasonably small free-stream turbulence. One might, however, expect the following trends to apply, judging from the body of literature surveyed in Chapter I:

(i) In the case of wall-cooling, the transition boundary of Figure 28 will be displaced to lower K and higher R_{δ_2}. Thus the design procedure of part 1 of this section is clearly conservative for this case.

(ii) The reverse is true for hot-wall boundary layers or for boundary layers having internal energy addition by any means, including chemical reaction.

(iii) The rough-wall case is less favorable for laminarisation.

(iv) The effect of wall curvature on the laminarisation phenomenon is probably additive, i.e. the convex-wall case is more favorable than the concave-wall case.

D. General Discussion

The use of the shape-factor change as an indicator for turbulent-laminar transition appears to be reliable and reproducible. Its use in further research into the phenomenon is to be recommended.

In view of the reservations expressed in Appendix I about the procedure used for correction of sublayer-fence readings for severe pressure-gradient effects, it is felt that the skin-friction values quoted should be treated with some caution for exact quantitative purposes, especially since these appear to be the first determinations of high-pressure-gradient transitional skin-friction by a quasi-direct method. Since the same correction

procedure has been consistently applied to all cases of this study, it does, however, seem valid to compare trends in the way discussed in part 1 of this section.

There is no apparent reason to doubt the usefulness of the single-sided fence geometry for measurements in very thin, compressible boundary layers in a small pressure-gradient. The universal calibration factors obtained in this study may be considered definitive for want of any other data. In the light of experience with Preston tubes, the calibration is likely to be invalid for fully laminar flows. The use of single-sided fences in this case will, therefore, require a new calibration. Non-adiabatic flows are also excluded from the turbulent calibration obtained in these studies.

It is probable that the profile measurements made in this study were in no case carried out sufficiently far downstream to be in a fully laminarised shear-layer. This was a dual consequence of the extremely thin shear-layers encountered and the appearance of bow-shocks on the probes, rendering further measurements of highly questionable accuracy. We have, however, the previous work of Launder[27,28] as a guide to the characteristics of a fully laminarised shear-layer.

V. CONCLUSIONS AND RECOMMENDATIONS FOR FURTHER STUDY

(i) It has been confirmed that an adiabatic turbulent boundary layer can be caused to enter turbulent-laminar transition for sufficiently low values of momentum thickness Reynold's number (R_{δ_2}) and sufficiently high values of a free-stream acceleration parameter (K).

(ii) Previously published incompressible results have been extended into the ranges of Mach and Reynold's numbers typical of actual engineering devices, viz: $M \approx 1$, $R_{\delta_2} \approx 10^4$.

(iii) It has been found that the behavior of a boundary layer in respect of turbulent-laminar transition may be described by consideration of its trajectory in the $K - R_{\delta_2}$ plane.

(iv) There exists a region of this plane, the boundary of which has been experimentally determined, inside of which turbulent-laminar transition occurs. Turbulent-laminar transition has not been observed outside this region.

(v) An ab initio design method has been developed which incorporates these findings and is capable of ensuring laminar flow upstream of, and at the throat of, a sufficiently small nozzle. As a by-product, there has resulted a computer program suitable for computation of turbulent or laminar, two-dimensional or axisymmetric, compressible boundary layers, with and without heat-transfer.

(vi) A new instrument of extremely small characteristic height, the single-sided sublayer fence, has been developed for measurements of wall shear-stress in thin, turbulent, adiabatic, compressible boundary layers with or without an imposed axial pressure-gradient.

(vii) A universal calibration function for this class of instrument has been developed.

(viii) Wall shear-stress measurements taken in regions of turbulent-laminar transition show a progressive reduction with streamwise distance when compared to measurements in non-laminarising boundary layers. These are believed to be the first measurements of wall shear-stress in a steep pressure-gradient by a quasi-direct method.

(ix) It is recommended that similar studies be performed in a larger facility to enable delineation of the turbulent-laminar transition boundary for still larger values of R_{δ_2}.

(x) The effects of heat-transfer on turbulent-laminar transition should be further investigated.

(xi) There is a need for more work on shear flows over imbedded small steps, both with and without an imposed pressure-gradient, and in the presence of heat-transfer to or from the wall.

VI. REFERENCES

1. Clauser, F.H., "Turbulent Boundary Layers in Adverse Pressure Gradients," J.A.S., XXI (1954), pp. 91-108.

2. Coles, D., "The Law of the Wake in the Turbulent Boundary Layer," J.Fl.Mech., I (1956), pp. 191-226.

3. Coles, D., The Turbulent Boundary Layer in a Compressible Fluid, Project RAND Report, R-403-PR (September 1962).

4. Crocco, L., "Transformation of the Compressible Turbulent Boundary Layer with Heat Exchange," AIAA Journal, I (1963), pp. 2723-2731.

5. Wilson, D.G. and J.A. Pope, "Convective Heat Transfer to Gas Turbine Blades," Proc. Inst. Mech. Engineers (1954).

6. Wilson, D.G., "Equilibrium Turbulent Boundary Layers in Favorable Pressure Gradients," (Cambridge, Massachusetts: Harvard University Division of Engineering and Applied Science, January 1957).

7. Sternberg, J., Transition from a Turbulent to a Laminar Boundary Layer, Ballistics Research Laboratory Report, No. 906 (May 1954).

8. Sergienko, A.H. and V.K. Gretsov, "Transition from a Turbulent into a Laminar Boundary Layer," S. S. Doklady, IV, pp. 275-276.

9. Hawthorne, W.R., On the Theory of Shear Flow, M.I.T. Gas Turbine Laboratory Report, No. 88 (October 1966). [See also Report No. 93 (1968) for addendum.]

10. Kutateladze, S.S. and A.J. Leont'ev, Turbulent Boundary Layers in Compressible Gases (London: Edward Arnold, 1964).

11. Senoo, Y., The Boundary Layer on the End Wall of a Turbine Nozzle Cascade, A.S.M.E. Paper, No. A-172 (1957).

12. Bartz, D.R., "A Simple Equation for Rapid Estimation of Rocket Nozzle Convective Heat Transfer Coefficients," Jet Propulsion, XXVII (January 1957), p. 49.

13. Neumann, H.E. and P.J. Bettinger, A Comparitive Analysis of Convective Heat Transfer in a Nuclear Rocket Nozzle, NASA Report, TN D-1742 (1963).

14. Fortini, A. and R.C. Ehlers, A Comparison of Experimental to Predicted Heat Transfer in a Bell Nozzle with Upstream Flow Disturbances, NASA Report, TN D-1473 (1963).

15. Welsh, W.E. and A.B. Witte, A Comparison of Analytical and Experimental Local Heat Fluxes in Liquid Propellant Rocket Thrust Chambers, J.P.L. Report, TR32-43 (1961).

16. Liebert, C.H. and R.C. Ehlers, Determination of Local Experimental Heat Transfer Coefficients on Combustion Side of an Ammonia-Oxygen Rocket, NASA Report, TN D-1048 (1961).

17. Preston, J.H., "The Minimum Reynolds Number for a Turbulent Boundary Layer and the Selection of a Transition Device," J.Fl.Mech., III (1958), p. 373.

18. Back, L.H., P.F. Massier and R.F. Cuffel, "Flow Phenomena and Convective Heat Transfer in a Conical Supersonic Nozzle," J. Spacecraft Rockets, IV (1967), pp. 1040-47.

19. Back, L.H., P.F. Massier and R.F. Cuffel, "Some Observations on Reduction of Turbulent Boundary Layer Heat Transfer in Nozzles," AIAA Journal, IV (1966), pp. 2226-29.

20. Back, L.H., P.F. Massier and R.F. Cuffel, "Effect of Inlet Boundary Layer Thickness and Structure on Heat Transfer in a Supersonic Nozzle," J. Spacecraft Rockets, V (1968), p. 121.

21. Schraub, F.A. and S.J. Kline, Department of Mechanical Engineering Report MD-12, Stanford University (Stanford, California).

22. Kline, S.J. et al., "The Structure of Turbulent Boundary Layers," J. Fluid Mechanics, XXX (1967), pp. 741-773.

23. Moretti, P.M. and W.D. Kays, "Heat Transfer to a Turbulent Boundary Layer with Varying Free-stream Velocity and Varying Surface Temperature - an Experimental Study," Int. J. Heat and Mass Transfer, VIII (1965), p. 1187.

24. O'Brien, R.L., Laminarisation of Nozzle Wall Boundary Layers as a Means of Reducing Heat Flux, AFRPL-TR-65-40 (February 1965).

25. McLafferty, G.H., Criteria for Laminar Flow in the Throats of Rocket Exhausts, United Aircraft Research Laboratories Report, A-110088-1 (February 1962).

26. Keilbach, J.R., Experimental Evaluation of a Scheme for Reducing Rocket Nozzle Heat Flux, United Aircraft Research Laboratories Report, UAC-B42 (March 1963).

27. Launder, B.E., The Turbulent Boundary Layer in a Strongly Negative Pressure Gradient, M.I.T. Gas Turbine Laboratory Report, No. 71 (1963).

28. Launder, B.E., Laminarisation of the Turbulent Boundary Layer by Acceleration, M.I.T. Gas Turbine Laboratory Report, No. 77 (1964).

29. Deich, M.E. and L. Ya. Lazarev, Study of the Transition of a Turbulent Boundary Layer Into a Laminar One, Johns Hopkins University, A.P.L. Bulletin, TG230-T470 (March 1966). [translation of Исследование перехода турьулентного пограничного слоя в ламинарный, Инженерно-Физический Журнал, том 7 по.4]

30. Deich, M.E. et al., Teploenergetika, XII (1954).

31. Hopkins, E.J. and E.R. Keener, Study of Surface Pitots for Measuring Turbulent Skin Friction at Supersonic Mach Numbers - Adiabatic Wall, NASA Report, TN D-3478 (1966).

32. Patel, V.C., "Calibration of the Preston Tube and Limitations on its Use in Pressure Gradients," J. Fluid Mechanics, XXIII (1965), pp.185-208.

33. Walz, A., "Ueber Fortschritte in Näherungstheorie und Praxis der Berechnung kompressibler laminarer und turbulenter Grenschichten mit Wärmeübergang," Z. Flugwissenschaft, XIII (1965), Heft 3, p. 89.

34. Walz, A., Strömungs- und Temperaturgrenzshichten, Braun Verlag, Karlsruhe. [Also to be published in English translation by the M.I.T. Press.]

35. Fernholz, H.H., "A Calculation Method for the Compressible Turbulent Boundary-layer with Zero Pressure Gradient, with and without Heat-transfer," to be published.

36. Escudier, M.P., "The Turbulent Incompressible Hydrodynamic Boundary Layer," (Doctoral dissertation, Imperial College of Science and Technology, London, October 1967).

37. Wisniewski, R.J., "Recent Studies on the Effect of Cooling on Boundary-Layer Transition at MACH4," J. Aerospace Science, XXVIII (March 1961) p. 250.

38. Jack, J.R., R.J. Wisniewski and N.S. Diaconis, Effect of Extreme Surface Cooling on Boundary-Layer Transition, NACA TN 4094 (1957).

39. Romanenko, P.N., A.J. Leont'ev and A.N. Oblivin, Investigation of Drag and Heat Transfer During Air Motion in Divergent and Convergent Nozzles, NASA Report, TT F-11,221 (1967). [translation of "Исследование Сопротивления и Теплообмена при Движении Воздуха в Дифузорах и Конфузорах," Общие вопроси Теплообмена (Москва, 1963), пп. 349-360.]

40. Preston, J.H., "The Determination of Turbulent Skin Friction by Means of Pitot Tubes," J. Royal Aero. Society, LVIII No. 109.

41. Staff of the Aerodynamics Division of the N.P.L., On the Measurement of Local Surface Friction on a Flat Plate by Means of Preston Tubes, Aero. Res. Council, R.&M. No. 3185 (1958).

42. Trilling, L. and R.J. Häkkinen, "The Calibration of the Stanton Tube as a Skin-friction Meter," from 50 Jahre Grenshichtforschung (Braunschweig: Friedr. Vieweg und Sohn), p. 201.

43. Sommer, S.C. and B.J. Short, Free-flight Measurements of Turbulent Boundary-layer Skin-friction in the Presence of Severe Aerodynamic Heating at Mach Numbers from 2.8 to 7.0, NACA Report TN3391 (1955).

44. Gadd, G.E., A Note on the Theory of the Stanton Tube, Aero. Res. Council R. & M. No. 3147 (1958).

45. Thom, A., The Flow at the Mouth of a Stanton Tube, Aero. Res. Council R. & M. No. 2984 (1952).

46. Hildebrand, F.B., Introduction to Numerical Analysis (New York: McGraw-Hill, 1956).

47. Van Driest, E.R., "Convective Heat Transfer in Gases," Vol.V, Section F, p. 382, of High Speed Aerodynamics and Jet Propulsion, C.C.Lin, ed. (Princeton, New Jersey: Princeton University Press, 1959).

48. Thompson, B.G.J., A Critical Review of Existing Methods of Calculating the Turbulent Boundary Layer, Aero. Res. Council R. & M. No. 3447 (1967).

49. Spalding, D.B., "Theories of the Turbulent Boundary Layer," Applied Mechanics Reviews, XX No.8 (1967), pp. 735-740.

50. Moses, H.L., The Behavior of Turbulent Boundary Layers in Adverse Pressure Gradients, M.I.T. Gas Turbine Laboratory Report, No. 73 (January 1964).

51. Taylor, G.I., "Measurements with a Half-pitot Tube," Roy. Soc. Proc. A, CLXVI (1938), pp. 476-481.

52. Oates, G.C., Ph.D. Thesis, California Institute of Technology, 1959.

53. Patankar, S.V. and D.B. Spalding, "A Finite-difference Procedure for Solving the Boundary-layer Equations for Two-dimensional Flows," Int. J. Heat and Mass Transfer, X (1967),

54. Marble, G. in High Speed Aerodynamics and Jet Propulsion, (Princeton, New Jersey: Princeton University Press, 1959).

55. Mellor, G.L. and D.M. Gibson, "Equilibrium Turbulent Boundary Layers," J. Fluid Mechanics XXIV (1966), p. 225.

56. Fernholz, H.H., Private communication.

57. Taylor, E.S., Dimensional Analysis for Engineers, M.I.T. Gas Turbine Laboratory Memorandum (1967).

58. Mangler, W., Kompressible Grenschichten bei drehsymmetrischer und bei zweidimensionaler Strömung, Laboratoire de Recherches Balistiques et Aérodynamiques, St. Louis (Elsaß), Bericht 7/47, Bd. I (1947).

59. Mellor, G.L., "Equilibrium Turbulent Boundary Layers," AIAA J., II (1964), p. 1650.

60. Rotta, J.C., Turbulent Boundary Layers in Incompressible Flow, Progress in Aero. Science II (London: Pergamon Press, 1962), p. 72.

61. Head, M.R., Entrainment in the Turbulent Boundary Layer, Aero. Res. Council R. & M. No. 3152 (1962).

62. Goldberg, P., Upstream History and Apparent Stress in Turbulent Boundary Layers, M.I.T. Gas Turbine Laboratory Report, No. 85 (May 1966).

63. Smith, D.W. and J.H. Walker, Skin-friction Measurements in Incompressible Flow, NASA Technical Report TR R-26 (1959)

APPENDIX I - THEORY OF THE SKIN-FRICTION FENCE

In 1953, Preston[40] showed that for incompressible turbulent boundary layers, if some form of universal "law of the wall" of form:

$$\frac{u}{u_\tau} = f\left(\frac{u_\tau y}{\nu_\delta}\right) \tag{I-1}$$

was assumed, and if no displacement effects were taken into account, then, from a dynamical similarity analysis for wall-pitots:

$$\frac{\Delta P\ d^2}{4\ \rho_\delta\ \nu_\delta^2} = f_P\left(\frac{\tau_w\ d^2}{4\ \rho_\delta\ \nu_\delta^2}\right) \tag{I-2}$$

He obtained an empirical form for f_P, and was followed by several other workers[32, 41, 42] who also obtained formulations for the incompressible calibration function f_P differing between themselves by up to 15%. In 1966 Hopkins and Keener[31] proposed a correlation method based on (I-2) which dealt highly successfully with flows up to M = 3.4. This requires non-dimensionalisation in the form:

$$f_2(T')\ R_d^2(M_s/M_\delta) = F[f_2(T')R_d\ c_f] \tag{I-3}$$

where

$$f_2(T') \equiv \left(\frac{\mu_\delta}{\mu'}\right)\ \frac{\rho'}{\rho_\delta} \tag{I-4}$$

the prime denoting evaluation of fluid properties at the Sommer and Short[43] reference temperature T' as defined in the notation. The remaining functions requiring definition are:

$$R_d \equiv (\rho_\delta\ u_\delta\ d)/\mu_\delta \tag{I-5}$$

$$M_s \equiv \left(\frac{2\ \Delta P}{\gamma\ P_s}\right)^{1/2} \tag{I-6}$$

It was found that this correlation collapsed all their supersonic Preston and Stanton tube data onto the original Preston incompressible calibration curve with quite astonishing accuracy, leading to substantial identification of the functions f_P and F above. Since the considerations leading to (I-3) are by no means specialised to Preston and Stanton tube geometries, this correlation method was adopted in calibrating the single-sided fences used in this study so as to account adequately for the effects of compressibility.

(I-4) was specialised for air by use of the Sutherland viscosity formula, yielding, with the assumption of an adiabatic wall:

$$T' = T_\delta \ (1 + 0.1142 \ M_\delta^2) \tag{I-7}$$

$$f_2(T') = \left(\frac{T' + 198.6}{T_\delta + 198.6}\right)^2 (1 + 0.1142 \ M_\delta^2)^{-4} \tag{I-8}$$

In 1965 Patel[32] discussed the application of wall pitots to shear measurements in pressure-gradients. He indicated that the sublayer fence was far less subject to error than Preston or Stanton tubes and presented a first-order analysis for the effect of pressure-gradient on fence readings. This may be rederived and further elaborated in a way relevant to the needs of the present study:

$$\tau \approx \rho_w \ \nu_w \ \frac{\partial u}{\partial y} \tag{I-9}$$

which, with the boundary condition at the wall:

$$\frac{\partial \tau}{\partial y} = \frac{dP}{dx} + \text{h.o.t.} \tag{I-10}$$

implies, after differentiating with respect to y:

$$\frac{d^2 \ u}{d \ y^2} = \frac{1}{\mu_w} \frac{dP}{dx} \tag{I-11}$$

This has the solution

$$u = \frac{\tau_w}{\mu_w} y + \frac{1}{2\mu_w} \left(\frac{dP}{dx}\right) y^2 \qquad \text{(I-12)}$$

This gives an estimate of the sign and magnitude of the curvature induced in the sublayer velocity profile by the imposed pressure gradient.

If we now assume, not unreasonably, that ΔP depends essentially on the momentum flux entering the region of influence of the fence, we can define a mean:

$$\overline{u^2} = \frac{1}{d} \int_o^d u^2 \, dy \qquad \text{(I-13)}$$

and, substituting from (I-12) supra,

$$\overline{u^2} = \frac{1}{d} \int_o^d \left(\frac{\tau_w}{\mu_w} y + \frac{1}{2\mu_w} \frac{dP}{dx} y^2\right) dy \qquad \text{(I-14)}$$

Now, for zero pressure gradient, the second RHS term of (I-12) falls away, and thus we get the comparison:

$$\frac{\Delta P_{dP/dx \neq 0}}{\Delta P_{dP/dx = 0}} = \frac{\int_o^d \left(\frac{\tau_w}{\mu_w} y + \frac{1}{2\mu_w} \frac{dP}{dx} y^2\right) dy}{\int_o^d \left(\frac{\tau_w}{\mu_w} y\right) dy}$$

$$= \left[1 + \frac{3}{4} \frac{d}{\tau_w} \frac{dP}{dx} + \frac{3}{4} \left(\frac{d}{\tau_w}\right)^2 \left(\frac{dP}{dx}\right)^2\right] \qquad \text{(I-15)}$$

Comparing surface-pitot data of many workers, Patel found that Reynold's number variation could be accounted for by writing

$$P = a\tau_w^{\,b} \qquad \text{(I-16)}$$

where $$b = b(R_d) \qquad \text{(I-17)}$$

and $$a = a\,(\rho_w,\ \nu_w,\ d) \qquad \text{(I-18)}$$

Experimental values of b for various geometries varied between 1 and 1.67.

The exponent b was determined as 1.31 for the data of the present study as described in Chapter II Section B.

Thus, finally, combining (I-16) and (I-15),

$$\Delta P_{\frac{dP}{dx}\neq 0} = \Delta P_{\frac{dP}{dx}=0} \left[1 + \frac{3}{4}\left(\frac{d}{\tau_w}\right)\left(\frac{dP}{dx}\right) + \frac{3}{4}\left(\frac{d}{\tau_w}\right)^2\left(\frac{dP}{dx}\right)^2\right]^{1.31} \qquad \text{(I-19)}$$

(I-19) thus allows the relation of a measurement made in a pressure gradient to a calibration made in a zero pressure gradient flow, although an iterative process is required, since the calibration formula and (I-19) both involve τ_w. Convergence is, however, rapid. Thus (I-19) taken in conjunction with the existence of a pre-determined F in (I-3) allows the interpretation of a sublayer fence measurement at arbitrary Mach number and pressure gradient. The machine realization of this procedure is treated in the following Appendix. See also Figure 30.

It must be realized that all of the above is merely a highly simplified model of an exceedingly complex flow-field involving separation and re-attachment with unsteady, eddying flow. The calibration procedure is to be defended in the last analysis by empiricism alone. The interpretation procedure rests on no more than a plausible foundation especially for fences extending substantially outside the "sublayer", and, this being so, must share the limbo of all hypotheses, standing until disproven or superceded.

APPENDIX II - FORTRAN IV PROGRAMS TO CALIBRATE AND INTERPRET SKIN FRICTION FENCE READINGS.

Program CALIBRATE is used to reduce the calibration data to a particular form of (I-3), viz.:

$$F_R = a_1 + a_2 \log_{10} F_L + a_3 (\log_{10} F_L)^2$$

or

$$F_R = b_1 + b_2 \log_{10} F_L \qquad \text{(II-1)}$$

where F_R is the RHS and F_L the LHS of (I-3).

The notation used in the program is consistent with this report.

Input quantities are:

AA, DD(J)	= d, the actual fence height (in inches)
NOR	integer label of the experiment run
PZERO	= P_o (in inches of mercury)
P	= static pressure (in inches of mercury)
TZERO	= T_o (in ^{o}R)
FACT	correction factor - $(T_o/T_{o\ std})\ (P_{o\ std}/P_o)$
NFENCE	integer fence label
DELP	= fence differential pressure reading ΔP (in mm. water)
DEL2	= δ_2 (in inches)

The program will print out and punch onto cards the coefficients of (II-1), and produce machine plots of the data points and curve-fits. Curve fitting is done by subroutine LSFIT using standard numerical techniques [46], and the relations of Fernholz [35] which are treated in Appendix VIII. Note that the coefficients associated with label numbers 29 and 30 are the

"universal" calibration, obtained by two and three term curve-fits to all the data of all the fences. See also Figure 29.

Program INTERPRET requires as input the deck of coefficients produced by CALIBRATE and some additional information about the readings to be interpreted:

A,B	array of coefficients for each fence as implied by (II-1)
H	fence heights (in inches)
NR	integer label of experiment run
NDATA	number of input values from that run which are to be interpreted
PZERO,TZERO	P_o, T_o, the actual values of the run (in "Hg and $^\circ$R)
PSTD, TSTD	= "standard values" of experiment run (in "Hg and $^\circ$R)
DELP	= fence reading (in mm. water)
N	= integer fence label
PR	local free-stream pressure ratio (P_{static}/P_o)
GRAD	= local pressure gradient, $\left\lvert \frac{d(P/P_o)}{dx} \right\rvert$ (in inches^{-1})

The program reverses the procedure of (II-1) and invokes the iterative pressure-gradient correction procedure described in Appendix I. Uncorrected and corrected c_f values are printed out, for two- and three-term calibration relations both of each individual fence, and the "universal" calibration. The notation is again consistent with this report. See also Figure 30.

```
C       PROGRAM CALIBRATE

      DIMENSION DD(28),XX(532),YY(532),X(19),Y(19),XA(532),YA(532)
     1 ,XAL(532),YAL(532),XL(19),YL(19),C(11),E(2),Q(2),R(100),S(100)
     2 ,SL(100)
      DIMENSION XLABEL(2),YLABEL(2)
      DATA XLABEL,YLABEL/' LOG FR ',' LOG FL '/
      CALL NEWPLT ('M5155','4862','WHITE ','BLACK')
      DO 39 J=1,28
      READ 40, AA
      DD(J) = AA
39    CONTINUE
      K = 1
      DO 200 JJ=1,19
44    CONTINUE
      READ 11, NOR
      READ 22, PZERO,P,TZERO,FACT
      DO 200 II=1,28
      NFENCE = II
      D = DD(II)
      DELP = FACT*DELP
      READ 22, DELP,DEL2
      D = D/12.0
      DEL2 = DEL2/12.0
      ACHM = (5.0*((PZERO/P)**0.2857 - 1.0))**0.5
      ACHMS = (5.0*(((P+DELP/345.18)/P)**0.2857 - 1.0))**0.5
      ROZERO = 1.32595*PZERO/TZERO
      RO = ROZERO/(1.0+0.2*ACHM*ACHM)**2.5
      T = TZERO/(1.0+0.2*ACHM*ACHM)
      VIS = 0.00001248*((T/540.0)**1.5)*738.0/(T+198.0)
      U = (12013.9*(TZERO-T))**0.5
      RD = RO*U*D/VIS
      TP = TZERO*(1.0+0.1142*ACHM*ACHM)
      F2 = ((TP+198.6)/(TZERO+198.6))**2.0*(1.0+0.1142*ACHM*ACHM)**
     1 (-4.0)
C     NOW INVOKE FERNHOLZ CF PROCEDURE
      NN = 0
      R1 = (1.0 + 0.176*ACHM*ACHM)**(-1.0)
      H32S = 1.80 + 0.0072*ACHM
      I = 0
      RDEL2 = RO*U*DEL2/VIS
      IF ( NN ) 1,1,2
1     SIGS = 1.001
      NN = NN + 1
2     CC = 0.01015/(RDEL2*SIGS)**0.15 + 0.786/(RDEL2*SIGS)
      H12 = (1.0 - ((0.5*CC)**0.5)*(7.506-0.08773*ALOG(RDEL2*SIGS)))
     1 **(-1.0)
      H12S = H12 + 0.4*ACHM*ACHM
      RAT = (H12S-0.176*ACHM*ACHM*H32S)/H12
100   SIGS = RAT**0.725
      I = I + 1
      IF (I-3) 3,4,4
3     GO TO 2
4     CF = R1*SIGS*CC
      FL = F2*RD*RD*(ACHMS/ACHM)**2.0
      FR = F2*RD*RD*CF
      YY(K) = FL
      XX(K) = FR
      K = K+1
```

```
200   CONTINUE
      JK = 0
      PRINT 302
      DO 300 KN=1,28
      NN = KN-1
      DO 3002 KM = 1,19
      JK = JK+1
      NJ = 1+(KM-1)*28 + NN
      X(KM) =XX(NJ)
      Y(KM) = YY(NJ)
      XL(KM) = ALOG10(XX(NJ))
      YL(KM) = ALOG10(YY(NJ))
      XA(JK) = XX(NJ)
      YA(JK) = YY(NJ)
      XAL(JK) = ALOG10(XX(NJ))
      YAL(JK) = ALOG10(YY(NJ))
3002  CONTINUE
      PRINT 301, KN
      PRINT 304, (XL(KM), KM=1,19)
      PRINT 304, (YL(KM), KM=1,19)
      IF (KN-28) 55,55,56
55    E(1) = 1.0
      Q(1) = 2.0
      E(2) = 6.0
      Q(2) = 7.0
56    CONTINUE
C     VALUE OF M DETERMINES TYPE OF FIT
      M = 1
      DO 54 J=1,11
54    C(J) = 0.0
      CALL LSFIT(YL,XL,C,19,2,M)
      PRINT 304, (C(I), I=1,2)
      C1 = C(1)
      C2 = C(2)
      PUNCH 306, C1,C2,KN
      CALL LSFIT(YL,XL,C,19,3,M)
      PRINT 304, (C(I), I=1,3)
      PUNCH 305, C(1),C(2),C(3),KN
      DO 890 K=1,100
      R(K) = 0.0
      SL(K) = 0.0
890   S(K) = 0.0
      DO 880 J=1,70
      R(J) = 2.1 + 0.1*J
      SL(J) = C1 + C2*R(J)
880   S(J) = C(1)+C(2)*R(J)+C(3)*R(J)*R(J)
      CALL PICTUR(10.,5.,XLABEL,-8,YLABEL,-8,E,Q,-2,0.1,-1,
     1 XL,YL,-19,0.1,-1,SL,R,45,0.,0,S,R,45,0.,0)
300   CONTINUE
      PRINT 304, (XAL(JK), JK=1,532)
      PRINT 304, (YAL(JK), JK=1,532)
      DO 17 L=2,5
      CALL LSFIT(YAL,XAL,C,532,L,M)
      PRINT 304, (C(I), I=1,L)
      IF (L-2) 70,70,17
70    C1 = C(1)
      C2 = C(2)
```

```
      KN = 29
      PUNCH 306, C1,C2,KN
17     CONTINUE
      CALL LSFIT(YAL,XAL,C,532,3,M)
      KN = 30
      PUNCH 305, C(1),C(2),C(3),KN
      DO 89 K=1,100
      R(K) = 0.0
      SL(K) = 0.0
89    S(K) = 0.0
      DO 88 J=1,70
      R(J) = 2.1 + 0.1*J
      SL(J) = C1 + C2*R(J)
88    S(J) = C(1)+C(2)*R(J)+C(3)*R(J)*R(J)
      PRINT 304, R
      PRINT 304, S
      PRINT 304, SL
      PRINT 307, M
C     N.B. R IS THE 'Y AXIS' AND S THE 'X AXIS'
C     N.B. Q IS THE 'Y AXIS' AND E THE 'X AXIS'
      CALL PICTUR(10C,5.,XLABEL,-8,YLABEL,-8,E,Q,-2,0.06,-1,
     1 XAL,YAL,-532,0.06,-1,SL,R,45,0.,0)
      CALL ENDPLT
40    FORMAT (F10.5)
151   FORMAT (25H1  FENCE HEIGHTS (INCHES)///)
12    FORMAT (36H1   SUBLAYER FENCE CALIBRATION DATA /  )
11    FORMAT (I3)
111   FORMAT  (11H RUN NO. K-,I3/ )
14    FORMAT (30H   FENCE       FL           FR / )
22    FORMAT (F12.6)
13    FORMAT (/I7,3X,2F12.0 )
15    FORMAT (9F12.5)
302   FORMAT (9H1WEED-OUT//)
47    FORMAT (10F10.0)
301   FORMAT (//15H  FENCE NUMBER ,I3/)
303   FORMAT (10F10.0)
9     FORMAT (2F12.4)
304   FORMAT (10F10.5)
305   FORMAT (3F20.10,9X,I3)
306   FORMAT (2F20.10,29X,I3)
307    FORMAT (//22H ***NOTA BENE*** M IS ,I1//)
      CALL EXIT
      STOP
      END
```

```
      SUBROUTINE LSFIT(X,Y,C,N,L,M)
C
C     IF M IS 1, SUBROUTINE GIVES (L-1)TH ORDER CURVE-FIT TO MINIMISE THE
C     SUM OF THE SQUARES OF THE ABSOLUTE ERRORS.
C     IF M IS 0, SUBROUTINE GIVES (L-1)TH ORDER CURVE-FIT TO MINIMISE THE
C     SUM OF SQUARES OF THE ERRORS RELATIVE TO THE MAGNITUDE OF THE DATA
C     MAXIMUM VALUE OF L IS 10
C     N IS THE NO. OF DATA PTS. TO BE FITTED, ARR. IN ARRAYS X AND Y
C     C IS THE ARRAY OF COEFFICIENTS OF THE RESULTING POLYNOMIAL,
C     THAT IS  Y = C(1) + C(2)*X + C(3)*X**2 + C(4)*X**3 + ..........
C
C
      DIMENSION X(600),Y(600),C(11),A(11,11),B(11),R(11)
      DO 1 I = 1,11
      B(I) = 0.
      DO 1  J = 1,11
1     A(I,J) = 0.0
      L1 = L+1
      DO 3 I = L1,11
3     A(I,I) = 1.
      DO 2 ID = 1,N
      IF (M) 5,9,10
9     WT = Y(ID)
      GO TO 11
10    WT = 1.0
11    DO 8 I=1,L
8     R(I) = X(ID)**(I-1)
C     R(I) ARE THE FUNCTIONS AS REQD. FOR FIT, IF NOT A POLYNOMIAL.
      DO 2 I = 1,L
      B(I) = B(I) + R(I)*Y(ID)/WT
      DO 2 J=1,L
2     A(I,J) = A(I,J) + R(I)*R(J)/WT
      CALL SIMQ(A,B,11,KS)
      IF (KS) 6,6,5
5     PRINT 7
7     FORMAT (18H NO SOLN IN LSFIT )
      RETURN
6     DO 4 I=1,L
4     C(I) = B(I)
      RETURN
      END
```

```
C       PROGRAM INTERPRET
C
C
        DIMENSION A(3,30),B(2,28),H(28)
        READ 13, A
        READ 14, B
        READ 4, H
        DO 5 K=1,28
5       H(K) = H(K)/12.0
10      READ 3, NR,NDATA
        READ 2, PZERO,TZERO,PSTD,TSTD
        PRINT 9, NR
        DO 6 L=1,NDATA
        READ 7, DELP,N,PR,GRAD
        GRAD = -GRAD*PZERO*848.72
        P = PZERO*PR
        DELP = DELP*(PSTD/PZERO)*(TZERO/TSTD)
        CONST = DELP
        M = 0
        KL = 0
        D = H(N)
        ACHM = (5.0*((PZERO/P)**0.2857 - 1.0))**0.5
1       ACHMS = (5.0*(((P+DELP/345.18)/P)**0.2857 - 1.0))**0.5
        ROZERO = 1.32595*PZERO/TZERO
        RO = ROZERO/(1.0+0.2*ACHM*ACHM)**2.5
        T = TZERO/(1.0+0.2*ACHM*ACHM)
        TE = T*(1.0+0.176*ACHM*ACHM)
        VISW = 0.00001248*((TE/540.)**1.5)*738./(T+198.)
        ROW = RO*TE/T
        VIS = 0.00001248*((T/540.0)**1.5)*738.0/(T+198.0)
        U = (12013.9*(TZERO-T))**0.5
        RD = RO*U*D/VIS
        TP = TZERO*(1.0+0.1142*ACHM*ACHM)
        F2 = ((TP+198.6)/(TZERO+198.6))**2.0*(1.0+0.1142*ACHM*ACHM)**
      1 (-4.0)
        FL = F2*RD*RD*(ACHMS/ACHM)**2.0
        FLL = ALOG10(FL)
        DELPL = ALOG10(DELP)
        FRL1= A(1,N)+A(2,N)*ALOG10(FL)+A(3,N)*ALOG10(FL)*ALOG10(FL)
        FRL2 = B(1,N)+B(2,N)*ALOG10(FL)
        FRL3 = A(1,30)+A(2,30)*ALOG10(FL)+A(3,30)*ALOG10(FL)*ALOG10(FL)
        FRL4 = A(1,29)+A(2,29)*ALOG10(FL)
        FR1 = 10.**FRL1
        FR2 = 10.**FRL2
        FR3 = 10.**FRL3
        FR4 = 10.**FRL4
        IF (M) 11,11,12
12      CF5 = FR1/(F2*RD*RD)
        CF6 = FR2/(F2*RD*RD)
        CF7 = FR3/(F2*RD*RD)
        CF8 = FR4/(F2*RD*RD)
        GO TO 15
11      CF1 = FR1/(F2*RD*RD)
        CF2 = FR2/(F2*RD*RD)
        CF3 = FR3/(F2*RD*RD)
        CF4 = FR4/(F2*RD*RD)
        TW = CF4*0.5*RO*U*U/32.17
```

```
      GO TO 18
15    TW = CF8*0.5*RO*U*U/32.17
18    TERM = D/TW*GRAD
      TWL = ALOG10(TW)
      IF (KL) 24,24,16
24    UTAU = (TW*32.17/ROW)**0.5
      DELTA = VISW/(ROW*ROW*UTAU**3.)*GRAD*32.17
      TERD = (DELTA*UTAU*D*ROW/VISW)
      CT = (1.0+0.75*TERM+0.75*TERM*TERM)**1.31
      DELP = CONST/CT
      IF (CT-1.0) 22,23,23
23    KL = 1
      M = M+1
      GO TO 1
22    M = M+1
21    IF (M-6) 1,1,16
16    PRINT 8, N,CF1,CF2,CF3,CF4,FLL,DELPL,TWL
      PRINT 17, CF5,CF6,CF7,CF8,DELTA,CT
6     CONTINUE
      GO TO 10
2     FORMAT (4F10.3)
3     FORMAT (2I3)
4     FORMAT (4F10.7)
7     FORMAT (F18.1,I2,2F20.5)
8     FORMAT (I6,F16.6,3F15.6,3X,3F10.2)
9     FORMAT (14H1***RESULTS***,30X,15H RUN NUMBER  D-,I2///76H FENCE NO
     1.     3 TERM IND.     2 TERM IND.     3 TERM UNIV.     2TERM UNIV.
     2              //)
13    FORMAT (3F20.10)
14    FORMAT (2F20.10)
17    FORMAT (7H CORR. ,4F15.6,3X,2F10.6/)
19    FORMAT (7F15.5)
      END
```

APPENDIX III - THEORY OF ASYMMETRIC TWO-DIMENSIONAL CONTRACTION FLOW

A first-order small-perturbation analysis, due to Oates[52] of the potential flow through an asymmetrically convergent channel is briefly summarised below. The solution provided by this analysis is exhibited parametrically in x and y for each of the contraction sections required to form the zero pressure-gradient calibration flows. Since the analysis is linear, the results may be subtracted from each other at each y for any constant x - graphically for the purpose at hand. This allows the determination of that relative position of the two nose-pieces which minimises the distortion of the free-stream flow downstream of the contraction.

Following Marble[54], with the assumption of incompressible, irrotational flow, with the usual stream function (ϕ) notation:

$$\frac{\partial^2\phi}{\partial x^2} + \frac{\partial^2\phi}{\partial y^2} = 0 \qquad \text{(III-1)}$$

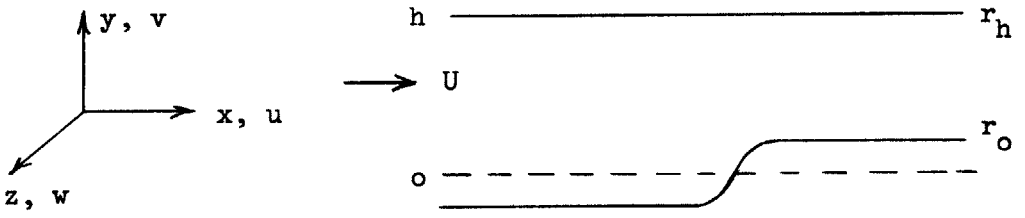

and, differentiating with respect to y:

$$\frac{\partial^2 u}{\partial x^2} + \frac{\partial^2 v}{\partial y^2} = 0 \qquad \text{(III-2)}$$

Now if we are given $r_o = f_o(x)$, the linearised boundary condition then becomes

$$v = 0 \quad \text{at} \quad r = r_h \qquad \text{(III-3)}$$

and introducing the axial velocity U,

$$\frac{v}{U} = \frac{dr_o}{dx} \quad \text{at} \quad r = r_o \tag{III-4}$$

and taking an integral transform by writing

$$\tilde{v}\,(y, k) = \frac{1}{\sqrt{2\pi}} \int_{-\infty}^{\infty} v\,(y, k)\, e^{-ikx}\, dx \tag{III-5}$$

we obtain the transformed equation

$$\frac{d^2\tilde{v}}{dy^2} - (i\,k)^2\, \tilde{v} = 0 \tag{III-6}$$

having boundary conditions

$$\tilde{v}\,(r_h, k) = \frac{1}{\sqrt{2\pi}} \int_{-\infty}^{\infty} v\,(r_h, x)\, e^{-ikx}\, dx \tag{III-7}$$

$$\tilde{v}\,(r_o, k) = \frac{U}{\sqrt{2\pi}} \int_{-\infty}^{\infty} \frac{dr_o}{dx}\, e^{-ikx}\, dx \quad U\, F_o(k) \tag{III-8}$$

where F_o is the transformed shape function.

Now (III-6) has a solution of the form

$$\tilde{v} = A \sin (iky) + B \cos (iky) \tag{III-9}$$

Application of (III-7) and (III-8) and taking $r_o = 0$, we obtain

$$\tilde{v} = U\, F_o(k)\, \frac{\sin [ik\,(r_h - y)]}{\sin ik\, r_h} \tag{III-10}$$

and, formally inverting:

$$\frac{v}{U} = \frac{1}{\sqrt{2\pi}} \int_{-\infty}^{\infty} F_o(k)\, \frac{\sin [ik\,(r_h - y)]}{\sin ik\, r_h}\, e^{ikx}\, dk \tag{III-11}$$

where $$F_o(k) = \frac{1}{\sqrt{2\pi}} \int_{-\infty}^{\infty} \frac{dr_o}{dx}\, e^{-ikx}\, dx \tag{III-12}$$

Now, the shape of the nose-pieces of the channel could be approximated by writing, with the notation implied by the sketch:

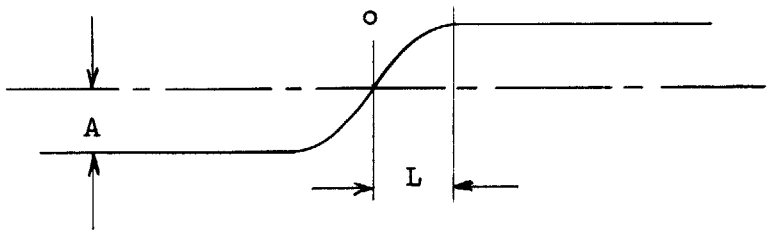

$$r_o = A \sin\left(\frac{\pi x}{2L}\right) , \quad -L \leq x \leq L \tag{III-13}$$

hence
$$\frac{dr_o}{dx} = \frac{\pi A}{2L} \cos\frac{\pi x}{2L} , \quad -L \leq x \leq L \tag{III-14}$$

$$= 0 , \quad |L| < x \tag{III-15}$$

this yields from (III-12)

$$F_o(k) = \frac{A}{2\sqrt{2\pi}} \left(\frac{\pi}{L}\right)^2 \frac{\cos kL}{\left(\frac{\pi}{2L}\right)^2 - k^2} \tag{III-16}$$

This, with (III-11) and after a contour integration procedure, leads to:

$$\frac{v}{U} = \left(\frac{2A}{r_h}\right) \sum_{n=1}^{\infty} \frac{\cosh \frac{n\pi L}{r_h}}{1 + \left(\frac{2nL}{r_h}\right)^2} \sin\left(\frac{n\pi y}{r_h}\right) e^{-\frac{n\pi x}{r_h}} \tag{III-17}$$

for $x \geq L$

Now, from continuity, the axial velocity follows:

$$u = v - \int \frac{\partial v}{\partial y} \, dx \tag{III-18}$$

and, since from the irrotationality, at $x = \infty$, u/U = constant, putting (III-17) into (III-18) yields for the shape of the axial velocity

distribution at exit from the contraction:

$$\frac{\Delta u}{U} = \left(\frac{2A}{r_h}\right) \sum_{n=1}^{\infty} \frac{\cosh\left(\frac{n\pi L}{r_h}\right)}{1 + \left(\frac{2nL}{r_h}\right)^2} \cos\left(\frac{n\pi y}{r_h}\right) \; e^{-\frac{n\pi x}{r_h}} \qquad \text{(III-19)}$$

and, since only the fundamental will predominate after one characteristic height or so, this is conveniently simplified to the approximate form:

$$\frac{\Delta u}{U} = \frac{A}{r_h} \frac{\cos \frac{\pi y}{r_h}}{1 + \left(\frac{2L}{r_h}\right)^2} \; e^{-\pi \left(\frac{x-L}{r_h}\right)} \qquad \text{(III-20)}$$

i.e., an axial velocity profile of the form:

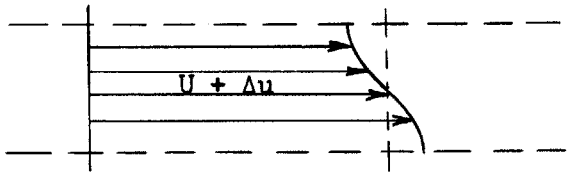

We can now superpose two solutions of the form (III-20) for the situation sketched below:

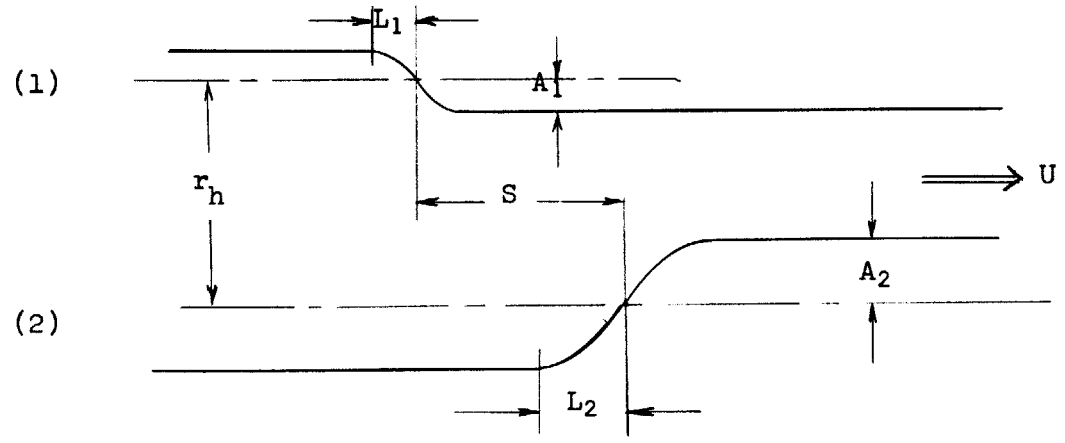

Furthermore, since $S = (x_1 - x_2)$, we can exhibit the quantity

$\left[\left|\left(\frac{\Delta u}{U}\right)_{(1)} - \left(\frac{\Delta u}{U}\right)_{(2)}\right|\right]$ at any x with S as parameter, and thus determine

that value of S which minimises this quantity.

For the purposes of this study, (III-20) was machine-calculated for cases (1) and (2) for several x, and the optimum value of S found by graphical superposition of the solutions.

APPENDIX IV - EXTRACT FROM THE EXPERIMENTAL DATA

TABLES

TABLE 1A - TEST SECTION PARAMETERS - NOZZLE A

x inches	U_δ, ft/sec (P_o=10"Hg.a.) (T_o=515°R)	M_δ	Channel depth inches	Kx10^6		
				P_o=5 T_o=515	10 520	20 525
20	162	.145	10.00	1.52	.71	.36
22	173	.155	10.00	2.88	1.41	.73
24	193	.174	10.00	3.96	1.97	.98
26	222	.200	8.74	4.83	2.52	1.20
28	281	.253	6.34	5.88	3.00	1.50
30	380	.344	4.43	5.06	2.51	1.27
32	521	.477	3.19	4.12	2.11	1.02
34	735	.688	2.42	3.12	1.71	.83
35	843	.801	2.34	2.29	1.21	.60
36	928	.894	2.28	1.50	.73	.38
37	983	.957	2.26	1.24	.60	.31
38	1057	1.044	2.33	2.08	1.06	.53
39	1221	1.252	2.58	3.94	1.99	.98
40	1421	1.546	2.82	3.22	1.64	.82
42	1652	1.970		1.98	1.01	.51
44	1686	2.045				

Sharp-edged geom. throat is at x = 37.75

TABLE 1B - TEST SECTION PARAMETERS - NOZZLE B

x inches	U_δ ft/sec (P_o=10"Hg.a.) (T_o=525°R)	M_δ	Channel depth inches	Kx10^6		
				P_o=5	10	20
				T_o=515	525	530
26	441	.399	10.00	.08	.04	.02
28	443	.401	10.00	.10	.05	.03
30	448	.405	10.00	.17	.08	.04
32	458	.415	10.00	.44	.22	.11
34	475	.431	10.00	.62	.31	.16
35	483	.440	10.00	.75	.37	.18
36	508	.462	10.00	1.51	.75	.40
37	544	.496	9.90	2.03	1.04	.52
38	600	.550	9.05	2.66	1.35	.69
39	685	.634	6.44	3.19	1.66	.82
40	812	.764	3.49	3.60	1.86	.94
41	979	.947	3.02	3.92	1.99	1.00
42	1187	1.200	4.00	3.94	1.98	1.02
43	1388	1.483	4.00	3.81	1.92	.96
44	1573	1.798	4.00	3.96	1.98	.99

Sharp-edged geometric throat is at x = 40.90"

TABLE 1C - TEST SECTION PARAMETERS - NOZZLE C

x inches	U_δ, ft/sec (P_o=10"Hg.a.) (T_o=515°R)	M_δ	Channel depth inches	Kx10^6		
				P_o=5 T_o=515	20 525	50 530
26	144	.130	10.00	.87	.19	.10
28	149	.134	10.00	1.51	.38	.15
30	156	.141	10.00	3.11	.77	.25
31	165	.149	10.00	4.55	1.10	.38
32	180	.162	10.00	5.43	1.43	.53
33	202	.183	10.00	6.18	1.69	.68
34	221	.200	9.14	6.76	1.84	.76
35	255	.231	7.79	7.26	1.93	.80
36	306	.278	6.45	7.39	1.95	.81
37	375	.341	5.11	7.35	1.91	.80
38	477	.437	3.86	7.08	1.80	.76
39	626	.582	2.78	6.47	1.64	.70
40	837	.800	2.22	5.66	1.45	.61
41	1097	1.099	3.23	4.66	1.28	.52
42	1314	1.392	4.00	3.99	1.08	.45
43	1496	1.685	4.00	3.50	.93	.28
44	1637	1.956	4.00	3.10	.84	.20
45	1726	2.157	4.00	2.72	.76	.13

Sharp-edged geom. throat is at x = 40.00

TABLE 2 - SHEAR LAYER MEASUREMENTS - NOZZLE A

	x inches	c_f	R_{δ_2}	H_{12}	H_{12}^*	H_{32}^*
P_o=5"Hg.abs.						
	19.0	.0038	2022	1.281	1.290	1.812
			2080	1.302	1.310	1.806
	23.0		1686	1.275	1.282	1.816
	24.0	.0057				
	26.0		1211	1.209	1.225	1.876
	28.0	.0068	944	1.141	1.167	1.896
	30.0		594	1.292	1.339	1.898
	32.0	.0051				
	32.8		420	1.471	1.601	1.848
	35.0	.0042	213	2.110	2.446	1.696
	38.0	.0039				
	41.0	.0038				
P_o=10						
	19.0	.0033	2830	1.251	1.260	1.825
				1.274	1.282	1.824
	23.0		2287	1.271	1.259	1.825
	24.0	.0047				
	26.0		1573	1.239	1.255	1.890
	28.0	.0061	1038	1.249	1.275	1.891
		.0056				
	30.0		885	1.330	1.377	1.896
	32.0	.0055				
		.0052				
	32.8		580	1.577	1.708	1.840
	35.0	.0047	394	2.026	2.346	1.767
			343	2.058	2.379	1.767
	38.0	.0045				
	41.0					
P_o=15						
	19.0	.0032	3699	1.270	1.279	1.824
	23.0		2981	1.261	1.270	1.827
	24.0	.0040				
	26.0		2010	1.234	1.251	1.882
	28.0	.0046	1546	1.194	1.220	1.879
			1485	1.190	1.216	1.891
	30.0		1217	1.275	1.323	1.896
	32.0	.0051				
	32.8		903	1.241	1.369	1.837
	35.0	.0054	724	1.785	2.092	1.795
	38.0	.0052				
	41.0	.0053				

	x inches	c_f	R_{δ_2}	H_{12}	H_{12}^*	H_{32}^*
P_o=20						
	19.0	.0030	4914	1.289	1.298	1.814
	23.0		4037	1.260	1.249	1.831
	24.0	.0038				
	26.0		3222	1.205	1.221	1.882
	28.0	.0056	1993	1.172	1.198	1.884
			2150	1.162	1.188	1.893
	30.0		1545	1.367	1.415	1.902
	32.0	.0055				
	32.8		1290	1.301	1.430	1.827
	35.0	.0054	1392	1.312	1.441	1.855
	38.0	.0055				
	41.0	.0056				

TABLE 3 - SHEAR LAYER MEASUREMENTS _ NOZZLE B

	x inches	c_f	R_{δ_2}	H_{12}	H_{12}^*	H_{32}^*
P_o=5"Hg.abs.						
	24.0	.0031				
	28.0	.0032	6501	1.429	1.493	1.763
	30.0		6593	1.414	1.469	1.758
	32.0	.0034				
	32.8		6102	1.360	1.420	1.780
	35.0	.0036				
	36.0		4793	1.281	1.384	1.834
	38.0	.0046	2785	1.277	1.370	1.885
	40.1		1289	1.356	1.719	1.913
	41.0	.0049				
P_o=10						
	24.0	.0030				
	28.0	.0030	9522	1.341	1.410	1.784
	30.0		9260	1.326	1.406	1.793
	32.0	.0032				
	32.8		8779	1.302	1.379	1.805
	35.0	.0037				
	36.0		7093	1.234	1.336	1.841
	38.0	.0047	4797	1.204	1.296	1.876
	40.1		2581	1.239	1.373	1.908
	41.0	.0051				
P_o=20						
	24.0	.0028				
	28.0	.0031	16210	1.257	1.323	1.820
	30.0		15800	1.249	1.315	1.818
	32.0	.0032				
	32.8		14840	1.229	1.287	1.833
	35.0	.0038				
	36.0		11120	1.182	1.281	1.857
	38.0	.0042	7525	1.184	1.307	1.896
	40.1		4003	1.159	1.361	1.901
	41.0	.0047				
P_o=30						
	28.0	.0027	21160	1.235	1.302	1.830
	32.8		19870	1.232	1.297	1.831
	36.0		16900	1.148	1.161	1.891
	38.0		12030	1.146	1.172	1.897

TABLE 4 - SHEAR LAYER MEASUREMENTS - NOZZLE C

	x inches	c_f	R_{δ_2}	H_{12}	H_{12}^*	H_{32}^*
P_o=5"Hg.abs						
	19.0	.0050				
	24.0	.0040				
	28.0	.0037	1899	1.250	1.271	1.835
	30.0		1962	1.256	1.275	1.837
	32.0	.0042				
		.0043				
	32.8		1352	1.249	1.269	1.855
	35.0	.0045				
		.0049	751	1.294	1.322	1.850
	36.0		495	1.451	1.486	1.861
	38.0	.0052	180	1.554	1.605	1.859
		.0058	241	1.565	1.616	1.857
	41.0	.0052				
		.0048				
P_o=10						
	19.0	.0055				
	21.9	.0052				
	24.0	.0052				
	25.9	.0050				
		.0054		1.229	1.244	1.845
	28.0	.0054	3261	1.240	1.258	1.835
	29.9	.0056				
		.0054				
	30.0		3024	1.241	1.262	1.838
	32.0	.0056				
	32.8		2127	1.237	1.253	1.869
				1.198	1.210	1.868
	32.9	.0055				
	35.0	.0056	1472	1.275	1.295	1.858
	35.9	.0056				
	36.0		908	1.451	1.481	1.881
	38.0	.0052	450	1.530	1.596	1.872
		.0048				
	38.9	.0050				
	41.0	.0047				
		.0044				
P_o=20						
	19.0	.0051				
	21.9	.0049				
	24.0	.0048				
	25.9	.0048	5561	1.218	1.228	1.844
	28.0	.0049	5449	1.231	1.245	1.820
		.0047				
	29.9	.0045				
	30.0		5008	1.228	1.241	1.849
	32.0	.0050				
	32.8		3109	1.219	1.235	1.833

	x inches	c_f	R_{δ_2}	H_{12}	H_{12}^*	H_{32}^*
	32.9	.0050				
		.0047				
			2459	1.211	1.230	1.859
	35.0	.0052	2397	1.222	1.252	1.852
	35.9	.0052				
	36.0		1763	1.373	1.403	1.855
			991	1.511	1.561	1.884
	38.0	.0051	890	1.532	1.591	1.873
	38.9	.0051				
		.0047				
	41.0	.0041				
P_o=30						
	19.0	.0046				
	21.9	.0036				
	24.0	.0036				
	25.9	.0035				
	28.0	.0035	7120	1.258	1.269	1.819
	29.9	.0045				
	30.0		6850	1.215	1.224	1.841
	32.0	.0045				
		.0043				
				1.204	1.211	1.897
	32.8		5176	1.183	1.198	1.892
	32.9	.0052				
	35.0	.0053	3398	1.212	1.235	1.881
	35.9	.0062				
	36.0		2238	1.231	1.265	1.885
	38.0	.0060	1803	1.250	1.292	1.887
	38.9	.0062				
	41.0	.0065				
		.0067				
P_o=50						
	19.0	.0038				
	21.9	.0031				
	24.0	.0032				
	25.9	.0033	10150	1.215	1.227	1.841
	28.0	.0035	10360	1.246	1.259	1.823
	29.9	.0040				
		.0043				
	30.0		10009	1.240	1.255	1.858
	32.0	.0051				
		.0039				
	32.8		8009	1.192	1.208	1.884
	35.0	.0041	3879	1.227	1.254	1.867
		.0047				
			3605	1.222	1.249	1.878
	36.0		3150	1.259	1.281	1.869
		.0051	2871	1.243	1.268	1.855
	38.0	.0053	2703	1.225	1.251	1.869
	41.0	.0062				
		.0066				

TABLE 5 - SHEAR LAYER MEASUREMENTS - NOZZLE C WITH SPOILER

	x inches	c_f	R_{δ_2}	H_{12}	H_{12}^*	H_{32}^*
P_o=10"Hg.abs.						
	19.0	.0051				
	24.0	.0049				
	28.0	.0049 .0052	4252	1.260	1.276	1.840
	30.0		3850	1.229	1.247	1.842
	32.0	.0053				
	32.8		2363	1.179	1.197	1.851
	35.0	.0058	1598	1.202	1.221	1.879
	36.0		1227	1.262	1.293	1.873
	38.0	.0056	590	1.558	1.645	1.905
	41.0	.0042				
P_o=15						
	19.0	.0046				
	24.0	.0041				
	28.0	.0041	5768	1.221	1.233	1.842
	30.0		5390	1.219	1.236	1.851
	32.0	.0045				
	32.8		3319	1.193	1.216	1.875
	35.0	.0051	1875	1.248	1.276	1.875
	36.0		1487	1.328	1.360	1.875
	38.0	.0050	910	1.571	1.702	1.887
	41.0	.0046				
P_o=20						
	19.0	.0049				
	24.0	.0047				
	28.0	.0048	6978	1.242	1.259	1.831
	30.0		6402	1.209	1.226	1.850
	32.0	.0045				
	32.8		3987	1.183	1.210	1.863
	35.0	.0054	2799	1.190	1.218	1.888
	36.0		2097	1.213	1.238	1.880
	38.0	.0053	1262	1.241	1.292	1.816
	41.0	.0054				

APPENDIX V - FORTRAN IV PROGRAM TO COMPUTE BOUNDARY LAYER DEVELOPMENT ACCORDING TO THE MODIFIED METHOD OF WALZ

This program has been written in such a way as to promote great flexibility of use, while nevertheless taking care of most routine calculations with a minimum of effort. The required input deck takes the following form:

First card: Operations card having 6 integer fields of 5 columns.

ID — An integer > 1 identifying the particular computation to the user.

NUMBER — An integer $0 < n \leq 9$ informing the program what type of boundary layer is under consideration. Table 6 lists the possibilities.

NIM — An integer ≥ 1 giving the number of x stations at which information about the free-stream is given.

NBUG — In the event that a detailed output is required for debugging purposes, this should be 1. For normal use, it should be left blank.

NHW — Can have values -1, 0 or 1. If -1, the Escudier auxiliary relations are used. If 0 (or left blank), the Walz auxiliary relations are used. If 1, the Fernholz relations are used.

ND — Can have values -2, -1, 0 or 1. If -2, free-stream information may be given in terms of (P/P_o) vs. x (see below), and output will be both printed out and punched onto cards. If -1, u_δ vs. x is required as input, and both printed and punched output results. If 0 (or blank)

u_δ vs. x input is required and only printed output results. If 1, (P/P_o) vs. x input is required, and only printed output results.

TABLE 6

Value of NUMBER	Type of Boundary Layer
1	Turb., 2-D, Adiabatic, Zero p.g., Fernholz incompressible aux. relations
2	Lam., Axisymmetric, Spec. Wall Temps.
3	Turb., 2-D, Adiabatic Wall.
4	Lam., 2-D, Adiabatic Wall.
5	Turb., 2-D, Spec. Wall Temps.
6	Lam., 2-D, Spec. Wall Temps.
7	Lam., Axisymm., Adiabatic Wall.
8	Turb., Axisymm., Spec. Wall Temps.
9	Turb., Axisymm., Adiabatic Wall

N.B. if NUMBER = 1, NHW must also be 1.

Second Card: Contains the parameters for the particular gas involved. The usual values for air are in parentheses. It has 4 decimal fields of 10 columns.

GAMMA Ratio of specific heats (1.4)

R Recovery factor (0.88 for turb., 0.86 for lam. b.l.)

RGAS Gas constant, (ft-lb/lb°R), (53.3)

CP Specific heat at constant pressure, (ft-lb/lb), (186)

Third Card: Contains initial values of boundary layer parameters, having 5 decimal fields of 10 columns.

DEL2U1 Value of $(\delta_2)_u$ at first x station, inches

DEL3U1 Value of $(\delta_3)_u$ at first x station, inches

P1 Value of static pressure at first x station, inches of mercury absolute.

TZERO Stagnation temperature of free-stream, °R (absolute).

SPACE Spacing, in inches, of the x stations at which the output is to be printed. The spacing of the input must be some even multiple or sub-multiple of this length.

Fourth and Successive Cards: These contain the free-stream information, one card for each x station. Each card has 4 decimal fields of 10 columns.

XIM(I) The i^{th} ($1 \leq i \leq$ NIM) value of x, in inches, to be given as input. Col. 1-10.

UIM(I) The value of u_δ, in ft/sec, at x_i. In the event that ND is -2 or 1, the value of (P_{static}/P_o) at x_i. Col. 11-20.

TIM(I) The value of T_w, in °R, at x_i. Col. 21-30. In the case of an adiabatic wall, these columns should be left blank.

RIM(I) The value of R, the radius of the flow passage, in inches, at x_i. Col. 31-40. In the case of a two-dimensional boundary layer, these columns should be left blank.

No further cards are required for non-zero pressure-gradient calculations. Thus the input data set for each separate computation has (NIM + 3) cards.

In the case of a zero pressure-gradient calculation, NIM = 1, and a final card, having 1 field of 10 columns, is required at the end of each data set, viz:

PZERO — Free-stream total pressure at x_1, in inches of mercury absolute.

When deciding on the value of NIM required for any given computation, it should be borne in mind that the machine will extrapolate the input between x_i and x_{i+1} by considering it to lie on that unique parabola which may be drawn through the input values of the required quantity at x_i, x_{i+1}, and x_{i+2}. Thus, for accuracy, closer spacing of the input is needed in regions of rapid free-stream changes. This variable spacing must, however, be an even multiple or sub-multiple of SPACE.

Any number of input data decks may be submitted simultaneously. Printout for each case will cover the range x_i to x_j, where $j \equiv NIM - 2$. The program will usually catch the impending numerical disaster associated with the prediction of a separation, and print out an appropriate series of messages. Not all types of disaster can be forseen, however, and unexplained stoppages should be further investigated by invoking the NBUG = 1 option on Card 1.

Typical output, with NBUG = 0 and 1, is shown at the end of the listing.

Exclusive of compilation time, a typical boundary layer calculation takes about 4 seconds on an IBM O/S 360, Mod. 65. The following library functions/subroutines are used (From the IBM Scientific Subroutines Package, Version II):

IFIX	ALOG
ABS	ALOG10
AMAX1	

```
C         WALZ METHOD   MOD 5  MAIN PROGRAM
C
      DIMENSION H(1000),HST(1000),U(1000),Z(1000),XA(1000),RR(1000),
     1 UIM(100),XIM(100),RIM(100),TIM(100),TA(1000),D(100)
     2 ,RN(1000),H12S(1000)
C
      COMMON P1,U1,PZERO,TZERO,UDEL,VISWAL,ACHM,RODEL,THETA,R,RGAS,
     1 GAMMA,NUMBER,ALPHA,BETA,H12,HSTAR,DELRAT,EN,BIGN,NN,NBUG
     2 ,MKS,RDEL2U,RDEL2,DEL12,DEL2,DELTAX,X,NHW,CP,TW
C
C     INITIALISE ARRAYS, INDICES AND TAGS
4     DO 44 I=1,100
      UIM(I) = 0.0
      XIM(I) = 0.0
      TIM(I) = 1.0
44    RIM(I) = 1.0
      NBUG = 0
      NHW = 0
      ND = 0
      NN = 0
      MKS = 0
      MKR = 0
      ID = 0
      J = 1
      MOD = 5
      E = 0.00001
C     READ INITIAL DATA
      READ 1, ID,NUMBER,NIM,NBUG,NHW,ND
      READ 11, GAMMA,R,RGAS,CP
      READ 2, DEL2U1,DEL3U1,P1,TZERO,SPACE
      DO 50 I=1,NIM
50    READ 3,XIM(I),UIM(I),TIM(I),RIM(I)
      IF (ND) 46,451,647
46    IF (ND+1) 647,451,932
647   DO 461 I=1,NIM
      TI = TZERO*UIM(I)**((GAMMA-1.)/GAMMA)
461   UIM(I) = (64.34*GAMMA*RGAS*(TZERO-TI)/(GAMMA-1.))**0.5
451   IF (NBUG) 932,15,16
16    PRINT 17
      PRINT 601, (XIM(I),I=1,NIM)
      PRINT 601, (UIM(I),I=1,NIM)
15    GO TO (7,45,7,7,8,8,9,45,9),NUMBER
7     DO 47 I=1,NIM
      TIM(I) = 1.0
47    RIM(I) = 1.0
      GO TO 45
8     DO 48 I=1,NIM
48    RIM(I) = 1.0
      GO TO 45
9     DO 49 I=1,NIM
49    TIM(I) = 1.0
C     ASSIGN THE STEP SIZE
45    IF (NIM-1) 932,74,75
74    READ 640, K
      GO TO 76
```

```
75    K = IFIX((XIM(NIM-1)-XIM(1))/SPACE)
76    IF (NIM-1) 932,467,468
468   D1 = ABS((UIM(2)-UIM(1))/UIM(1))
      DO 462 I=2,NIM
      D(I) = ABS((UIM(I)-UIM(I-1))/UIM(I-1))
462   D1 = AMAX1(D(I),D1)
      DO 463 I=2,NIM
      D(I) = ABS((UIM(I)-UIM(I-1))/UIM(I-1))+.0001
      IF (D(I)-D1) 463,464,464
464   L = I
      GO TO 465
463   CONTINUE
465   KKB = 2*IFIX((UIM(L)-UIM(L-1))/(UIM(L-1)*0.03))
      IF (KKB-2) 71,72,72
71    KKB = 2
72    GO TO 469
467   DELTAX = SPACE/120.0
      KK = 10
      KKB = 10
      GO TO 73
469   DELTAX = (XIM(L)-XIM(L-1))/(12*KKB)
      IF (DELTAX-SPACE/12.) 648,747,747
747   DELTAX = SPACE /12.
648   KK = IFIX(SPACE/(12.0*DELTAX) + .001)
73    IF (NBUG) 932,18,19
19    PRINT 10, K,D1,L,KKB,KK,DELTAX
18    DO 466 I=1,NIM
      XIM(I) = XIM(I)/12.0
466   RIM(I) = RIM(I)/12.0
      X = XIM(1)
C     CREATE DETAILED DATA ARRAYS
      IF (NIM-1) 932,470,471
470   XY = XIM(1) - DELTAX
      MKK = K*KK+1
      DO 472 I=1,MKK
      XY = XY+DELTAX
      U(I) = UIM(1)
      RR(I) = RIM(1)
      TA(I) = TIM(1)
472   XA(I) = XY
      GO TO 473
471   NIMM = NIM-1
      U(1) = UIM(1)
      XA(1) = XIM(1)
      TA(1) = TIM(1)
      RR(1) = RIM(1)
599   MM = 2
      DO 600 IM = 2,NIMM
      MK = IFIX((XIM(IM)-XIM(IM-1))/DELTAX + .001)
      IF (IM - 2) 932,503,504
503   MKK = MK + 1
      GO TO 505
504   MKK = MM + MK - 1
      IF (MKK-1000) 505,505,506
506   PRINT 507, ID
      GO TO 932
```

```
505   DO 500 I = MM,MKK
      X = X + DELTAX
      XA(I) = X
      Y1 = UIM(IM-1)
      Y2 = UIM(IM)
      Y3 = UIM(IM+1)
      XX1 = XIM(IM-1)
      XX2 = XIM(IM)
      XX3 = XIM(IM+1)
      S1 = RIM(IM-1)
      S2 = RIM(IM)
      S3 = RIM(IM+1)
      T1 = TIM(IM-1)
      T2 = TIM(IM)
      T3 = TIM(IM+1)
      U(I) = Y3*(X-XX1)*(X-XX2)/(XX3-XX1)/(XX3-XX2) + Y2*(X-XX3)*(X-XX1)
     1 /(XX2-XX3)/(XX2-XX1) + Y1*(X-XX2)*(X-XX3)/(XX1-XX2)/(XX1-XX3)
      TA(I)= T3*(X-XX1)*(X-XX2)/(XX3-XX1)/(XX3-XX2) + T2*(X-XX3)*(X-XX1)
     1 /(XX2-XX3)/(XX2-XX1) + T1*(X-XX2)*(X-XX3)/(XX1-XX2)/(XX1-XX3)
      RR(I)= S3*(X-XX1)*(X-XX2)/(XX3-XX1)/(XX3-XX2) + S2*(X-XX3)*(X-XX1)
     1 /(XX2-XX3)/(XX2-XX1) + S1*(X-XX2)*(X-XX3)/(XX1-XX2)/(XX1-XX3)
500   CONTINUE
      MM = MKK + 1
600   CONTINUE
473   IF (NBUG) 932,475,474
474   PRINT 476, MKK,XA(MKK),XA(MKK-1),U(MKK),U(MKK-1),TA(MKK),
     1  TA(MKK-1),RR(MKK),RR(MKK-1)
      PRINT 601, (U(I),I=1,MKK)
475   PZERO = P1*(1.0-((GAMMA-1.0)*UIM(1)*UIM(1))/(2.0*GAMMA*RGAS
     1 *TZERO*32.17))**(-GAMMA/(GAMMA-1.0))
      X = XIM(1)
      DEL2U1 = DEL2U1/12.0
      DEL3U1 = DEL3U1/12.0
      P1 = 70.72622 * P1
      PZERO = 70.72622*PZERO
C     CALCULATE INITIAL VALUES FOR PRINTOUT
121   UU = U(J)
      TW = TA(1)
      U1 = U(1)
      CALL PROPS (J,UU)
      HH = DEL3U1/DEL2U1
      RDEL2U = RODEL*UDEL*DEL2U1/VISWAL
C     GUESS INITIAL VALUE OF 'DELRAT' THEN ITERATE 3 TIMES
      RDEL2 = RDEL2U*0.998
      DO 783 IJK=1,3
      GO TO (78,13,78,13,78,13,13,78,78),NUMBER
13    CALL BLAM (HH)
      GO TO 782
78    CALL TURB (HH)
782   DEL2 = DEL2U1*DELRAT
      RDEL2 = RODEL*UDEL*DEL2/VISWAL
      RN(1) = RDEL2
      H12S(1) = DEL12
      IF (MKS) 783,783,932
783   CONTINUE
```

```
      Z(1) = DEL2*RDEL2**EN
      HST(1) = HSTAR
      H(1) = HH
      CALL HEAD (NUMBER,MOD,ID)
      IF (NBUG) 932,884,883
883   PRINT 70, J
884   CALL PRINT (U1,HSTAR,HH)
      LL = KK + 1
      L  = 2
      DO 200  N = 1,K
      DO 100  I = L,LL
      IF (MKK - I) 927,927,22
22    JJ = 0
C     GUESS NEXT VALUE OF 'HSTAR' THEN ITERATE UNTIL
C     DIFFERENCE BETWEEN SUCCESSIVE VALUES IS LESS THAN 'E'
      IF (I - 2) 20,20,21
20    HST(2) = HST(1) - 0.001
      GO TO 210
21    HST(I) = HST(I-1)+0.5*(HST(I-1)-HST(I-2))
210   PSI = 0.0114*ACHM*(2.0-THETA)**0.8
      H(I) = (1.0+2.0*PSI-((1.0+2.0*PSI)**2.0-4.0*PSI*HST(I))**0.5)
     1  /(2.0*PSI)
      HBAR = (H(I) + H(I-1))*0.5
      GO TO (23,14,23,14,23,14,14,23,23),NUMBER
14    CALL BLAM (HBAR)
      GO TO 891
23    CALL TURB (HBAR)
891   JJ = JJ + 1
      IF (MKS) 116,116,932
116   IF (JJ-20) 24,24,114
24    CALL FUNCT (F1,F2,F3,F4,HBAR)
      UU = U(I)
      TW = TA(I)
      CALL PROPS (I,UU)
      U(I) = UDEL
      M = I - 1
      UA = U(M)
      UB = U(I)
      ZA = Z(M)
      HSTA = HST(M)
      RA = RR(M)
      RB = RR(I)
      CALL SOLVE(F1,F2,F3,F4,ZA,ZB,HSTA,HSTB,UA,UB,DELTAX,NBUG,RA,RB,EN)
      VAL = ABS(HST(I) - HSTB)
      IF (VAL - E) 32,32,31
31    HST(I) = HSTB
      GO TO 210
32    Z(I) = ZB
      HST(I) = HSTB
      RDEL2 = (RODEL*UB*ZB/VISWAL)**(1.0/(1.0+EN))
      RDEL2U = RDEL2/DELRAT
      RN(I) = RDEL2
```

```
      H12S(I) = DEL12
      II = I
      HHH = H(I)
      X = X + DELTAX
      IF (NBUG) 932,100,638
638   PRINT 639, JJ
100   CONTINUE
C     AFTER KK STEPS, PRINT OUT VALUES
      GO TO (5,6,5,6,5,6,6,5,5),NUMBER
6     CALL BLAM (HHH)
      GO TO 915
5     CALL TURB (HHH)
      IF (NBUG) 932,918,915
915   PRINT 70, II
918   RDEL2 = (RODEL*UB*ZB/VISWAL)**(1.0/(1.0+EN))
      RDEL2U = RDEL2/DELRAT
      DEL2 = ZB/(RDEL2**EN)
      CALL PRINT (UB,HSTB,HHH)
      L = LL + 1
      LL = (N+1)*KK + 1
200   CONTINUE
927   DEL2U1 = DEL2U1 * 12.0
      DEL3U1 = DEL3U1 * 12.0
      P1 = P1/70.72622
      PZERO = PZERO/70.72622
      PRINT 303, DEL2U1,DEL3U1,P1,U1,TZERO,PZERO
      GO TO 932
114   MKR = MKR+1
      IF (MKR-1) 120,120,118
120   PRINT 117
      E = E*10
      NN = 0
      J = 1
      X = XIM(1)
      GO TO 121
118   PRINT 115
932   PRINT 311
      IF (ND) 641,642,642
641   MKKN = MKK - 1
      PUNCH 640, ID
      DO 643 I=1,MKKN
643   PUNCH 644, XA(I),U(I),RN(I),H12S(I),HST(I)
642   GO TO 4
1     FORMAT (6I5)
2     FORMAT (2F10.6,3F10.4)
3     FORMAT (4F10.4)
10    FORMAT (//' ***ARRAY PARAMS.***',I5,F10.4,3I6,F12.5//)
11    FORMAT (4F10.5)
17    FORMAT ('1 *** INPUT DEBUG ***'///)
70    FORMAT ( 3H I=,I5 )
```

```
101   FORMAT (//I3)
115   FORMAT (///69H *****NO CONVERGENCE AFTER OVER  20  ITERATIONS. CAS
     1E ABANDONED.*****///)
117    FORMAT(///' ***NO CONVERGENCE. NEW ATTEMPT WITH WEAKER CONVERGENC
     1E CRITERION FOLLOWS***')
303   FORMAT (//46H ***END OF COMPUTATION HAVING STARTING VALUES  ,
     1          /8H DEL2U1=,F9.5 ,9H  DEL3U1=,F9.5 ,5H  P1=,F7.3,
     2  5H  U1=,F8.2,8H  TZERO=,F5.0,8H  PZERO=,F7.3)
311   FORMAT (//33H ***QUIT***VRYSTAAT INTEENDEEL***)
476   FORMAT (12H ***INPUT***,I6,8F11.5//)
601   FORMAT (2X,10F10.4)
507   FORMAT ('1***COMPUTATION NUMBER',I5,' REQUIRES TOO MUCH STORAGE.
     1BREAK IT UP INTO SHORTER PARTS***'//)
639   FORMAT (19H **NEXT STEP AFTER ,I2,13H ITERATIONS**)
640   FORMAT (I5)
644   FORMAT (5F13.5)
      END
```

```
      SUBROUTINE PROPS (I,UU)
C
C     MOD 5
C
      COMMON P1,U1,PZERO,TZERO,UDEL,VISWAL,ACHM,RODEL,THETA,R,RGAS,
     1 GAMMA,NUMBER,ALPHA,BETA,H12,HSTAR,DELRAT,EN,BIGN,NN,NBUG
     2 ,MKS,RDEL2U,RDEL2,DEL12,DEL2,DELTAX,X,NHW,CP,TW
C
      IF (NUMBER-1) 1,1,10
1     IF (I - 1) 6,6,7
6     ACHM1 = ((2.0/(GAMMA - 1.0))*((PZERO/P1)**((GAMMA-1.0)/GAMMA)
     1  - 1.0))**0.5
      ROZERO = PZERO/(RGAS*TZERO)
      TDEL1 = TZERO/(1.0 +((GAMMA-1.0)/2.0)*ACHM1*ACHM1   )
      TE1 = TDEL1*(1.0 + R*((GAMMA-1.0)/2.0)*ACHM1*ACHM1   )
      RODEL1 = ROZERO*(P1/PZERO)**(1.0/GAMMA)
      VIS1 = 0.00001248*((TE1/540.0)**1.5)*738.0/(TE1 + 198.0)
7     ACHM = ACHM1
      RODEL = RODEL1
      VISWAL = VIS1
      GO TO (8,9,8,8,9,9,8,9,8),NUMBER
8     THETA = 0.0
      GO TO 11
9     THETA = 64.34*CP*(TE1-TW)/(U1*U1)
11    TDEL = TDEL1
      TE = TE1
      UDEL = U1
      GO TO 2
10    UDEL = UU
      ACHM = (2.0/(GAMMA-1.0)*((2.0*GAMMA*32.174*TZERO*RGAS)
     1 /((2.0*GAMMA*RGAS*32.174*TZERO) - (GAMMA-1.0)*UU*UU) - 1.0 )
     2 )**0.5
      ROZERO = PZERO/(RGAS*TZERO)
      TDEL  = TZERO/(1.0 +((GAMMA-1.0)/2.0)*ACHM *ACHM    )
      TE  = TDEL *(1.0 + R*((GAMMA-1.0)/2.0)*ACHM *ACHM    )
      RODEL =ROZERO/(1.+(GAMMA-1.)*.5*ACHM*ACHM)**(1./(GAMMA-1.))
      VISWAL=0.00001248*((TE /540.0)**1.5)*738.0/(TE  + 198.0)
      GO TO (12,13,12,12,13,13,12,13,12),NUMBER
12    THETA = 0.0
      GO TO 2
13    THETA = 64.34*CP*(TE-TW)/(UU*UU)
2     IF (NBUG) 4,4,5
5     PRINT 3, UDEL,ACHM,ROZERO,TDEL,TE,RODEL,VISWAL,THETA
4     RETURN
3     FORMAT (9H **PROPS ,8F13.8)
      END
```

```
      SUBROUTINE TURB (H)
C
C     MOD 5
C
C     THIS SUBROUTINE CALLS 'HANS' OR 'WALZ' OR 'MARCEL' TO COMPUTE
C     VALUES OF ALPHA BETA H12 DEL12 PHI PSI HSTAR AND DELRAT DEPENDING
C     ON THE VALUE GIVEN TO PARAMETER 'NHW'
C     NHW= 1 GETS ALL THE ABOVE FROM 'HANS'
C     NHW= 0 GETS ALL THE ABOVE FROM 'WALZ'
C     NHW=-1 GETS ALL THE ABOVE FROM 'MARCEL'
C
      COMMON P1,U1,PZERO,TZERO,UDEL,VISWAL,ACHM,RODEL,THETA,R,RGAS,
     1 GAMMA,NUMBER,ALPHA,BETA,H12,HSTAR,DELRAT,EN,BIGN,NN,NBUG
     2 ,MKS,RDEL2U,RDEL2,DEL12,DEL2,DELTAX,X,NHW,CP,TW
C
C     TEST VALUE OF SHAPE FACTOR
      NMJ = NN
      IF (H - 1.57) 2,2,1
2     IF (NN-1) 3,3,19
3     PRINT 4
      NN = NN+1
19    IF (H-1.50) 20,20,1
20    IF (NN-4) 23,23,1
23    PRINT 21
      NN = NN+1
      IF (H-1.49) 5,5,1
5     PRINT 6
      MKS = 1
      GO TO 18
1     IF (NHW) 8,12,11
8     CALL MARCEL (H)
      GO TO 9
12    CALL WALZ (H)
      GO TO 9
11    CALL HANS (H)
9     IF (ALPHA) 14,14,10
14    IF (NN-6) 16,16,10
16    PRINT 15
      MKS = 1
      GO TO 18
10    EN = 0.268
      BIGN = 0.168
      IF (NBUG) 17,17,18
18    PRINT 13, ALPHA,BETA,H12,DEL12,HSTAR,DELRAT,H,NMJ
17    CONTINUE
7     RETURN
4     FORMAT ('0**SEPARATION IMMINENT.  H32 L.T. 1.57 '/)
6     FORMAT ('0**CASE ABANDONED**   H32 L.T. 1.49'/)
13    FORMAT (8H **TURB ,7F12.6,I3)
15    FORMAT ('0**NEGATIVE WALL SHEAR STRESS COMPUTED**'/)
21    FORMAT ('0**SEPARATION REACHED BY WALZ CRITERION  H32 L.T. 1.50'/)
      END
```

```
      SUBROUTINE BLAM (H)
C
C     MOD 5
C
      COMMON P1,U1,PZERO,TZERO,UDEL,VISWAL,ACHM,RODEL,THETA,R,RGAS,
     1 GAMMA,NUMBER,ALPHA,BETA,H12,HSTAR,DELRAT,EN,BIGN,NN,NBUG
     2 ,MKS,RDEL2U,RDEL2,DEL12,DEL2,DELTAX,X,NHW,CP,TW
C
C     TEST H
      IF (H - 1.5151) 16,16,3
3     ALPHA = 1.441*(H-1.515)**0.66
      BETA = (0.1573 + 1.691*(H-1.515)**1.637)*((1.0+0.6667*R*((GAMMA-
     1 1.0)/2.0)*ACHM*ACHM*(1.0-0.75*THETA))**0.65)
      H12 = 4.03-4.183*(H-1.515)**0.3945
      PHI = 0.936-0.0572*ACHM
      PSI = 0.0114*ACHM*(2.0-THETA)**0.8
      IF (ALPHA - 0.001) 14,14,100
14    IF (NN-2) 16,16,100
16    PRINT 15
      NN = NN + 1
      MKS = NN
      GO TO 7
100   HSTAR = H *(1.0 + (2.0 - H)*PSI)
      DELRAT = (1.0 + R*((GAMMA-1.0)/2.0)*ACHM*ACHM*(HSTAR-THETA)*
     1  (2.0 - H)*PHI)**(-1.0)
      DEL12 = H12/DELRAT+R*((GAMMA-1.0)/2.0)*ACHM*ACHM*(HSTAR-THETA)
      EN = 1.0
      BIGN = 1.0
      IF (NBUG) 17,17,18
18    PRINT  13, ALPHA,BETA,H12,DEL12,PHI,PSI,HSTAR,DELRAT,H
17    CONTINUE
7     RETURN
15    FORMAT (///49H ****BOUNDARY LAYER HAS NOW REACHED SEPARATION***//)
13    FORMAT (8H **BLAM ,9F12.6)
      END


      SUBROUTINE FUNCT (F1,F2,F3,F4,HBAR)
C
C     MOD 5
C
      COMMON P1,U1,PZERO,TZERO,UDEL,VISWAL,ACHM,RODEL,THETA,R,RGAS,
     1 GAMMA,NUMBER,ALPHA,BETA,H12,HSTAR,DELRAT,EN,BIGN,NN,NBUG
     2 ,MKS,RDEL2U,RDEL2,DEL12,DEL2,DELTAX,X,NHW,CP,TW
C
      DEL43 = R*((GAMMA-1.0)/2.0)*ACHM*ACHM*(HSTAR-THETA)/HSTAR
      F1 = 2.0 + EN + (1.0+EN)*DEL12 - ACHM*ACHM
      F2 = (1.0+EN)*DELRAT*ALPHA
      F3 = 1.0 - DEL12 + 2.0*DEL43
      F4 = DELRAT*(2.0*BETA*RDEL2**(EN-BIGN) - ALPHA*HSTAR)
      IF (NBUG) 3,3,1
1     PRINT 2, HBAR,DEL43,F1,F2,F3,F4
3     RETURN
2     FORMAT (9H **FUNCT ,6F13.7)
      END
```

```
      SUBROUTINE HEAD (NUMBER,MOD,ID)
C
C     MOD 5
C
      PRINT 10
      PRINT 20, NUMBER,MOD,ID
      GO TO (1,2,3,4,5,6,7,8,9),NUMBER
1     PRINT 11
      GO TO 69
2     PRINT 21
      GO TO 69
3     PRINT 31
      GO TO 69
4     PRINT 41
      GO TO 69
5     PRINT 51
      GO TO 69
6     PRINT 61
      GO TO 69
7     PRINT 71
      GO TO 69
8     PRINT 81
      GO TO 69
9     PRINT 91
69    PRINT 70
      PRINT 80
      RETURN
10    FORMAT ( '1  COMPRESSIBLE BOUNDARY LAYER CALCULATION BY THE METHOD
     1 OF WALZ ET AL.')
20    FORMAT ('0  CASE NUMBER',I3,'    PROGRAM MOD. ',I2, 9X,' COMPUTATI
     1ON NUMBER ',I5)
11     FORMAT ('0    TURBULENT, ZERO PRESSURE GRADIENT, ADIABATIC WALL,
     1 TWO DIMENSIONAL, FERNHOLZ (1967) INCOMPRESSIBLE RELATIONS')
21    FORMAT ('0    LAMINAR, AXISYMMETRIC, SPECIFIED WALL TEMPERATURE')
31    FORMAT ('0  TURBULENT, TWO DIMENSIONAL, ADIABATIC WALL')
41    FORMAT ('0    LAMINAR, TWO DIMENSIONAL, ADIABATIC WALL')
51    FORMAT ('0  TURBULENT, TWO DIMENSIONAL, SPECIFIED WALL TEMPS.')
61    FORMAT ('0    LAMINAR, TWO DIMENSIONAL, SPECIFIED WALL TEMPS.')
71    FORMAT ('0    LAMINAR, AXISYMMETRIC, ADIABATIC WALL')
81    FORMAT ('0  TURBULENT, AXISYMMETRIC, SPECIFIED WALL TEMPERATURE')
91    FORMAT ('0  TURBULENT, AXISYMMETRIC, ADIABATIC WALL')
70    FORMAT (/         '  POSN.  VELOCITY  SKIN FRIC. MACH  HT.TFR. SHP.
     1FCT. MOM.THK.   MOM.THK.   DISP.   SHP. FCT.  INCOMP. ')
80    FORMAT (          '  X IN.  FT/SEC.   CF LOCAL   NO.   PARAM.  H12
     1(S)  INCHES     REN. NO.   THK.    H32 (S)    H12 '//)
      END
```

```
      SUBROUTINE HANS (H)
C
C     MOD 5
C
C     THIS SUBROUTINE COMPUTES VALUES OF ALPHA,BETA,H12,DEL12,PHI,PSI,
C     HSTAR AND DELRAT ACCORDING TO RELATIONS OF FERNHOLZ (1967) FOR
C     THE TURBULENT BOUNDARY LAYER ON A FLAT PLATE
C
      COMMON P1,U1,PZERO,TZERO,UDEL,VISWAL,ACHM,RODEL,THETA,R,RGAS,
     1 GAMMA,NUMBER,ALPHA,BETA,H12,HSTAR,DELRAT,EN,BIGN,NN,NBUG
     2 ,MKS,RDEL2U,RDEL2,DEL12,DEL2,DELTAX,X,NHW,CP,TW
      R1 = (1.+R*(GAMMA-1.)/2.*ACHM*ACHM*(1.-THETA))**(-1.)
      H32S = 1.80 + 0.0072*ACHM
      F2THET = 1.
      I = 0
      SIGS = 1.002
2     CC = 0.01015/(RDEL2*SIGS)**0.15 + 0.786/(RDEL2*SIGS)
      H12 = (1.0 - ((0.5*CC)**0.5)*(7.506-0.202*ALOG10(RDEL2*SIGS)))
     1 **(-1.0)
      H12S = H12 + .4*ACHM*ACHM*F2THET
      RAT = (H12S - R*(GAMMA-1.)/2.*ACHM*ACHM*(H32S-THETA))/H12
      SIGS = RAT**0.7
      I = I + 1
      IF (I-5) 3,4,4
3     GO TO 2
4     CF=R1*(.01015*(RAT**.595)/(RDEL2**.15)+.786/RDEL2)
      ALPHA1 = 0.5*CF*RAT*(RDEL2**0.268)
      CFU = 0.01015/(RDEL2U**0.150) + 0.786/RDEL2U
      ALPHA2= CFU*0.5*(RDEL2U**0.268)
      IF (NUMBER-1) 7,6,5
6     ALPHA = ALPHA2
      GO TO 17
5     ALPHA = ALPHA1
17    IF (NUMBER-1) 7,13,9
13    BETA = 0.25*CFU*(H + 0.017)*RDEL2U**0.168
      GO TO 11
9     BETA = 0.25*CF*H32S*(RDEL2**0.168)*RAT
11    DEL12 = H12S
      DELRAT = 1.0/RAT
      PSI = 0.0114*ACHM*(2.0 - THETA)**0.8
      HSTAR = H *(1.0 + (2.0 - H)*PSI)
      IF (NBUG) 7,102,103
103   PRINT 20, H,PSI,R1,SIGS,RAT,CF,CFU,NN,NHW,MKS
102   GO TO 12
7     MKS = 1
12    RETURN
20    FORMAT (8H **HANS ,7F12.8,3I5)
      END
```

```
      SUBROUTINE MARCEL (H)
C
C     MOD 5
C
C     THIS SUBROUTINE COMPUTES VALUES OF ALPHA,BETA AND H12 ACCORDING TO
C     RELATIONS OF ESCUDIER ET AL (1966).  VALUES OF THE COMPRESSIBILITY-
C     CORRECTED QUANTITIES DEL12 AND HSTAR ARE ACCORDING TO WALZ (1965)
C     CORRECTION RELATIONS
C
      COMMON P1,U1,PZERO,TZERO,UDEL,VISWAL,ACHM,RODEL,THETA,R,RGAS,
     1 GAMMA,NUMBER,ALPHA,BETA,H12,HSTAR,DELRAT,EN,BIGN,NN,NBUG
     2 ,MKS,RDEL2U,RDEL2,DEL12,DEL2,DELTAX,X,NHW,CP,TW
C
      H12 = 1.55/(.0971+(.009428-3.1*(1.431-H))**0.5)
      PHI = 1.0 - 0.0719*ACHM + 0.00419*ACHM*ACHM
      PSI = 0.0114*ACHM*(2.0 - THETA)**0.8
      HSTAR = H *(1.0 + (2.0 - H)*PSI)
      DELRAT = (1.0 + R*((GAMMA-1.0)/2.0)*ACHM*ACHM*(HSTAR-THETA)*
     1 (2.-H)*PHI)**(-1.)
      DEL12 = H12/DELRAT+R*((GAMMA-1.0)/2.0)*ACHM*ACHM*(HSTAR-THETA)
      HT = 2.*H/3.
      ZETA = HT-1.+(HT*(HT-1.))**0.5
      IF (ZETA-1.) 1,1,2
1     TERM = .00565*(1.-ZETA)**2.715
      GO TO 3
2     TERM = .01*(ZETA-1.)**3.
3     EL = ALOG(3.389*RDEL2*ZETA/((1.-ZETA)*(1.+2.*ZETA)))
      SS = (.243*ZETA*ZETA+.0376*ZETA-.00106+.0914*ZETA*ZETA/
     1 (1.+65./ZETA))/(EL*EL)
C     BY USUAL DEFN.  CF = 2.*SS
      ALPHA = SS*(RDEL2**.268)/DELRAT
      SBAR = (2.*ZETA+1.)*SS/3. + TERM
      BETA = SBAR*(RDEL2**.168)/DELRAT
      IF (NBUG) 5,5,6
6     PRINT 4, H,PHI,PSI,HT,ZETA,EL,SS,SBAR
5     RETURN
4     FORMAT (' **MARCEL ',8F12.8)
      END


      SUBROUTINE PRINT (U,HST,H)
C
C     MOD 5
C
      COMMON P1,U1,PZERO,TZERO,UDEL,VISWAL,ACHM,RODEL,THETA,R,RGAS,
     1 GAMMA,NUMBER,ALPHA,BETA,H12,HSTAR,DELRAT,EN,BIGN,NN,NBUG
     2 ,MKS,RDEL2U,RDEL2,DEL12,DEL2,DELTAX,X,NHW,CP,TW
C
2     CF = ALPHA*DELRAT/(RDEL2**EN)*2.0
3     QX = 12.0*X
      QDEL2 = 12.0*DEL2
      QDLTAX = 12.0*DELTAX
      DEL1 = QDEL2*DEL12
      PRINT 13, QX,U,CF,ACHM,THETA,DEL12,QDEL2,RDEL2,DEL1,HST,H12
      RETURN
13    FORMAT (1X,F6.2,3X,F7.2,3X,F8.6,2X,F5.3,2X,F6.3,F8.4,3X,F6.4,
     1 1X,F10.0,3X,F6.4,3X,F7.4,F9.4/)
      END
```

```
      SUBROUTINE SOLVE (F1,F2,F3,F4,ZA,ZB,HSTA,HSTB,UA,UB,DELTAX,
     1  NBUG,RA,RB,EN )
C
C     MOD 5
C
      UR = (UA/UB)
      IF (UR - 1.0) 2,3,2
3     AZ = 1.0
      BZ = 1.0
      AH = 1.0
      BH = 1.0
      GO TO 4
2     AZ = UR**F1
      BZ = (1.0 - AZ*UR)/((1.0 + F1)*(1.0 - UR))
      AH = UR**F3
      BH = (1.0 - AH*UR)/((1.0 + F3)*(1.0 - UR))
4     ZB = ZA*(RA/RB)**(1.0+EN)*(AZ+(BZ*F2*DELTAX/ZA)*(1.0+(RB/RA)
     1 **(1.0+EN))/2.0)
      HSTB = HSTA * (AH + BH*F4*DELTAX*2.0/(HSTA*(ZB + ZA)))
      IF (NBUG) 13,13,17
17    PRINT 5, UR,ZA,ZB,HSTA,HSTB,AZ,BZ,AH,BH,RA,RB
13    CONTINUE
      RETURN
5     FORMAT (9H **SOLVE ,11F10.6)
      END



      SUBROUTINE WALZ (H)
C
C     MOD 5
C
C     THIS SUBROUTINE COMPUTES VALUES OF ALPHA,BETA,H12,DEL12,PHI,PSI,
C     HSTAR AND DELRAT ACCORDING TO RELATIONS OF WALZ (1965) FOR A
C     TURBULENT BOUNDARY LAYER.
C
      COMMON P1,U1,PZERO,TZERO,UDEL,VISWAL,ACHM,RODEL,THETA,R,RGAS,
     1 GAMMA,NUMBER,ALPHA,BETA,H12,HSTAR,DELRAT,EN,BIGN,NN,NBUG
     2 ,MKS,RDEL2U,RDEL2,DEL12,DEL2,DELTAX,X,NHW,CP,TW
C
      ALPHA = 0.0566*H - 0.0842
      BETA = 0.0056
      H12 = 1.0 + 1.48 *(2.0-H) + 104.0 * (2.0-H)**6.7
      PHI = 1.0 - 0.0719*ACHM + 0.00419*ACHM*ACHM
      PSI = 0.0114*ACHM*(2.0 - THETA)**0.8
      HSTAR = H *(1.0 + (2.0 - H)*PSI)
      DELRAT = (1.0 + R*((GAMMA-1.0)/2.0)*ACHM*ACHM*(HSTAR-THETA)*
     1  (2.0 - H)*PHI)**(-1.0)
      DEL12 = H12/DELRAT+R*((GAMMA-1.0)/2.0)*ACHM*ACHM*(HSTAR-THETA)
      IF (NBUG) 3,3,2
2     PRINT 1, H,PHI,PSI,NN,NHW,MKS
3     RETURN
1     FORMAT (8H **WALZ ,3F12.8,48X,3I5)
      END
```

COMPRESSIBLE BOUNDARY LAYER CALCULATION BY THE METHOD OF WALZ ET AL.

CASE NUMBER 3 PROGRAM MOD. 5 COMPUTATION NUMBER 4

TURBULENT, TWO DIMENSIONAL, ADIABATIC WALL

POSN. X IN.	VELOCITY FT/SEC.	SKIN FRIC. CF LOCAL	MACH NO.	HT.TFR. PARAM.	SHP.FCT. H12 (S)	MOM.THK. INCHES	MOM.THK. REN. NO.	DISP. THK.	SHP. FCT. H32 (S)	INCOMP. H12
16.00	85.00	0.003161	0.075	0.0	1.4529	0.0570	2387.	0.0828	1.7130	1.4505
18.00	85.00	0.003240	0.075	0.0	1.4349	0.0602	2521.	0.0863	1.7219	1.4325
20.00	85.00	0.003271	0.075	0.0	1.4240	0.0634	2658.	0.0903	1.7275	1.4217
22.00	84.65	0.003237	0.074	0.0	1.4214	0.0676	2821.	0.0961	1.7289	1.4191
24.00	84.01	0.003169	0.074	0.0	1.4233	0.0726	3008.	0.1034	1.7279	1.4211
26.00	83.15	0.003082	0.073	0.0	1.4279	0.0784	3215.	0.1120	1.7255	1.4256
28.00	82.10	0.002981	0.072	0.0	1.4346	0.0850	3441.	0.1220	1.7221	1.4324
30.00	80.85	0.002765	0.070	0.0	1.4576	0.0958	3780.	0.1396	1.7105	1.4555
32.00	76.91	0.002409	0.068	0.0	1.5065	0.1129	4281.	0.1701	1.6886	1.5046
34.00	72.22	0.001789	0.063	0.0	1.6330	0.1436	5115.	0.2345	1.6444	1.6312
36.00	67.52	0.000996	0.059	0.0	1.9401	0.1865	6213.	0.3618	1.5799	1.9383

**SEPARATION IMMINENT. H32 L.T. 1.57

**SEPARATION IMMINENT. H32 L.T. 1.57

**SEPARATION REACHED BY WALZ CRITERION H32 L.T. 1.50

```
 COMPRESSIBLE BOUNDARY LAYER CALCULATION BY THE METHOD OF WALZ ET AL.

 CASE NUMBER  1    PROGRAM MOD.  5          COMPUTATION NUMBER    24

   TURBULENT, ZERO PRESSURE GRADIENT, ADIABATIC WALL,  TWO DIMENSIONAL, FERNHOLZ (1967) INCOMPRESSI

 POSN.  VELOCITY  SKIN FRIC. MACH  HT.TFR. SHP.FCT. MOM.THK.   MOM.THK.   DISP.   SHP. FCT.  INCOMP.
 X IN.  FT/SEC.   CF LOCAL   NO.   PARAM.  H12 (S) INCHES     REN. NO.   THK.    H32 (S)    H12


I=    1
 15.75    350.22   0.0027C5  C.309   0.0    1.3671   0.0246      8250.   0.0336    1.7477   1.3289

**HANS   1.74442863  0.006135C7  0.98346382  1.00416279  1.C0595188  0.00010180  0.00271660    1
**TURB     0.015251    0.C05448    1.328911    1.367126    1.747163    0.994083    1.744429  1
**FUNCT     1.7444286    C.0168149    3.9059753    0.0192235   -0.3334967    0.0002004
**PROPS  350.21655273   0.30909413   0.15144247 534.78198242 543.77392578   0.14444309   0.00001255
**SOLVE   1.000000  0.022937  C.023258  1.747667  1.747810  1.000000  1.000000  1.000000  1.000000
**HANS   1.74500656  0.006135C7  0.98346382  1.00416279  1.00595188  0.00010180  0.00271660    1
**TURB     0.015251    0.005450    1.328911    1.367126    1.747735    0.994083    1.745007  1
**FUNCT     1.745CC66    C.0168149    3.9059753    0.0192235   -0.3334967    C.0002005
**PROPS  350.21655273   0.30909413   0.15144247 534.78198242 543.77392578   0.14444309   0.00001255
**SOLVE   1.000000  0.C22937  0.C23258  1.747667  1.747810  1.000000  1.000000  1.000000  1.000000
**NEXT STEP AFTER  2 ITERATIONS**
**HANS   1.74511051  0.006135C7  C.98346382  1.00416470  1.00595474  0.00010069  0.00271127    1
**TURB     0.015266    0.005449    1.328420    1.366635    1.747838    0.994080    1.745111  1
**FUNCT     1.7451105    C.0168149    3.9053526    0.0192421   -0.3330055    C.0002007
**PROPS  350.21655273   0.30909413   0.15144247 534.78198242 543.77392578   0.14444309   0.00001255
**SOLVE   1.000000  0.C23258  0.C23578  1.747810  1.747952  1.000000  1.000000  1.000000  1.000000
**HANS   1.74514484  0.00613507  0.98346382  1.00416470  1.00595474  0.00010069  0.00271127    1
**TURB     C.015266    0.C05449    1.328420    1.366635    1.747872    0.994080    1.745145  1
**FUNCT     1.7451448    0.0168149    3.9053526    0.0192421   -0.3330C55    C.0002007
**PROPS  350.21655273   0.30909413   0.15144247 534.78198242 543.77392578   0.14444309   C.00001255
**SOLVE   1.000000  0.023258  0.C23578  1.747810  1.747952  1.000000  1.000000  1.000000  1.000000
**NEXT STEP AFTER  2 ITERATIONS**
**HANS   1.74525166  0.006135C7  0.98346382  1.00416565  1.00595665  0.00009961  0.00270603    1
**TURB     C.015280    0.C05449    1.327935    1.366151    1.747977    0.994079    1.745252  1
**FUNCT     1.7452517    C.0168149    3.9047375    0.0192605   -0.3325211    C.0002009
**PROPS  350.21655273   0.30909413   0.15144247 534.78198242 543.77392578   0.14444309   0.00001255
**SOLVE   1.000000  0.023578  0.C23899  1.747952  1.748091  1.000000  1.000000  1.000000  1.000000
**HANS   1.74528599  0.006135C7  0.98346382  1.00416565  1.00595665  0.00009961  0.00270603    1
**TURB     C.01528C    0.005449    1.327935    1.366151    1.748012    0.994079    1.745286  1
**FUNCT     1.7452860    C.0168149    3.9047375    0.0192605   -0.3325211    C.0002009
**PROPS  350.21655273   0.3C9C9413   0.15144247 534.78198242 543.77392578   0.14444309   0.CCCC1255
**SOLVE   1.000CC0  0.023578  0.C23899  1.747952  1.748091  1.000000  1.000000  1.000000  1.000000
**NEXT STEP AFTER  2 ITERATIONS**
**HANS   1.7453928C  0.006135C7  C.98346382  1.C0416756  1.00595856  0.00009855  C.00270087    1
```

APPENDIX VI - NOTES ON EXPERIMENTAL DATA USED FOR TESTING THE WALZ METHOD

Moses[50] #5.

Since no tabulated values were available, δ_2 ($\approx(\delta_2)_u$) and H_{12} were read off the plots for x = 0" as 0.02" and 1.35 respectively. This value of H_{12} was used with eqn. (46) to compute a value of H_{32}, and hence to obtain a value of δ_3 at x = 0. The actual value of u_δ at x = 0 was not given, but was assumed to be 100 ft/sec. This enabled a computation of u_δ at each succeeding data point. $P_{x=0}$ was assumed to be 30.0" Hg.abs. and T_o to be 540 °R.

Moses #6.

The identical starting values were used for this case.

Goldberg[62] #3.

Values of δ_2 ($\approx(\delta_2)_u$) and δ_3 ($\approx(\delta_3)_u$) were read off the published plots at x = 4" as 0.033" and 0.0575" respectively. The report stated that the free-stream velocity in the test-section was "about 85 ft/sec" and this number was used for u_δ at x = 4" to initiate the calculations. $P_{x=4}$ was assumed to be 30.0 "Hg.abs. and T_o to be 540 °R.

Goldberg #6

The same procedure yielded δ_2 = 0.057, δ_3 = 0.0976, the other starting quantities being unchanged for a computation starting at x = 16".

Launder[28] case (a), (i)

Tabulated values of u_δ and R_{δ_2} were available for x = 11". With the assumption of ν = 0.00017 ft^2/sec, this yielded $(\delta_2)_u$ = 0.04321". H_{12} was given as 1.68 and equation (46) was used

to estimate H_{32} as 1.673, giving $(\delta_3)_u$ = 0.07229". The tabulated experimental values of u_δ vs. x were plotted, and values of u_δ read off a faired curve through the data at one inch intervals up to x = 31". $P_{x=11}$ was assumed to be 30.0 "Hg.abs. and T_o to be 540 °R.

Smith and Walker[63]

Data was extracted from the complete tabulations of this report for cases where $M_\delta \approx 0.309$ and $P_o \approx 30.55$ psia. The tabulated values of energy and momentum thickness at x = 15.75" were assumed to correspond to the δ_2 and δ_3 definitions of the present report, although it is not clear whether Smith and Walker made any density corrections in evaluating either their velocity-profiles or integral parameters. Consequently, the auxiliary relations of the present report were used to produce values of $(\delta_2)_u$ and $(\delta_3)_u$ consequent upon M_δ = 0.309. (It might be remarked that this is rather too large a Mach no. to allow the accurate evaluation of shape-factors without density corrections being applied both to the derivation of velocity-profiles from ΔP data and to the evaluation of integral parameters.)

The consequent values of $(\delta_2)_u$ and $(\delta_3)_u$ were 0.0247" and 0.0431". Mean values of P_o and T_o over the data were calculated, which, with adoption of M_δ = 0.3095 yielded values of $P_{x=15.75}$ = 58.213 "Hg.abs. and T_o = 545 °R.

Data of the present study.

In each case, the experimental data tabulated in Tables 1-5 were used, in conjunction with the associated experimental values of $(\delta_2)_u$ and $(\delta_3)_u$, to initiate computations.

APPENDIX VII - THE SKIN FRICTION LAW OF FERNHOLZ

In 1967 Fernholz[35] produced a new form of correlation for the wall shear stress in the turbulent compressible flat plate boundary layer with or without heat transfer. When specialised to the adiabatic wall case, this may be presented in the following form:

$$c_f = \frac{\rho_w}{\rho_\delta} \sigma^* (\overline{c_f})_u = f(M_\delta, R_{\delta_2}) \qquad \text{(VII-1)}$$

where $$\frac{\rho_w}{\rho_\delta} = [1 + 0.176 M_\delta^2]^{-1} \qquad \text{(VII-2)}$$

and $$(\overline{c_f})_u = \frac{0.01015}{(R_{\delta_2} \sigma^*)^{0.15}} + \frac{0.786}{(R_{\delta_2} \sigma^*)} \qquad \text{(VII-3)}$$

and σ^*, the Coles[3] transform function takes the form

$$\sigma^* = \left[\frac{(\delta_2)_u}{\delta_2}\right]^{0.7} \qquad \text{(VII-4)}$$

Now the correlation for $[(\delta_2)_u/\delta_2]$ takes the form

$$(\delta_2)_u/\delta_2 = [H_{12}^* - 0.176 M_\delta^2 H_{32}^*] H_{12}^{-1} \qquad \text{(VII-5)}$$

where $$H_{12} = \{1 - [\tfrac{1}{2} (\overline{c_f})_u]^{1/2} [7.506 - 0.202 \log_{10}(R_{\delta_2} \sigma^*)]\}^{-1} \qquad \text{(VII-6)}$$

and $$H_{12}^* = H_{12} + 0.4 M_\delta^*$$

and $$H_{32}^* = 1.80 + 0.0072 M_\delta$$

This cascaded series of relations clearly requires iteration on σ^* for final evaluation, given R_{δ_2} and M_δ, but this converges very quickly. This procedure is realised in Appendix II.

APPENDIX VIII - THE TEMPERATURE PROFILE RELATION OF VAN DRIEST[47]

Solution of the energy equation for the turbulent compressible flow in the shear layer of a flat plate with a negligible longitudinal enthalpy gradient, unity Prandtl number and constant c_p yields, for the time-averaged quantities:

$$\frac{T}{T_\delta} = \frac{T_w}{T_\delta} - \left(\frac{T_w}{T_\delta} - 1\right) \frac{u}{u_\delta} - \frac{\gamma - 1}{2} M_\delta^2 \frac{u}{u_\delta} \left(1 - \frac{u}{u_\delta}\right) \qquad \text{(VIII-1)}$$

This, together with the usual relation for the recovery temperature of an adiabatic wall, viz.

$$T_w = T \left(1 + r \frac{\gamma - 1}{2} M_\delta^2\right) \qquad \text{(VIII-2)}$$

allows determination of the temperature and hence density profile of a shear layer given only the mean velocity profile, Mach number and local free-stream properties. The LHS of (VIII-1) is close to unity for all the cases treated in this report.

APPENDIX IX - FORTRAN IV PROGRAM TO COMPUTE BOUNDARY LAYER INTEGRAL PARAMETERS FROM RAW DATA

This program provides for the computation of δ_1, δ_2, δ_3, $(\delta_1)_u$, $(\delta_2)_u$, $(\delta_3)_u$, H_{12}, H_{12}^*, H_{32}, H_{32}^*, $\delta_2/(\delta_2)_u$, u_δ, R_{δ_2} and M_δ, given either values of ΔP vs. y only or values of (u/u_δ) and (T/T_δ) vs. y. In the former case, density corrections are put in according to the relation of Van Driest set out in Appendix VIII. The required input deck is:

NSER An integer tag identifying the computation to the user.

STN The value of x at which the profile was measured.

MOD If this is 1, (u/u_δ) and (T/T_δ) must be given vs. y. If it is 3, ΔP (in any units) must be given vs. y (in any units).

PZERO Free-stream stagnation pressure in inches of mercury absolute.

P Local static pressure, inches of mercury absolute.

TZERO Free-stream stagnation temperature, in °R.

DISP The effective displacement, if any, of the probe tip from the y coördinates quoted below. (e.g. in the present study, this was half the y O.D. dimension, in inches, of the probe tips used, since y = 0 was declared to be the case of the probe touching the wall.)

YSCALE A scale factor relating the numbers given for y coördinates below to the actual physical lengths. This is useful if data is read off X-Y plots of varying scales.

There are now two possibilities:

(i) If MOD = 3, a table of values of ΔP vs. y follows, a pair of values to a card [USQ(I) and Y(I)]. This must terminate with a card having only the quantity "-1.0" punched in columns 11-14.

(ii) If MOD = 1, the following card contains the value of T at the first y station, and is followed by a table of y, (T/T_δ) and (u/u_δ), a triplet of values to a card, [Y(I), TS(I), and U(I)] which must terminate with "-1.0" punched in columns 1-4.

Any number of such data sets may be submitted simultaneously. A trapezoidal integration rule is followed, except for the first element. To attenuate the inaccuracy introduced by the finite size of the first experimental y value, the profile is automatically assigned a spurious value of (u/u_δ) at y = 0 by extrapolating to y = 0 that unique parabola which may be drawn through the data of the first, second and third given y stations.

A sample printout is given at the end of the listing.

```
C      COMPRESSIBLE BOUNDARY LAYER PROFILES --- INTEGRATED QUANTITIES
C
C      THE VALUE OF 'MOD' DETERMINES THE FORMAT OF THE DATA
C      MOD = 1 REQUIRES BOTH VELOCITY RATIO AND STATIC TEMP. RATIO TO BE
C      GIVEN IN TERMS OF COORDINATE 'Y'
C      MOD = 3 REQUIRES ONLY VALUES OF DELTAP FOR EACH Y. DENSITY
C      CORRECTIONS ARE PUT IN THROUGH RELATION OF VAN DRIEST.
C      ARRAY 'A' REFERS TO AXISYMMETRIC CASE NOT IMPLEMENTED HERE
C
       DIMENSIONF(6,50),T(6),Y(50),U(50),USQ(50),TS(50),XI(50),A(50)
C
111    PRINT 211
       NCOM = 0
       NCOM2 = 0
       READ 75, NSER
       READ 82, STN
       READ 80, MOD
       READ 82, PZERO,P,TZERO,DISP,YSCALE
       ACHM = (5.0*((PZERO/P)**0.2857-1.0))**0.5
       TFS = TZERO/(1. + .2*ACHM*ACHM)
       TWALL = TFS*(1. + .176*ACHM*ACHM)
       VISC = .00001248*((TWALL/540.)**1.5)*738./(TWALL+198.)
       RODEL = P*70.72622/(53.3*TFS)
       VEL = ((1.4*53.3*32.17*TFS)**0.5)*ACHM
       TR = 1.0 + 0.176*ACHM*ACHM
       PRINT 10
       I = 1
       IF (MOD-3) 98,44,21
44     I = I + 1
       READ 13, USQ(I),Y(I)
       Y(I) = Y(I) + DISP*YSCALE
       IF (Y(I)) 33,44,44
33     IMAX = I - 1
       UMAX = (USQ(IMAX))**0.5
       DO 15 J=2,IMAX
       U(J) = (USQ(J)**0.5)/UMAX
       IF (U(J)-1.00001) 71,71,72
72     NCOM2 = 1
71     TS(J) = TR-(TR-1.)*U(J)+.2*ACHM*ACHM*U(J)*(1.-U(J))
       U(J) =  U(J)*TS(J)**0.5
15     Y(J) = Y(J)/YSCALE
       GO TO 66
98     READ 82, TS(1)
4      I = I + 1
       READ 2, Y(I),TS(I),U(I)
       IF (Y(I)) 3,4,4
3      IMAX = I - 1
C      SET ARRAY 'A' TO ZERO FOR 2-DIM. CASE
66     DO 58 IJKL = 1,IMAX
58     A(IJKL) = 0.0
       Y(1) = 0.0
       U(1) = U(4)*(Y(1)-Y(2))*(Y(1)-Y(3))/(Y(4)-Y(2))/(Y(4)-Y(3))
     1      + U(3)*(Y(1)-Y(4))*(Y(1)-Y(2))/(Y(3)-Y(4))/(Y(3)-Y(2))
     2      + U(2)*(Y(1)-Y(3))*(Y(1)-Y(4))/(Y(2)-Y(3))/(Y(2)-Y(4))
       IF (U(1)) 14,14,151
14     U(1) = 0.1
```

```
      NCOM = 1
151   TS(1) = TR-(TR-1.)*U(1)+.2*ACHM*ACHM*U(1)*(1.-U(1))
      DO 6 I=1,IMAX
      XI(I) = 1.0/TS(I)
      X=XI(I)
       F(1,I) = (1.-X*U(I))*(1.+A(I))
       F(2,I) = U(I)*X*(1. - U(I))*(1. + A(I))
       F(3,I) = U(I)*X*(1. - U(I)*U(I)) *(1.+A(I))
       F(4,I) = (1. - U(I))*(1. + A(I))
       F(5,I) = U(I)*(1. - U(I))*(1. + A(I))
       F(6,I) = U(I)*(1. - U(I)*U(I))*(1. + A(I))
6     PRINT 7, Y(I),U(I),XI(I)
      DO 8 L=1,6
      T(L) = 0.0
      DO 8 I=2,IMAX
      DY = Y(I) - Y(I-1)
8     T(L) = T(L) + 0.5*(F(L,I)+F(L,I-1))*DY
      PRINT 9, (T(L),L=1,6)
      H12 = T(4)/T(5)
      H32 = T(6)/T(5)
      H12S = T(1)/T(2)
      H32S = T(3)/T(2)
      RATD2 = T(2)/T(5)
      RENO = RODEL*VEL*T(2)/(VISC*12.)
      PRINT 11, H12S,H32S
      PRINT 12, H12,H32
      PRINT 756, PZERO,P,TZERO,RATD2,ACHM,VEL,RENO
      PRINT 74, STN,NSER
      IF (NCOM) 16,16,17
17    PRINT 18
16    IF (NCOM2) 25,25,26
26    PRINT 27
25    PRINT 20
      GO TO 111
21    CALL EXIT
2     FORMAT (3F10.5)
7     FORMAT (2X,3F9.4)
9     FORMAT (//14H DELTA 1,2,3 =,3X,3F13.5//
     117H (DELTA 1,2,3)U = ,3F13.5//)
10    FORMAT ('        Y        U/UD    RHO/RHOD'/)
11    FORMAT (' COMP. H12S,H32S =',2F9.4/)
12    FORMAT (' INCOMP. H12,H32 =',2F9.4/)
13    FORMAT (2F10.5)
18    FORMAT (//' **** SUSPECT DATA NEAR WALL ****')
20    FORMAT (//'**COMPRESSIBLE BOUNDARY LAYER** MK III **')
27    FORMAT (//' ****SPURIOUS DATA MAXIMUM ****')
74    FORMAT (//' STATION X =',F6.2,10X,'SERIAL NO.',I4)
75    FORMAT (I2)
80    FORMAT (I1)
82    FORMAT (F10.5)
211   FORMAT ('1***NEXT PROFILE***'//)
756   FORMAT (' PZERO,P,TZERO,D2/D2U = ',2F9.3,F7.1,F7.4//
     1' MACH NO.,FREESTREAM VEL., REN. NO. = ',F6.3,F6.1,F8.0)
      END
```

NEXT PROFILE

Y	U/UD	RHO/RHOD
0.0	0.3551	0.9750
0.0055	0.4761	0.9775
0.0155	0.6143	0.9816
0.0254	0.6479	0.9828
0.0354	0.6712	0.9837
0.0454	0.6830	0.9841
0.0653	0.7203	0.9856
0.0853	0.7420	0.9865
0.1052	0.7579	0.9872
0.1252	0.7734	0.9879
0.1551	0.7900	0.9886
0.1850	0.8028	0.9892
0.2448	0.8303	0.9906
0.3047	0.8517	0.9916
0.4044	0.8801	0.9931
0.5041	0.8959	0.9939
0.6038	0.9258	0.9956
0.7035	0.9448	0.9967
0.8033	0.9623	0.9977
0.9030	0.9760	0.9985
1.0526	0.9878	0.9992
1.2021	0.9934	0.9996
1.3517	0.9950	0.9997
1.5013	0.9956	0.9997
1.6509	0.9967	0.9998
1.8005	0.9983	0.9999
1.9999	1.0000	1.0000

DELTA 1,2,3 = 0.13222 0.10152 0.18577

(DELTA 1,2,3)U = 0.12651 0.10245 0.18740

COMP. H12S,H32S = 1.3023 1.8298

INCOMP. H12,H32 = 1.2349 1.8292

PZERO,P,TZERO,D2/D2U = 30.080 26.925 534.0 0.9910

MACH NO.,FREESTREAM VEL., REN. NO. = 0.401 446.9 21164.

STATION X = 28.00 SERIAL NO. 81

*COMPRESSIBLE BOUNDARY LAYER** MK III **

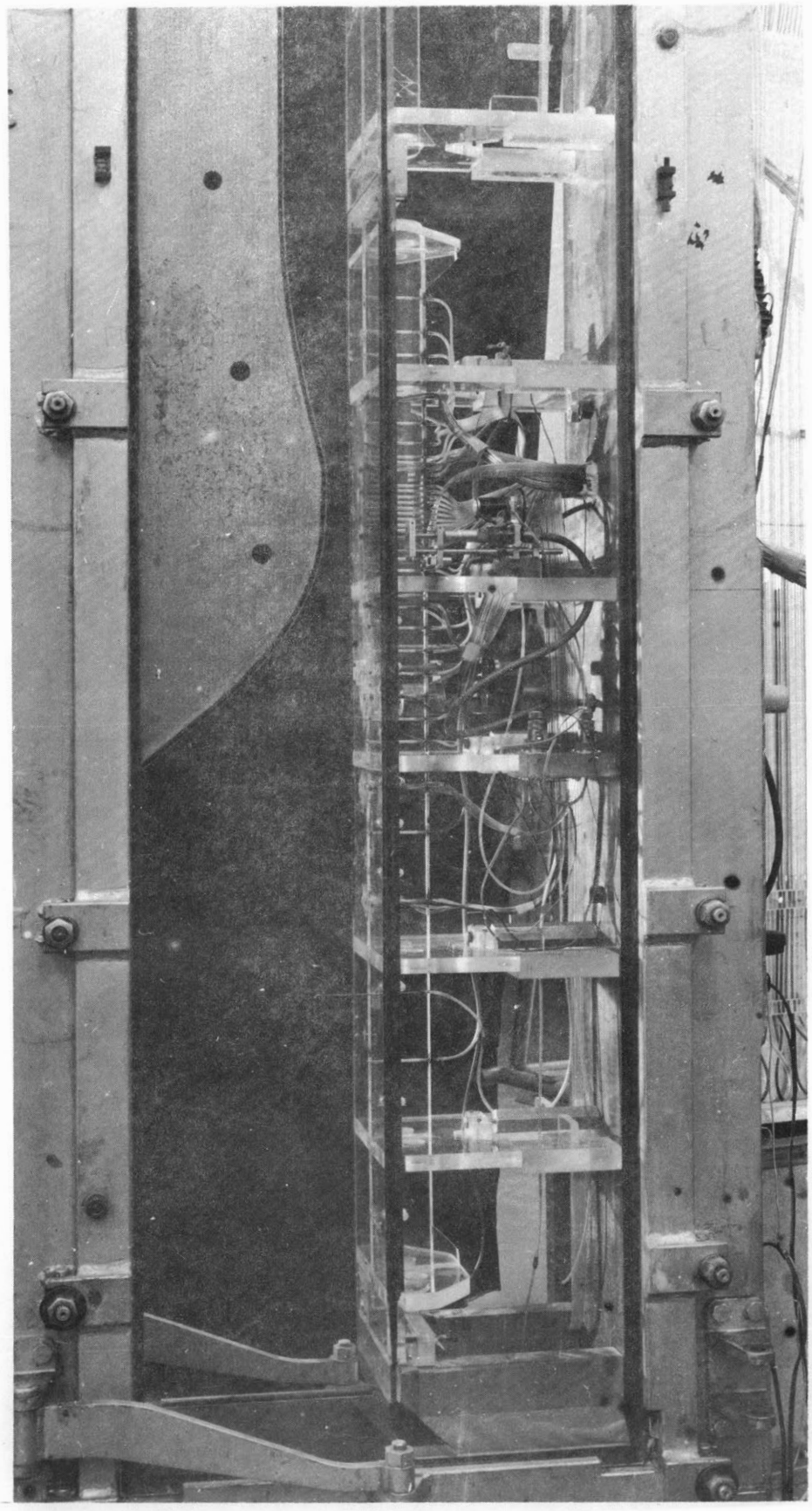

FIG. 1 TEST SECTION OF G.T.L.
SUPERSONIC WIND TUNNEL

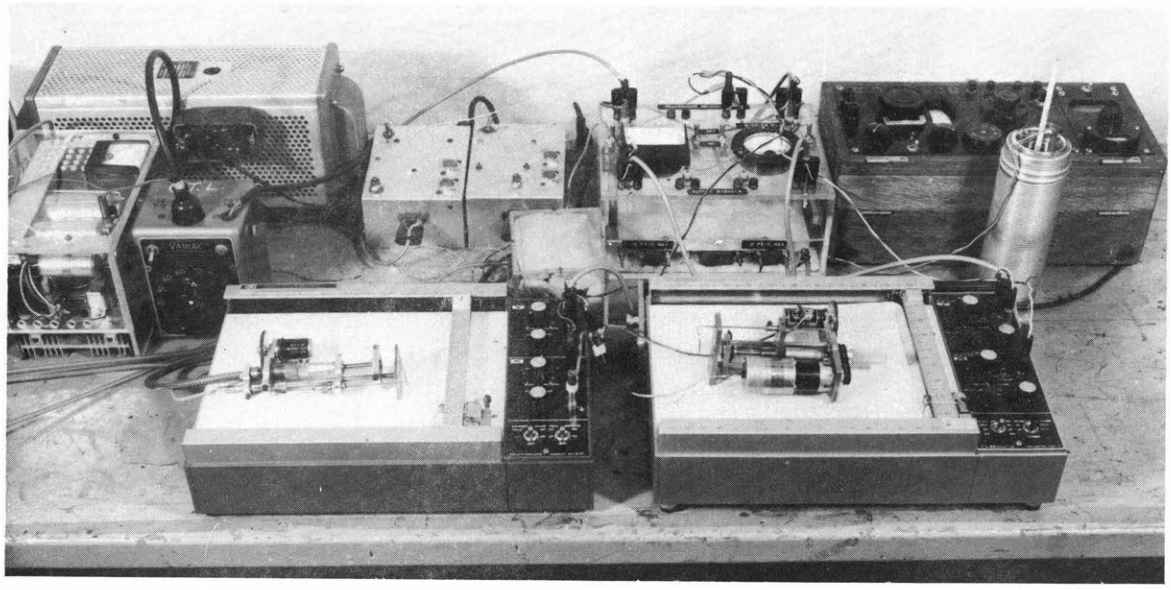

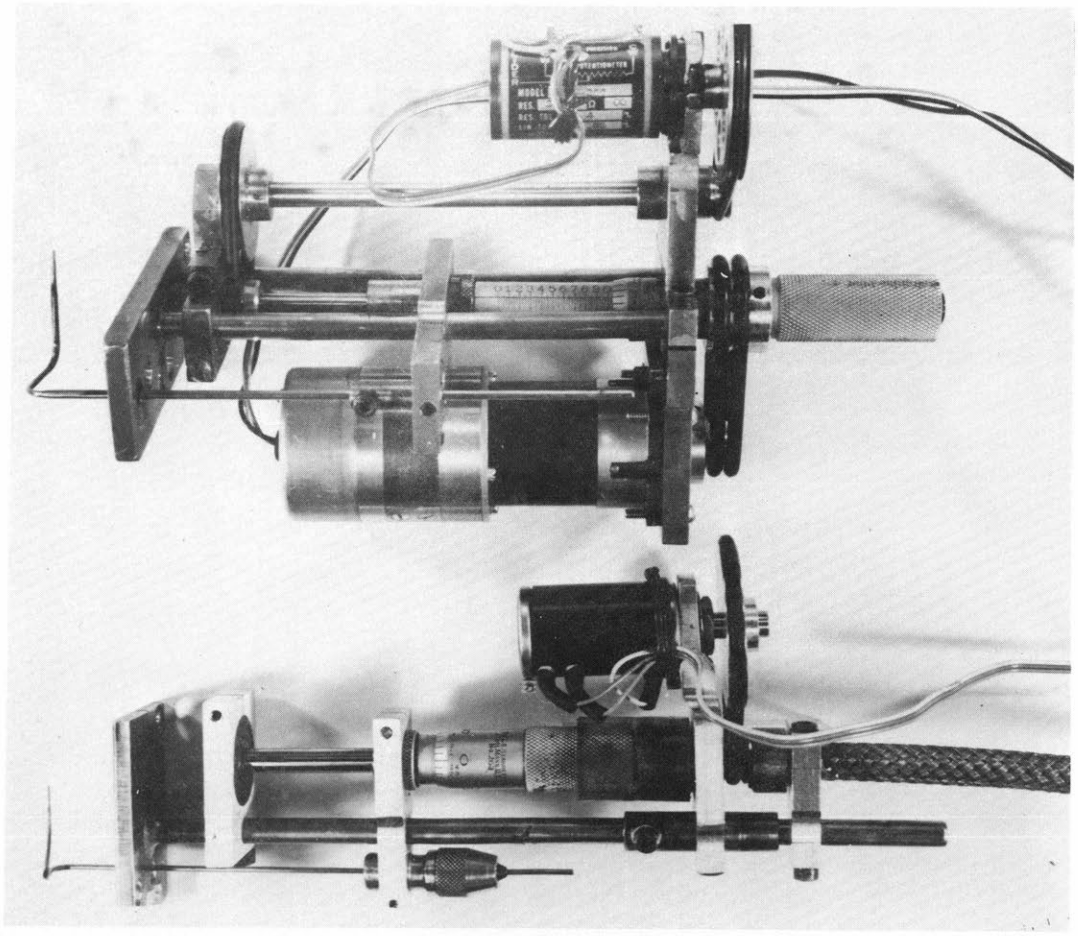

FIG. 2 TEST EQUIPMENT AND TRAVERSING RIGS

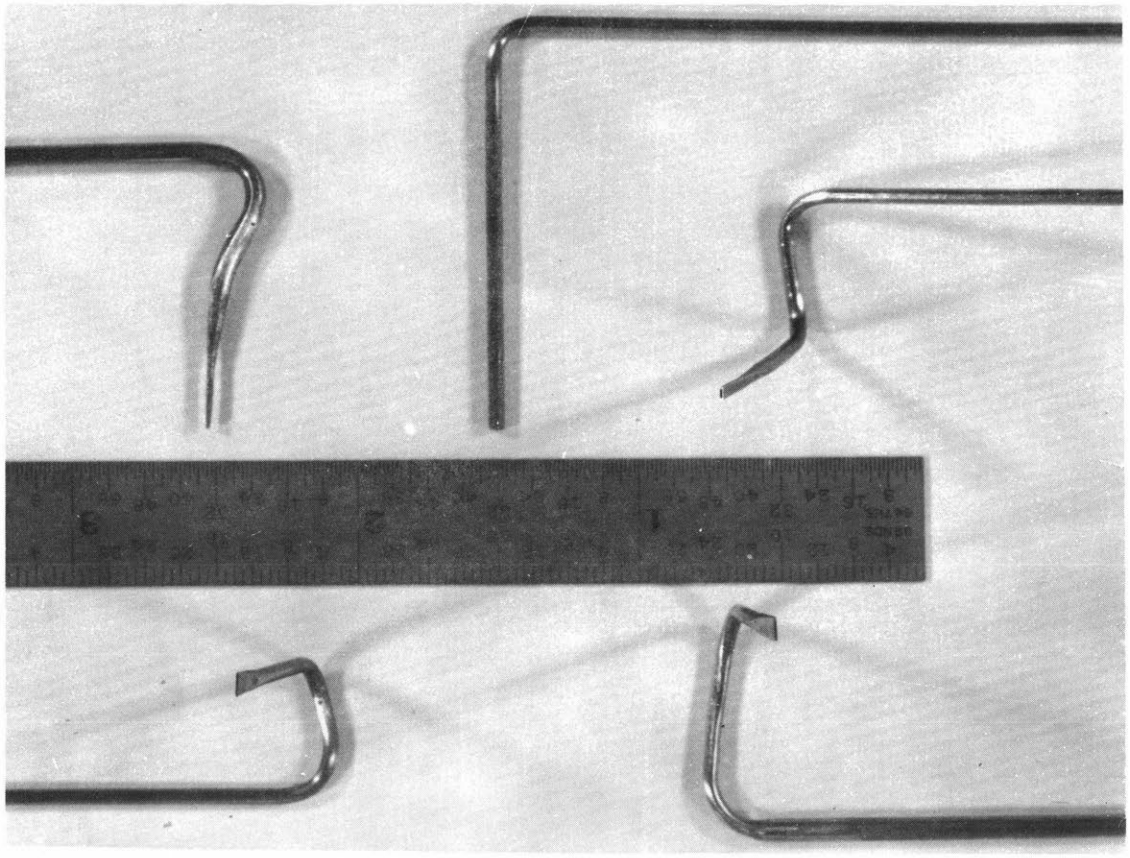

FIG. 3 MINIATURE TOTAL-HEAD PROBES.

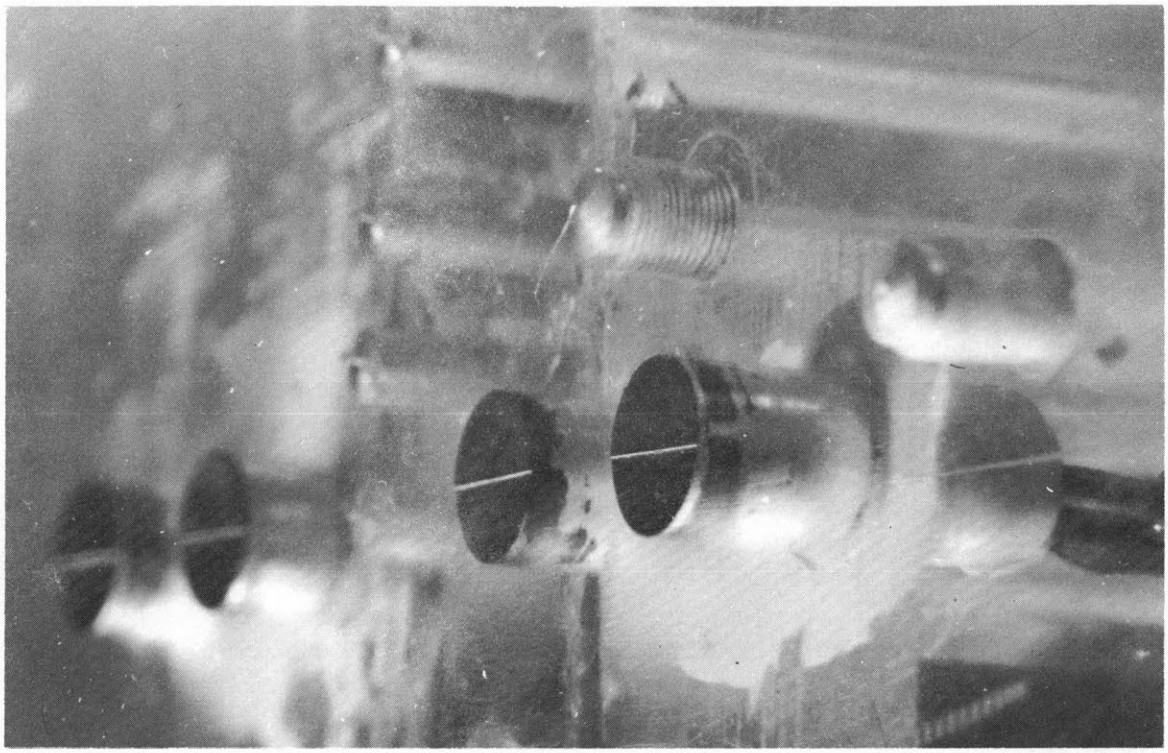

FIG. 4 SKIN-FRICTION FENCES

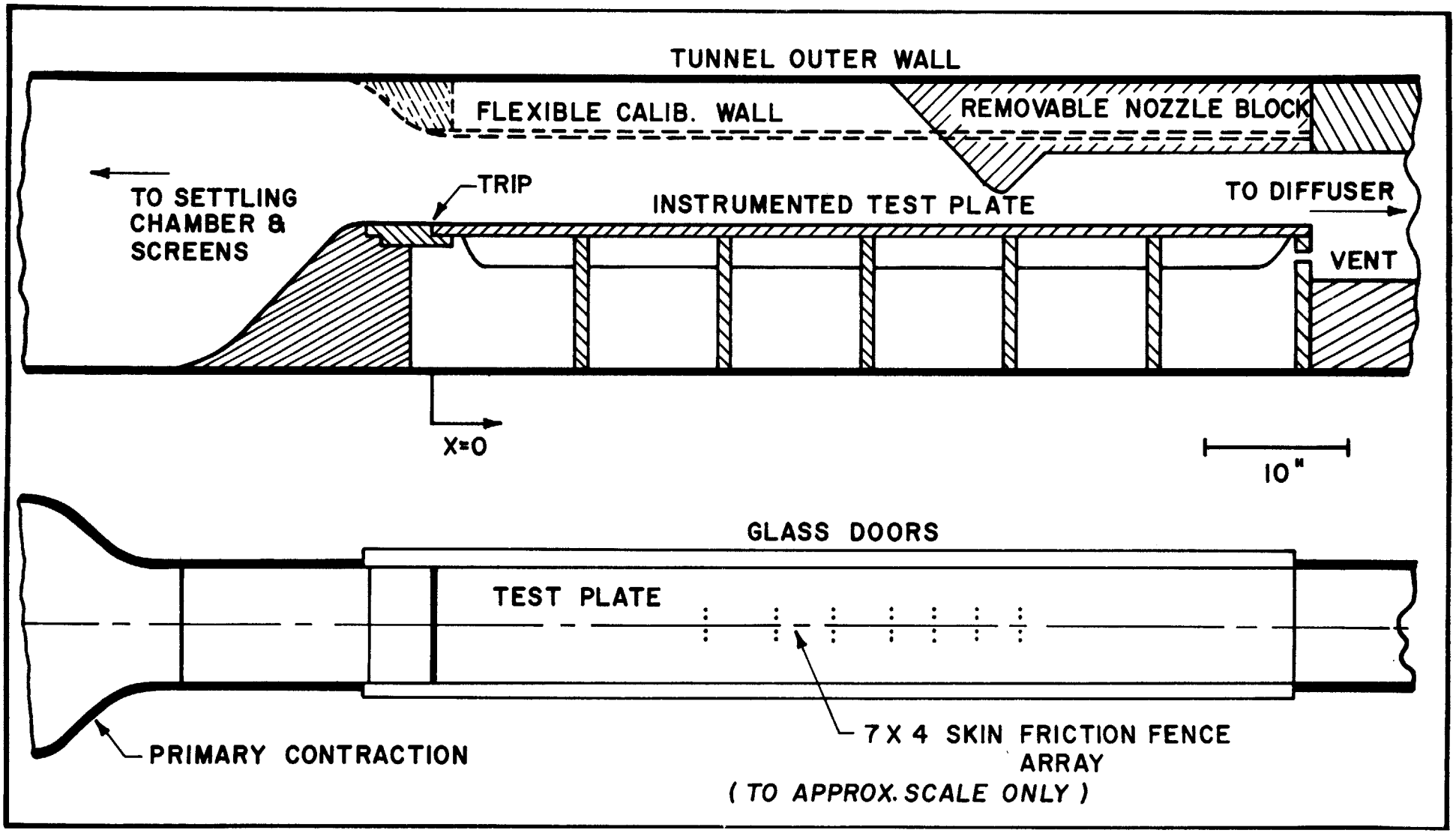

FIG. 5 SCHEMATIC LAYOUT OF TEST SECTION

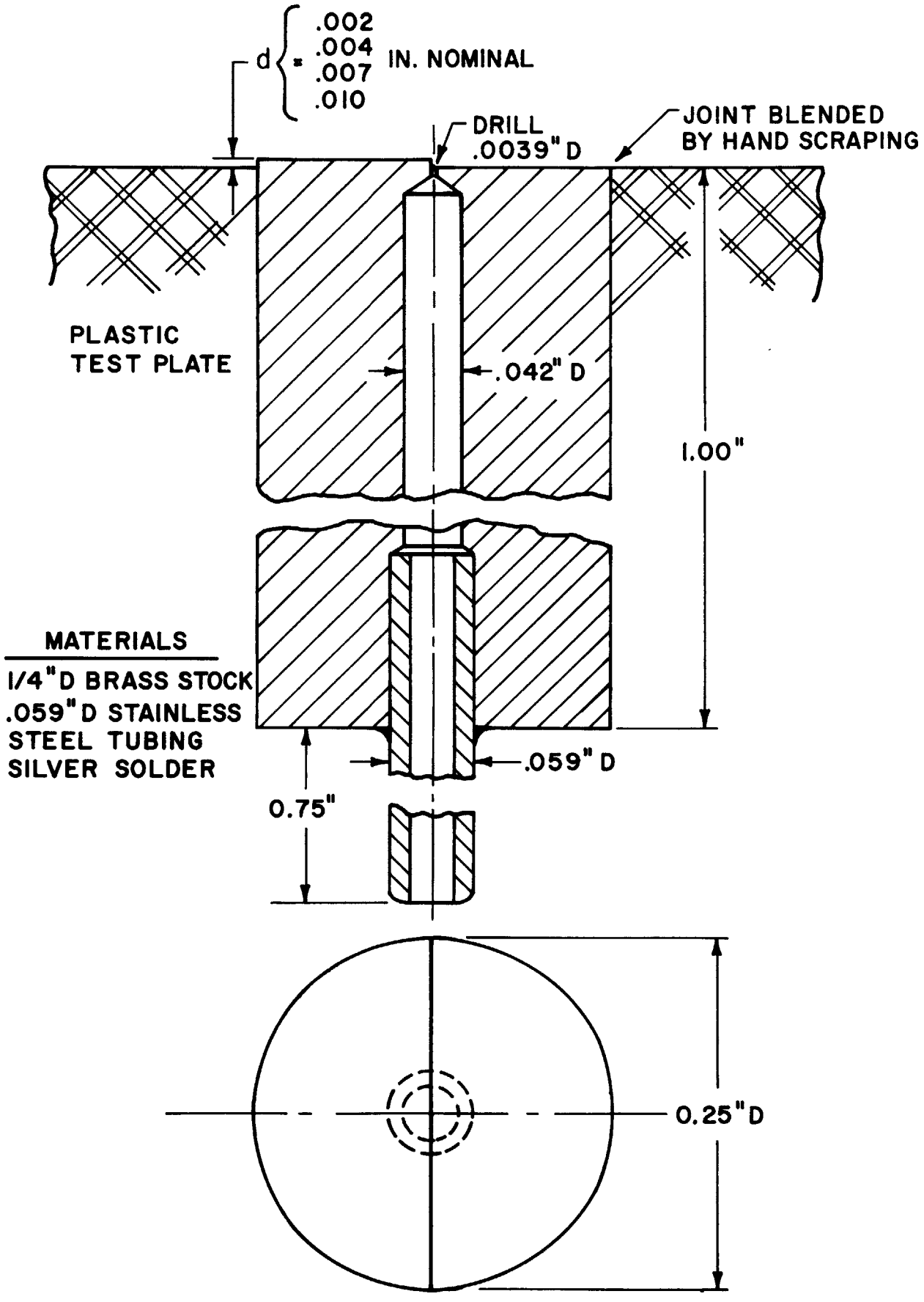

FIG. 6 CONSTRUCTION OF SKIN-FRICTION FENCES

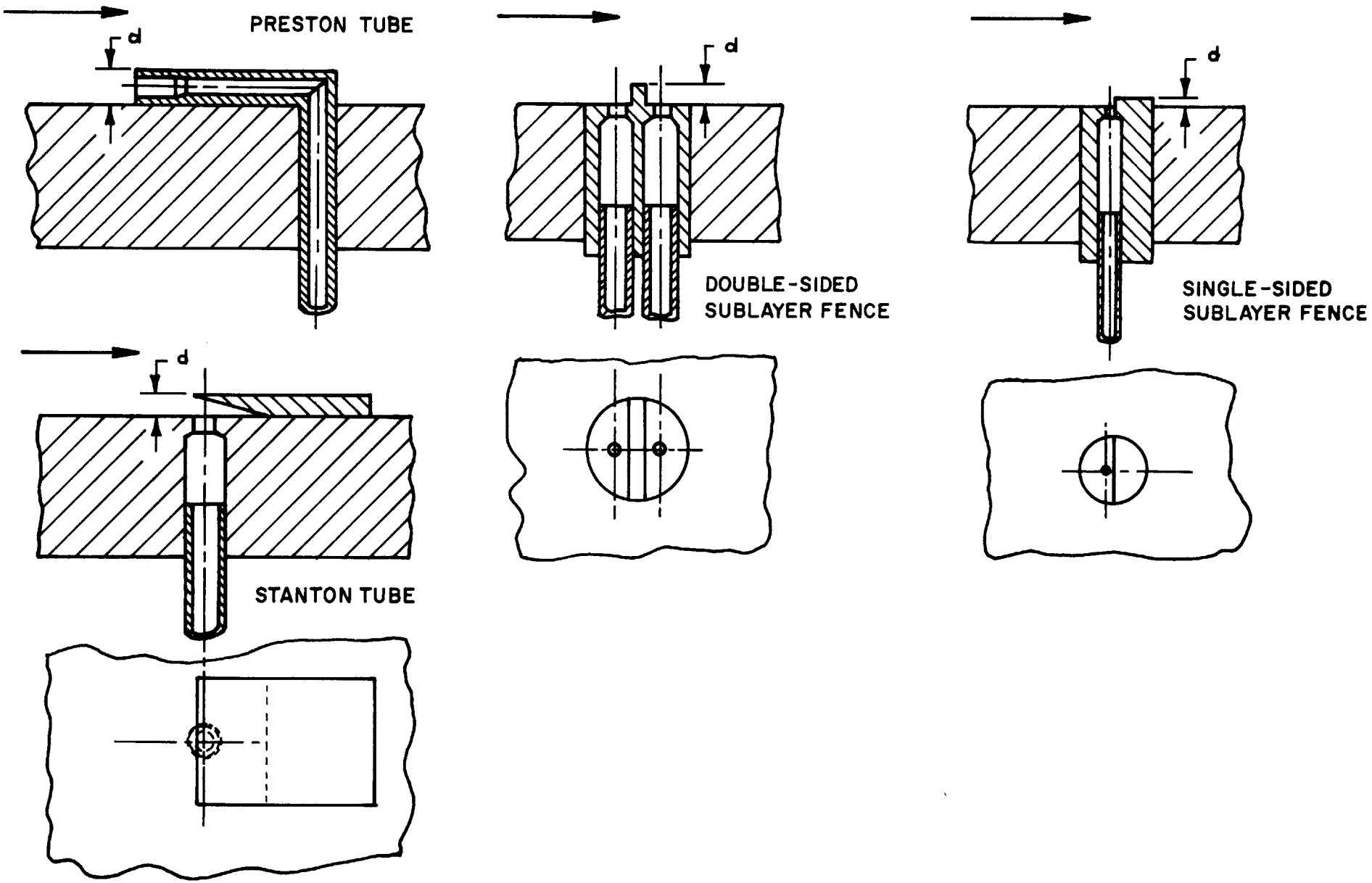

FIG. 7 VARIOUS WALL-PITOT GEOMETRIES

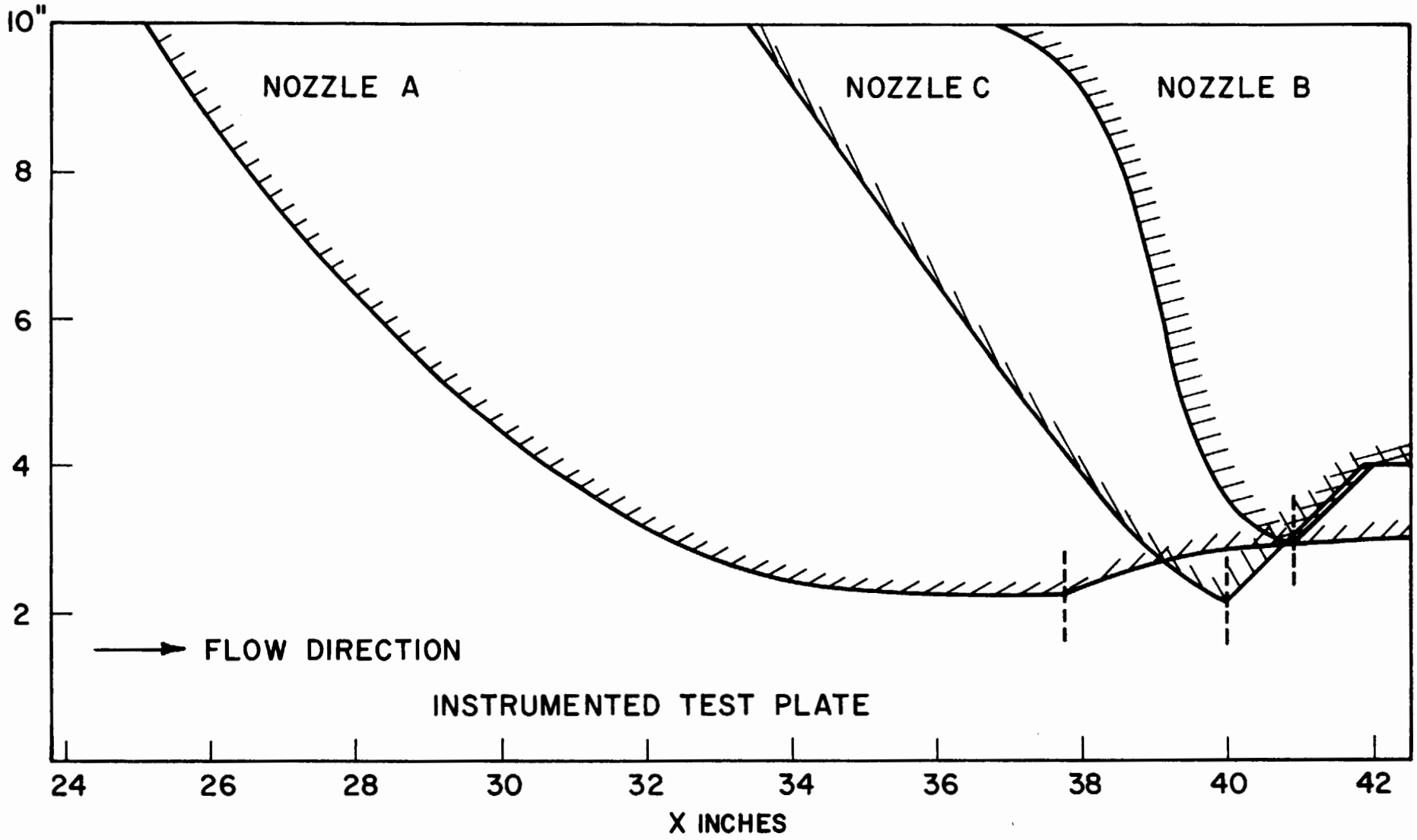

FIG 8. TEST-SECTION NOZZLE PROFILES

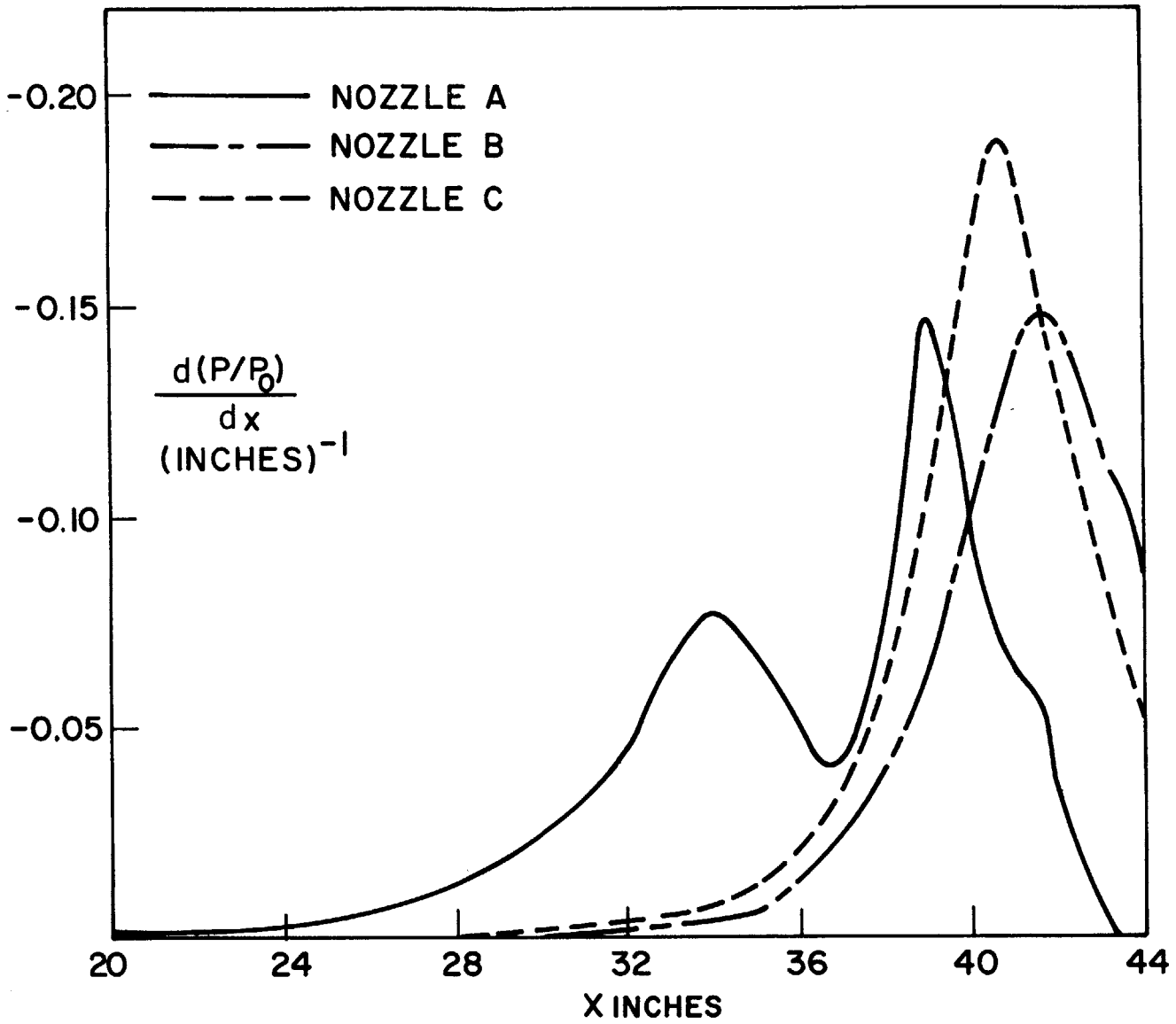

FIG. 9 (CONTINUED) TEST SECTION PRESSURE GRADIENT DISTRIBUTIONS

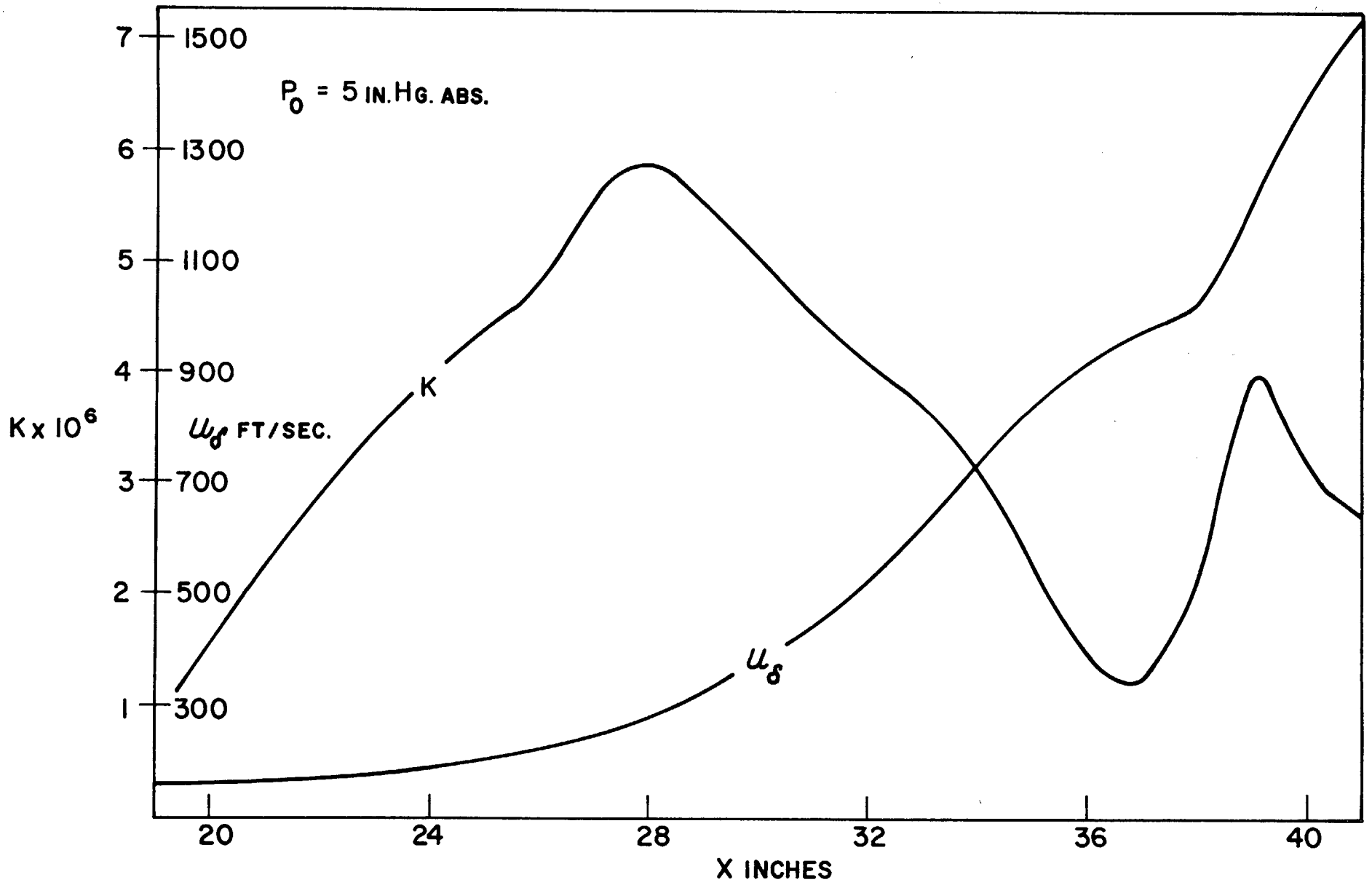

FIG. 9 VELOCITY AND ACCELERATION PARAMETER DISTRIBUTIONS — NOZZLE A

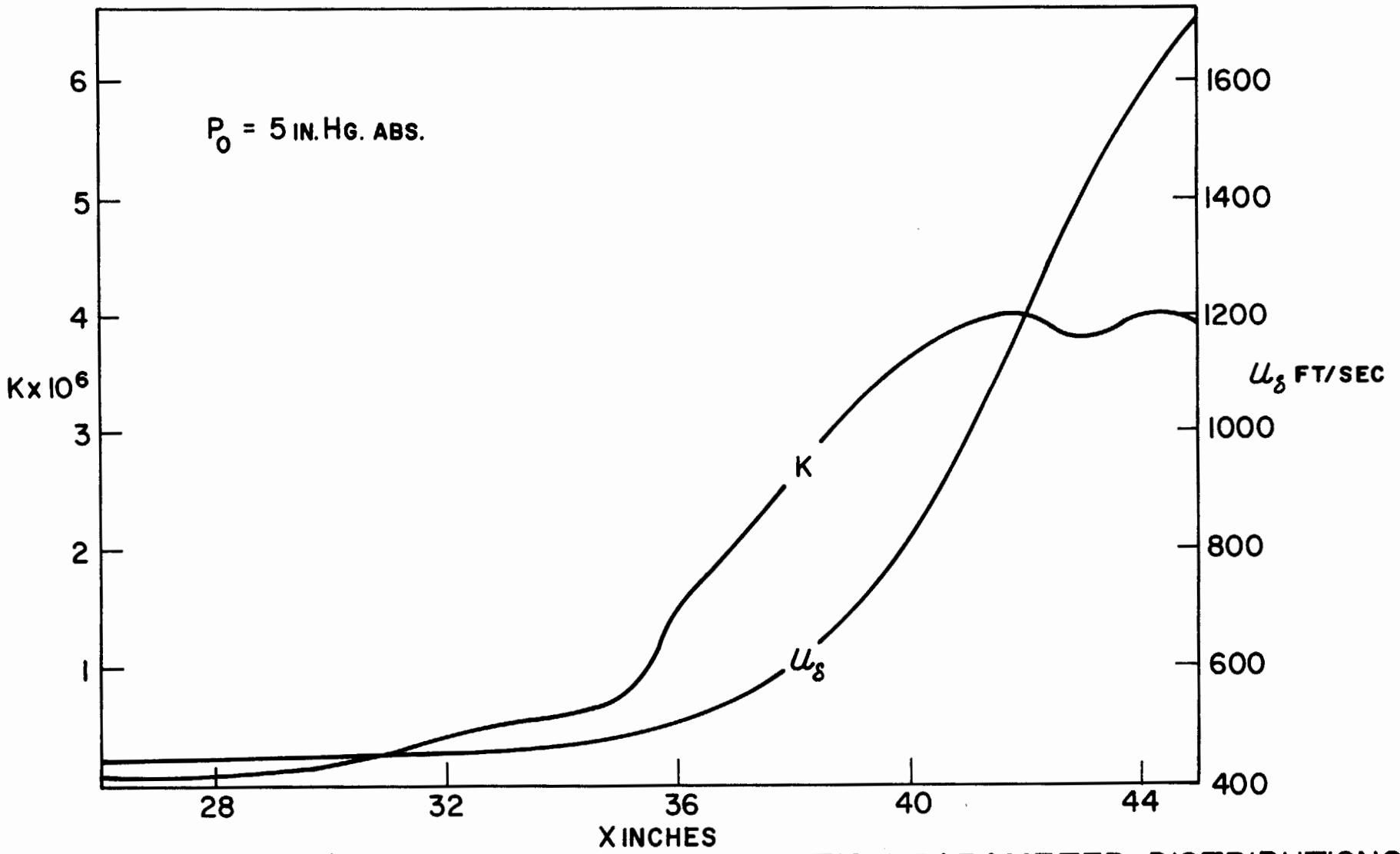

FIG. 9 (CONTINUED) VELOCITY AND ACCELERATION PARAMETER DISTRIBUTIONS
NOZZLE B

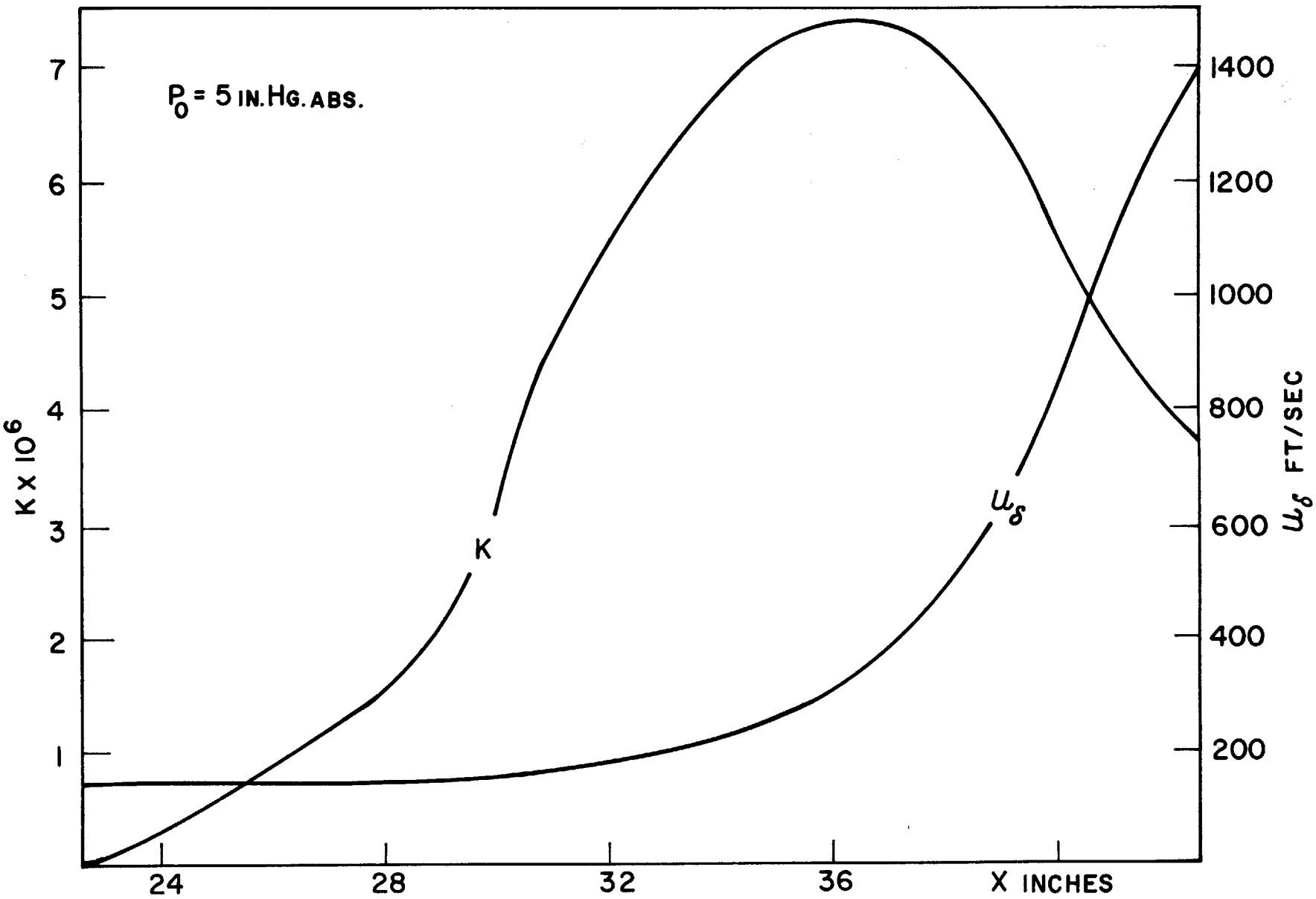

FIG. 9 (CONT) VELOCITY AND ACCELERATION PARAMETER DISTRIBUTIONS
NOZZLE C

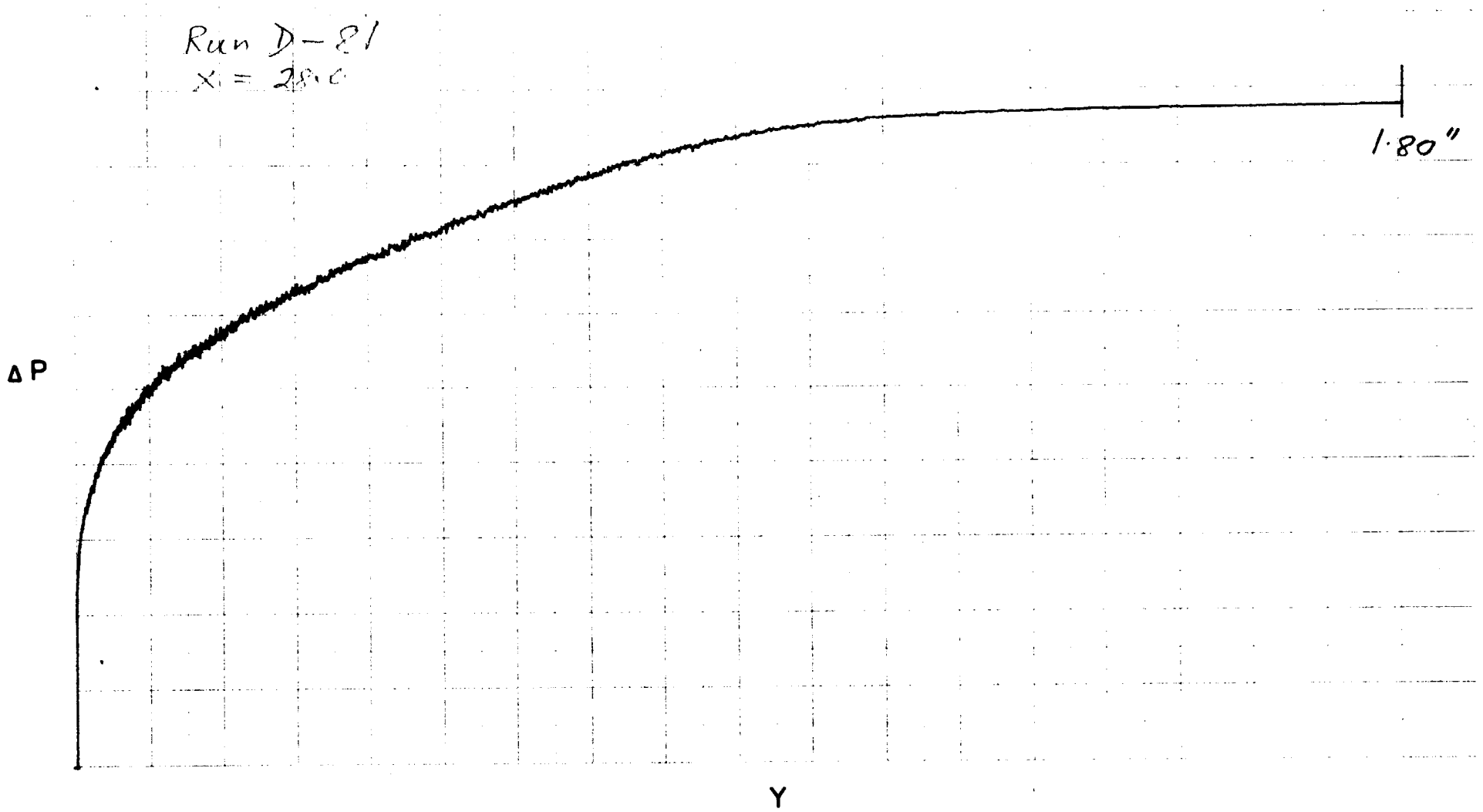

FIG. 10 TYPICAL X-Y RECORDER TRACE

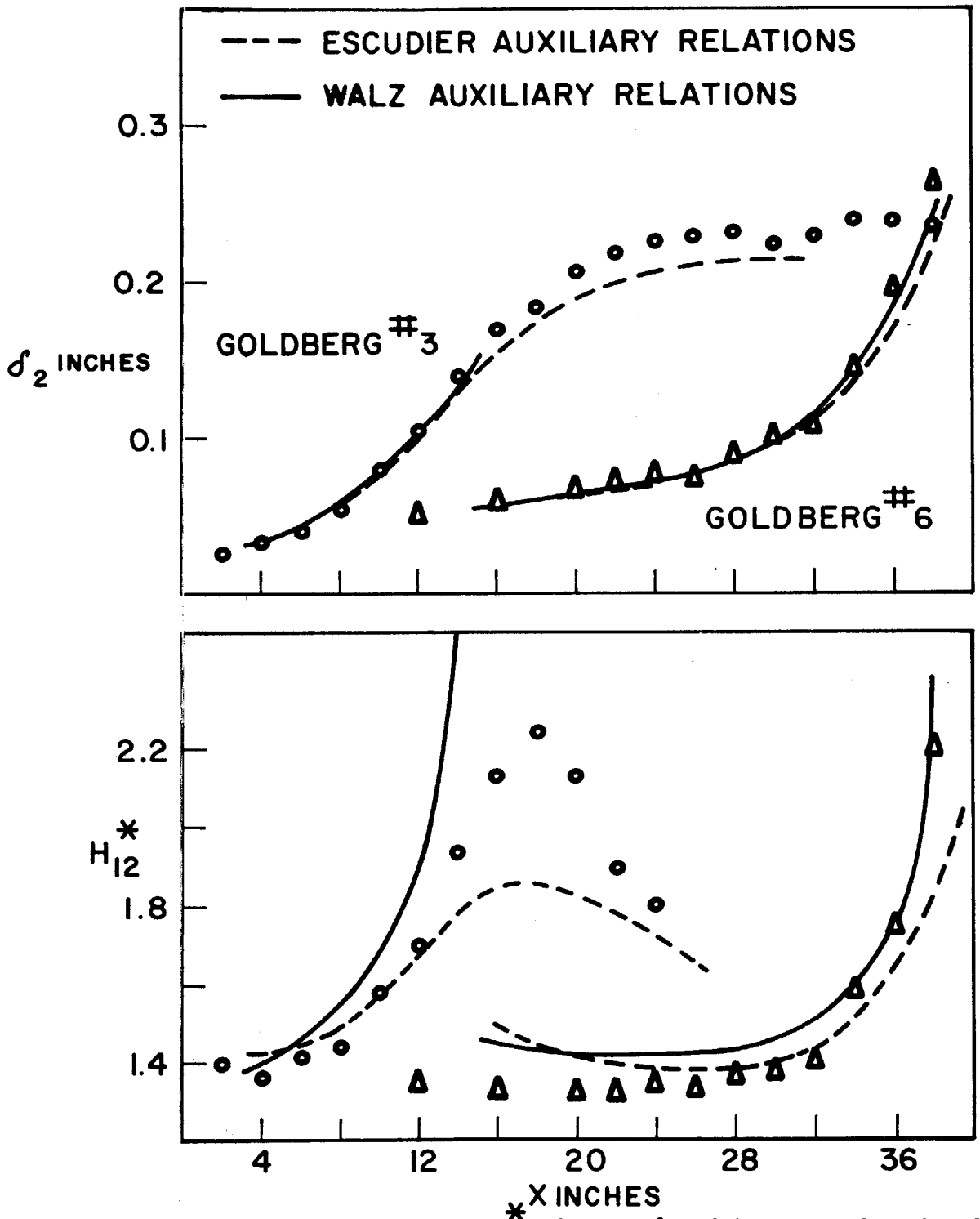

FIG. 11 COMPARISON OF H_{12}^* AND δ_2 CALCULATIONS WITH DATA OF MOSES[50] AND GOLDBERG[62] IN ADVERSE PRESSURE GRADIENTS

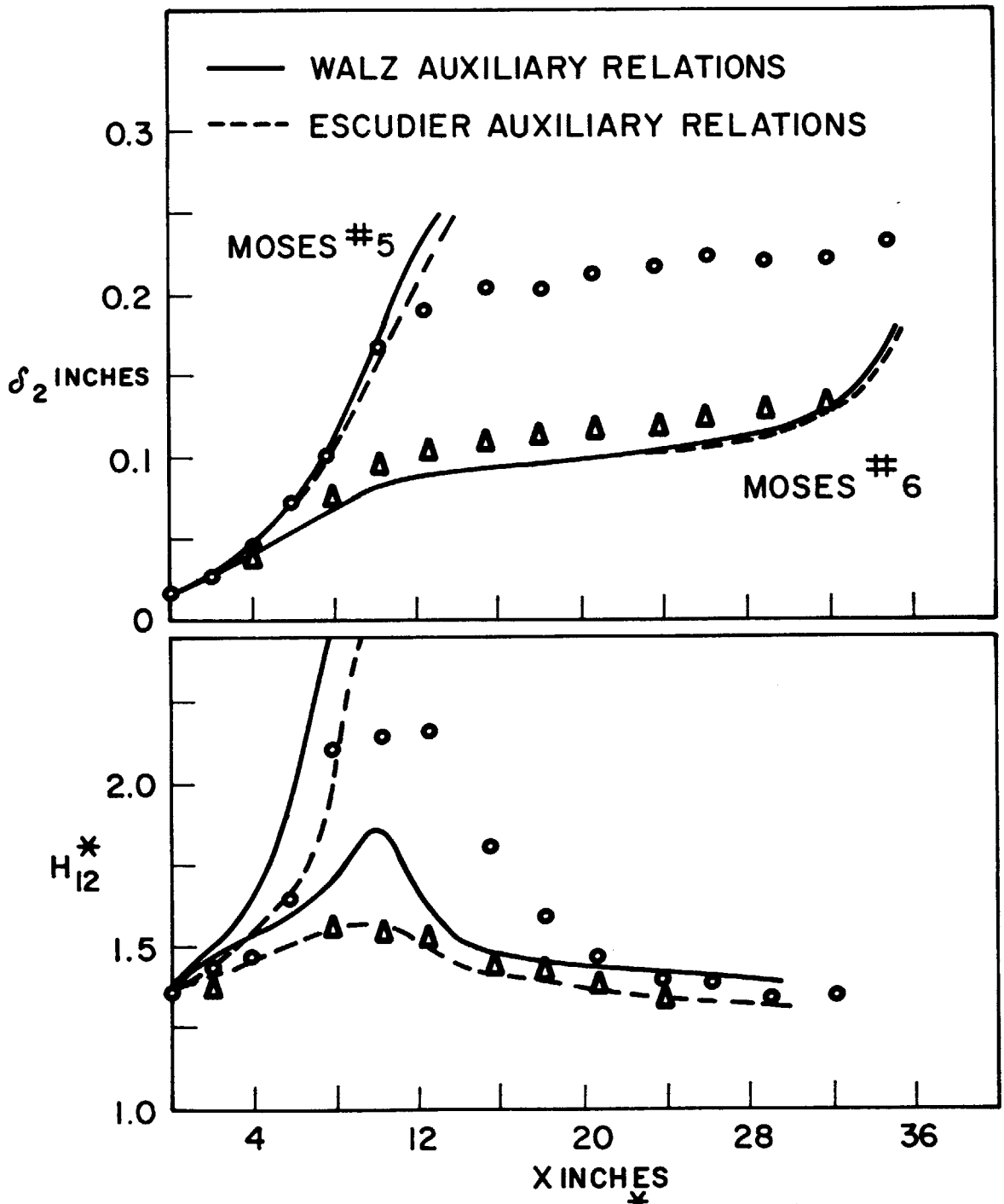

FIG. 11 (CONT.) COMPARISON OF H_{12}^* AND δ_2 CALCULATIONS WITH DATA OF MOSES[50] AND GOLDBERG[62] IN ADVERSE PRESSURE GRADIENTS

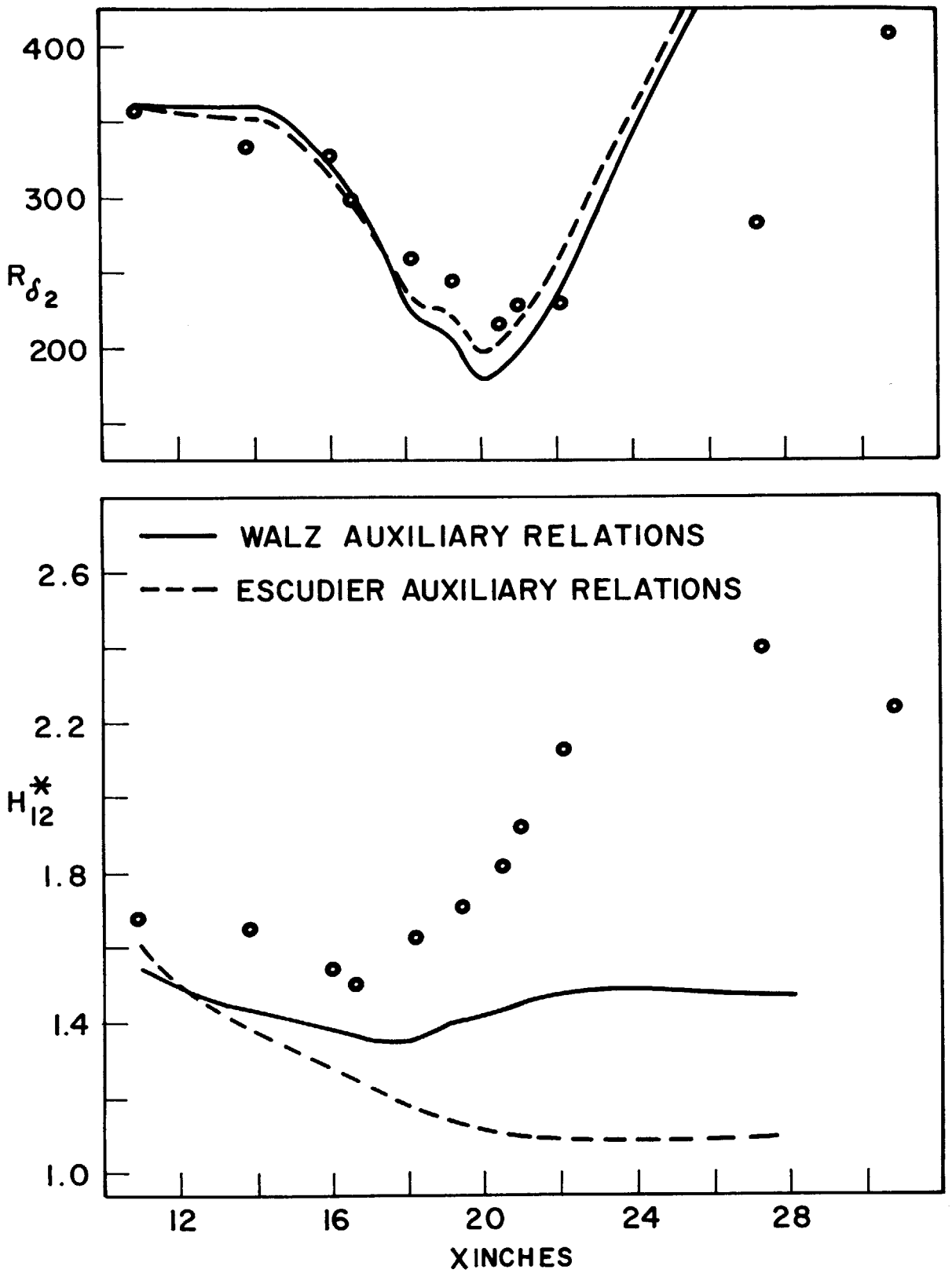

FIG. 12 COMPARISON OF H_{12}^* AND R_{δ_2} CALCULATIONS WITH DATA OF LAUNDER[28] IN A FAVORABLE PRESSURE GRADIENT

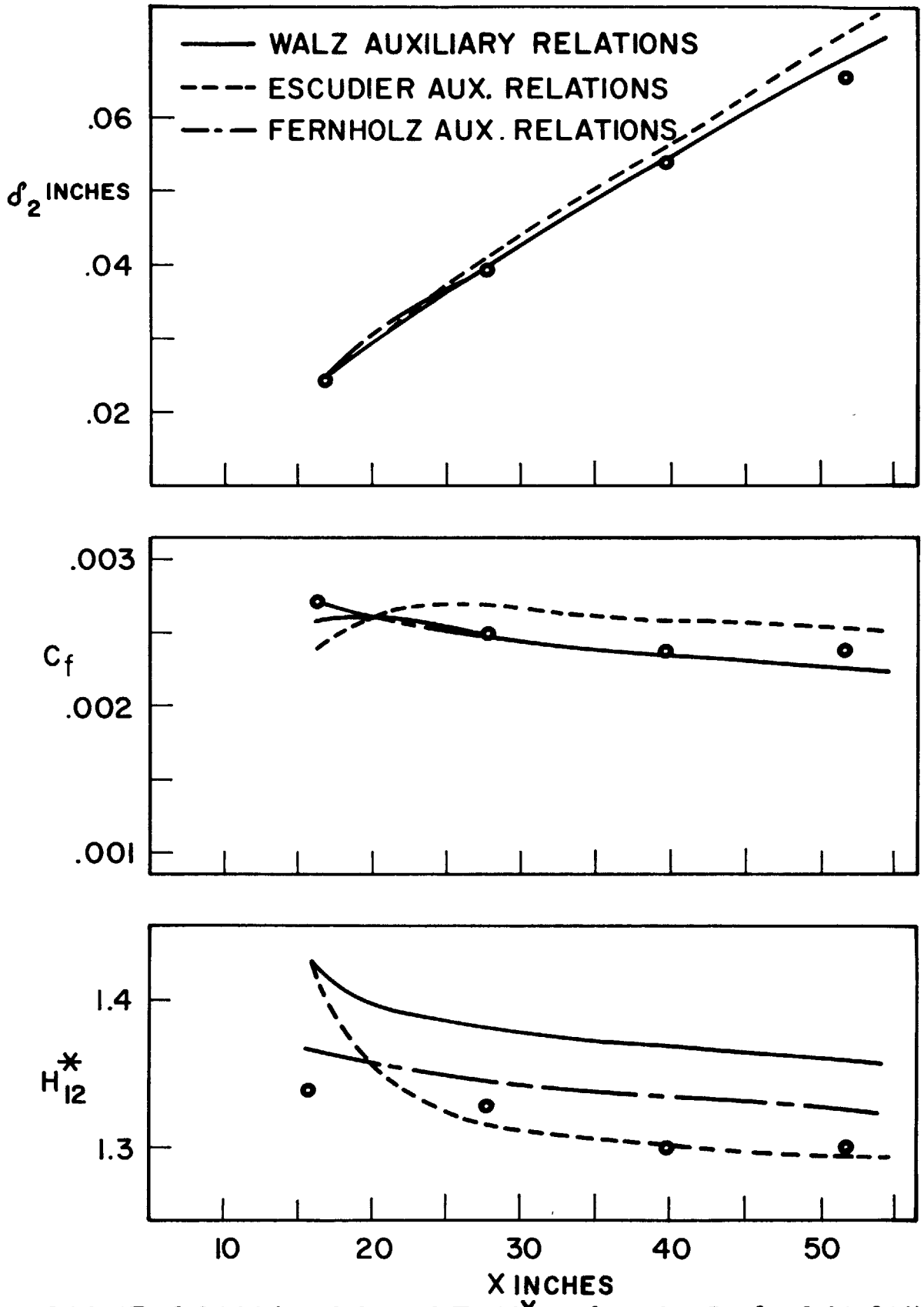

FIG. 13 COMPARISON OF H_{12}^*, C_f AND δ_2 CALCULATIONS WITH DATA OF SMITH AND WALKER[63] IN ZERO PRESSURE GRADIENT

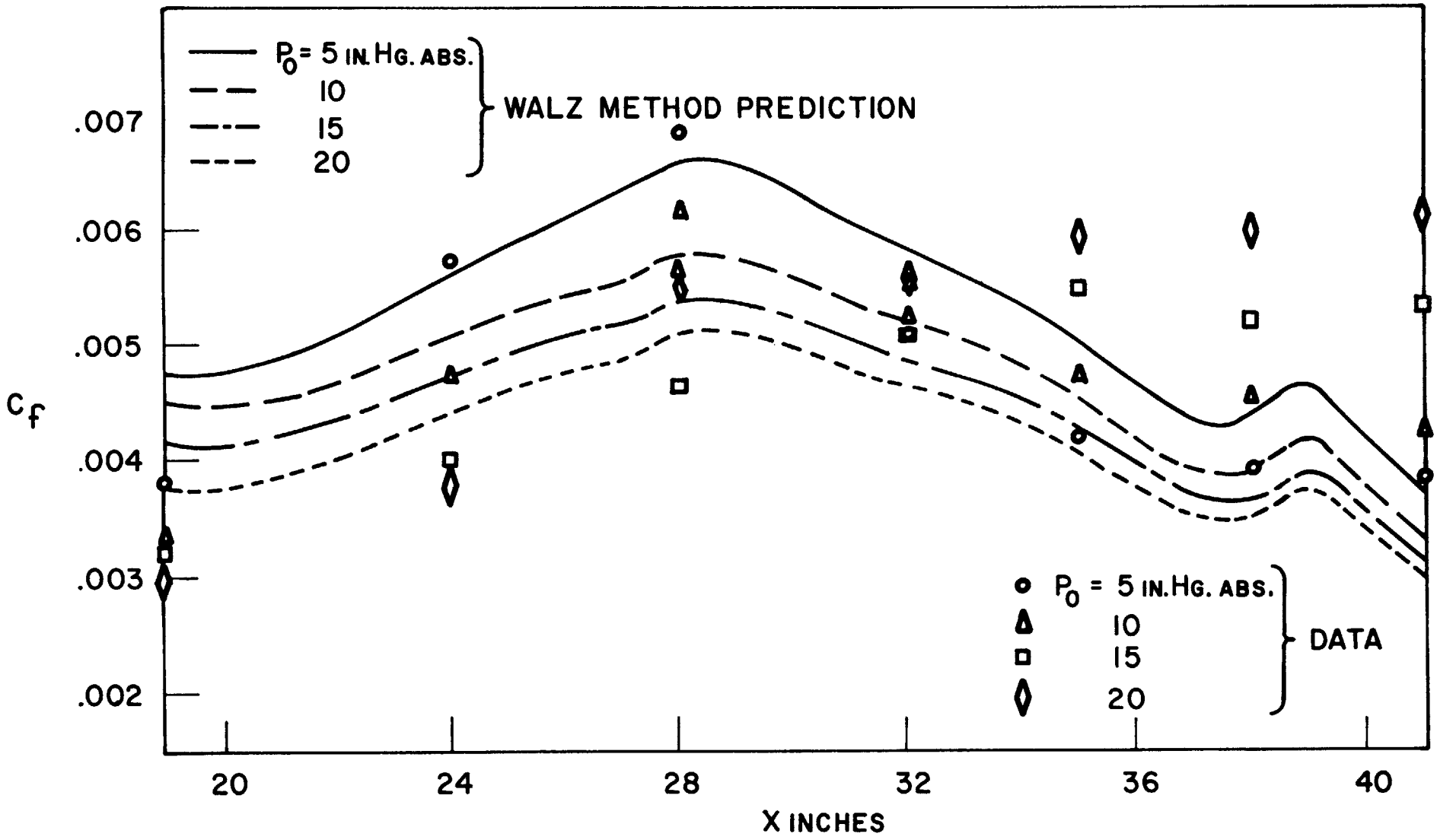

FIG. 14 COMPARISON OF MEASURED AND PREDICTED SKIN FRICTION NOZZLE A

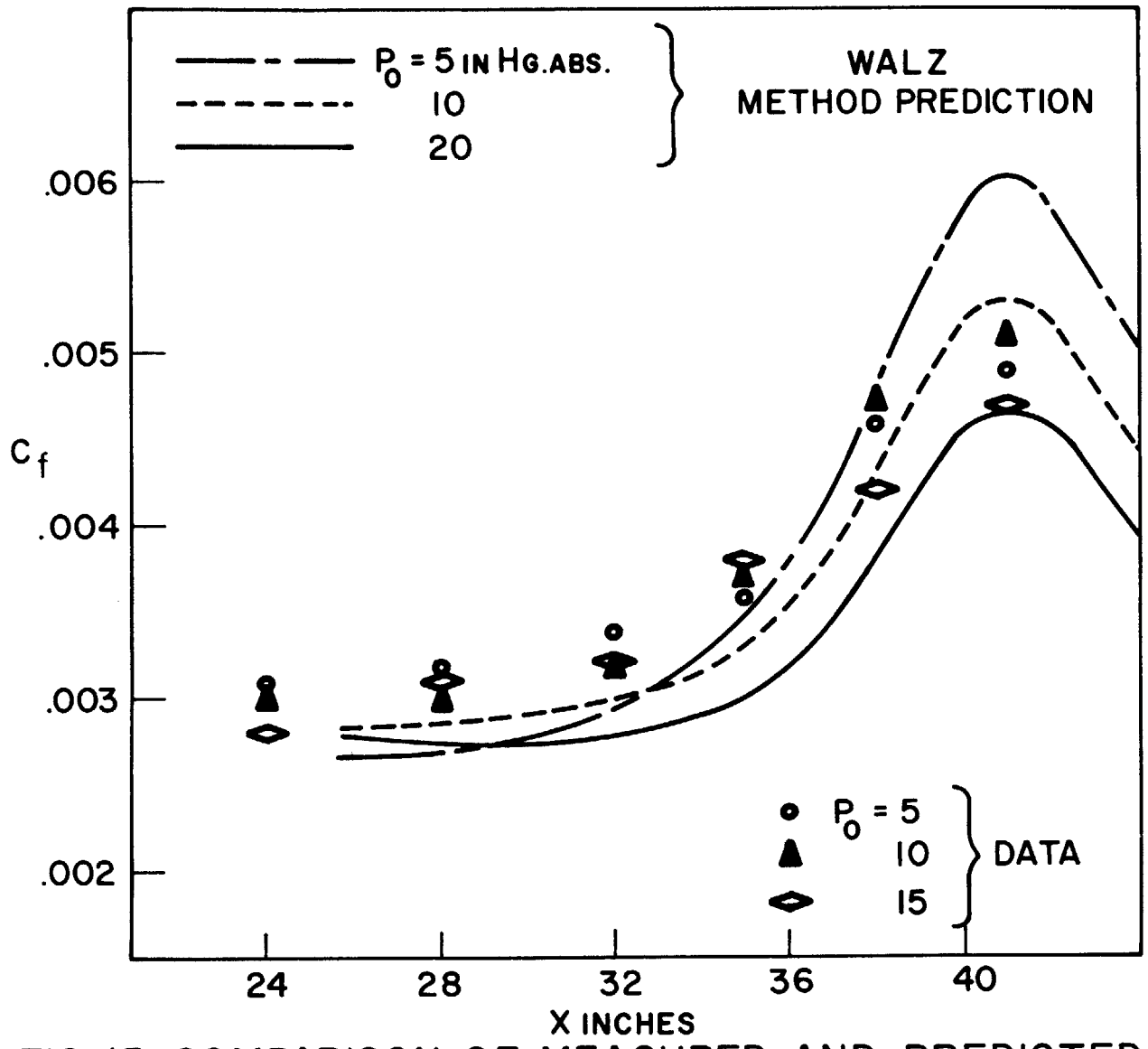

FIG. 15 COMPARISON OF MEASURED AND PREDICTED SKIN FRICTION- NOZZLE B

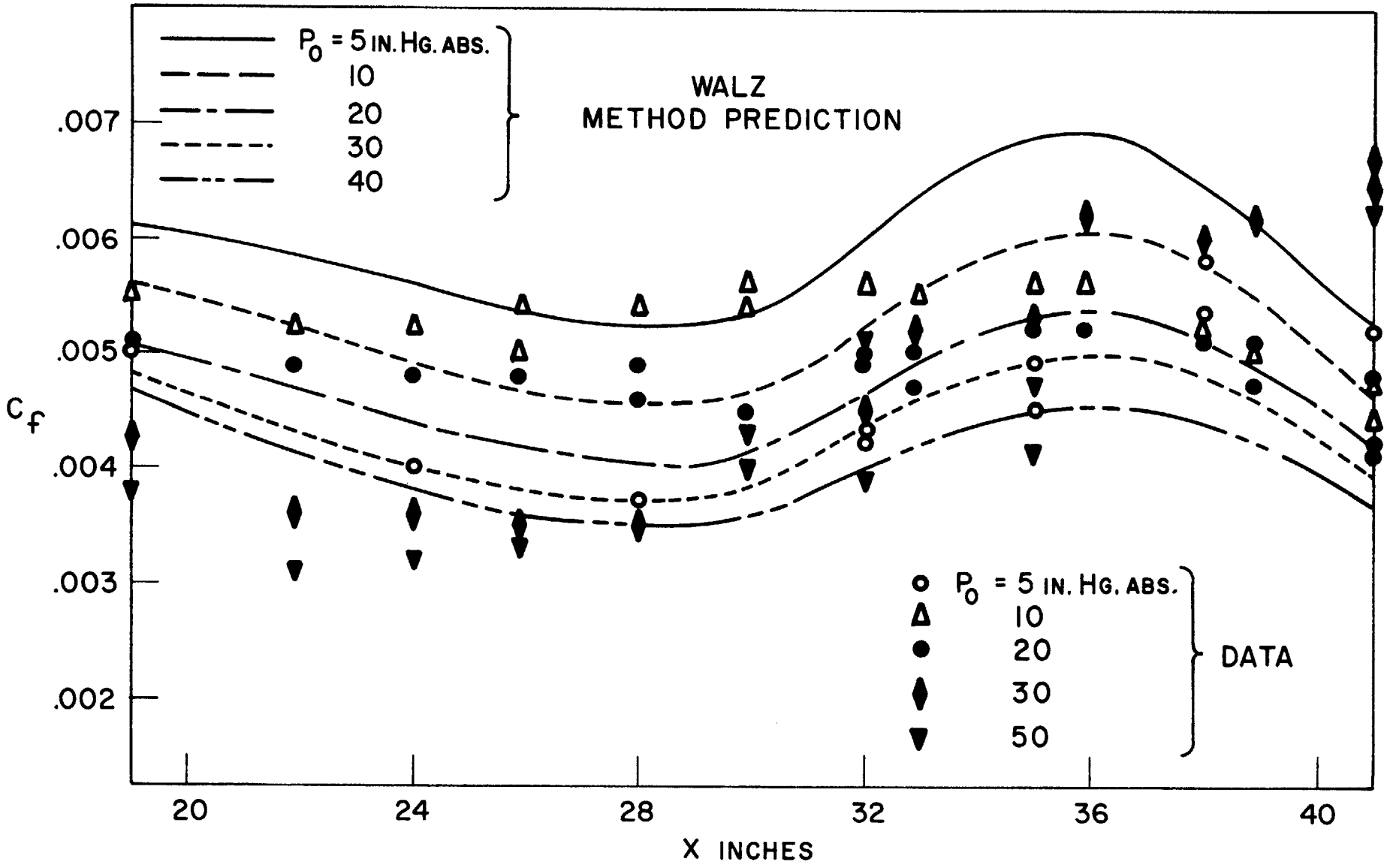

FIG. 16 COMPARISON OF MEASURED AND PREDICTED SKIN FRICTION NOZZLE C

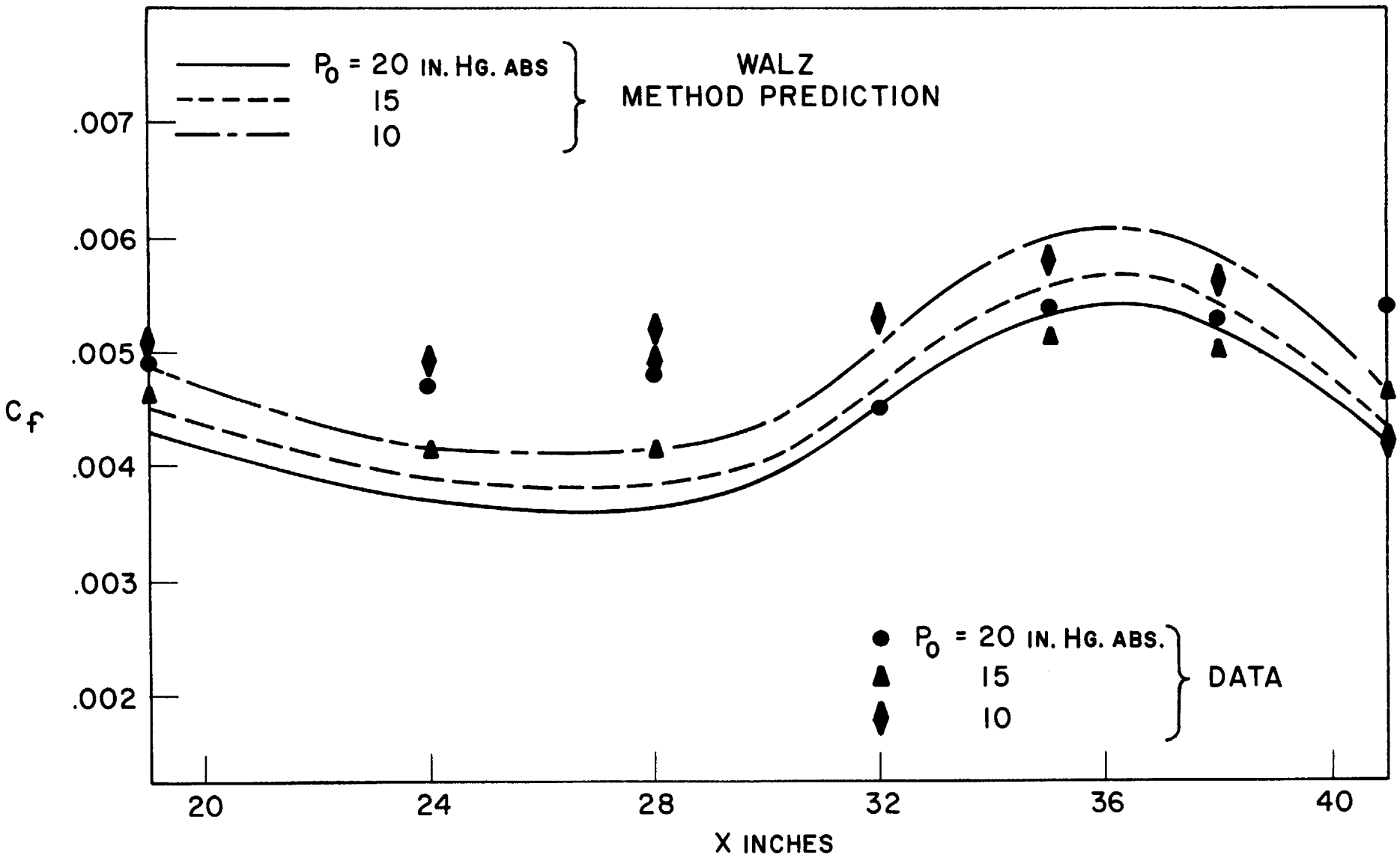

FIG. 17 COMPARISON OF MEASURED AND PREDICTED SKIN FRICTION NOZZLE C WITH SPOILER

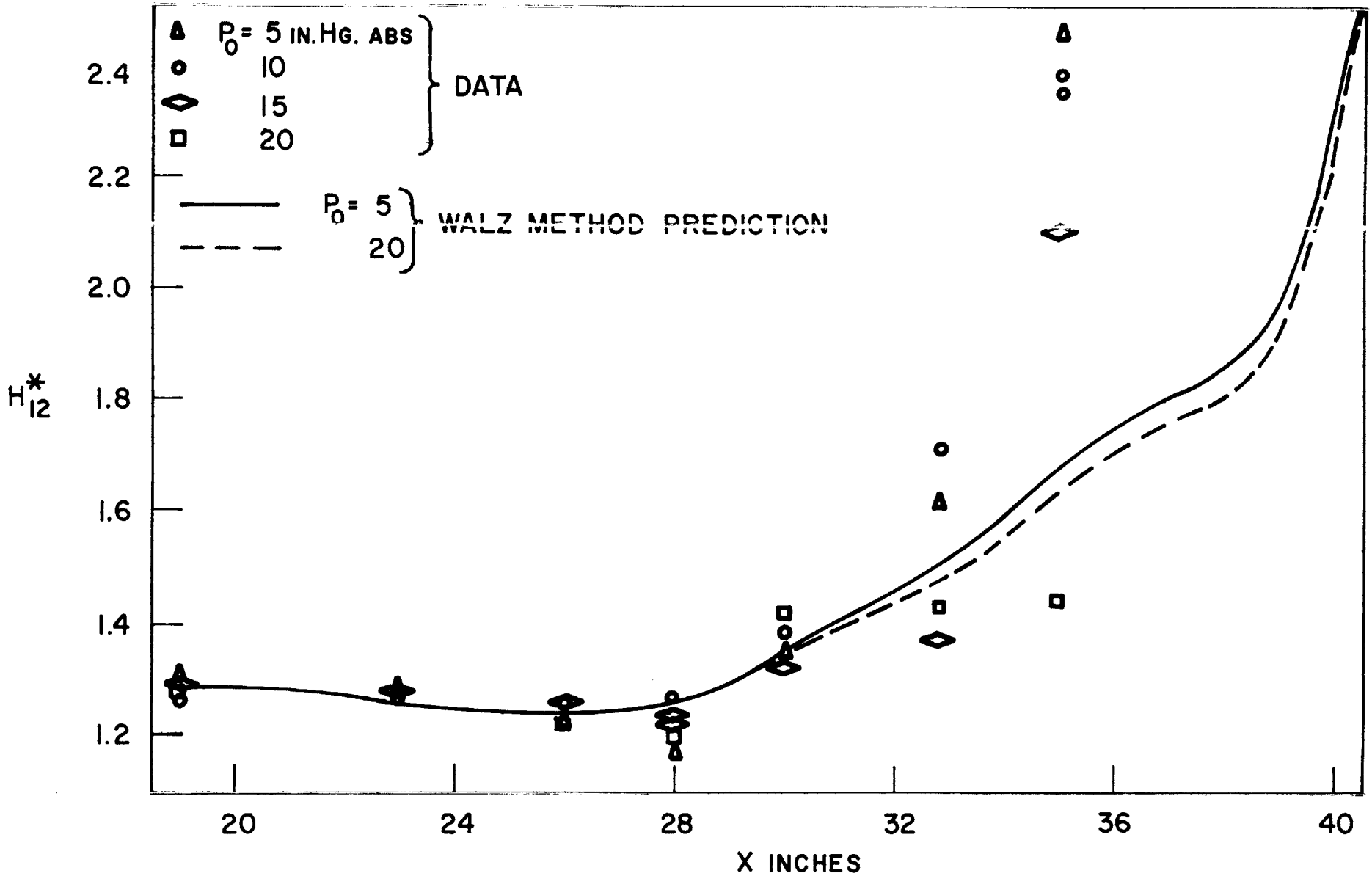

FIG. 18 SHAPE FACTORS DEVELOPMENT
NOZZLE A

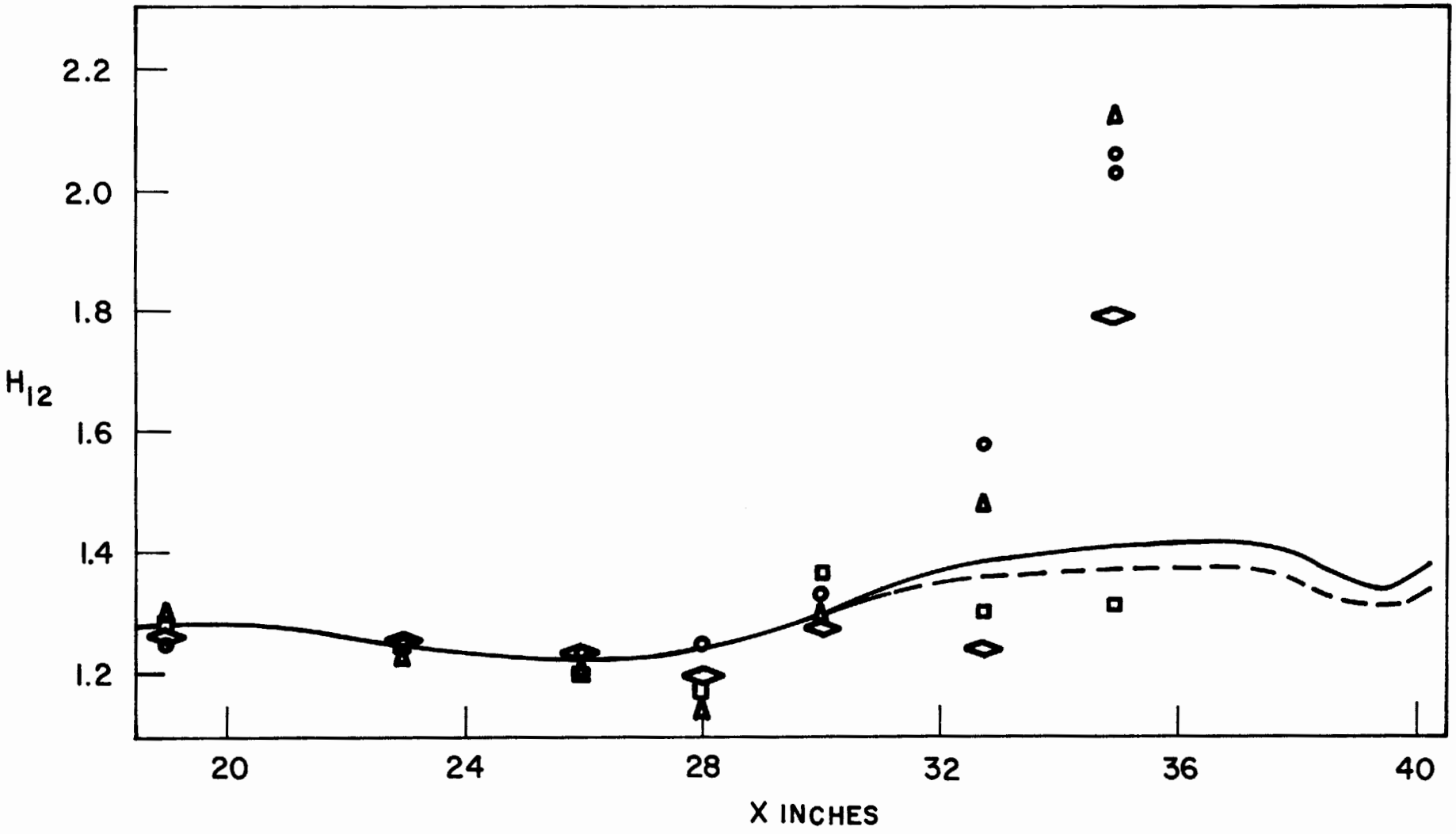

FIG. 18 (CONTINUED) SHAPE FACTORS DEVELOPMENT
NOZZLE A

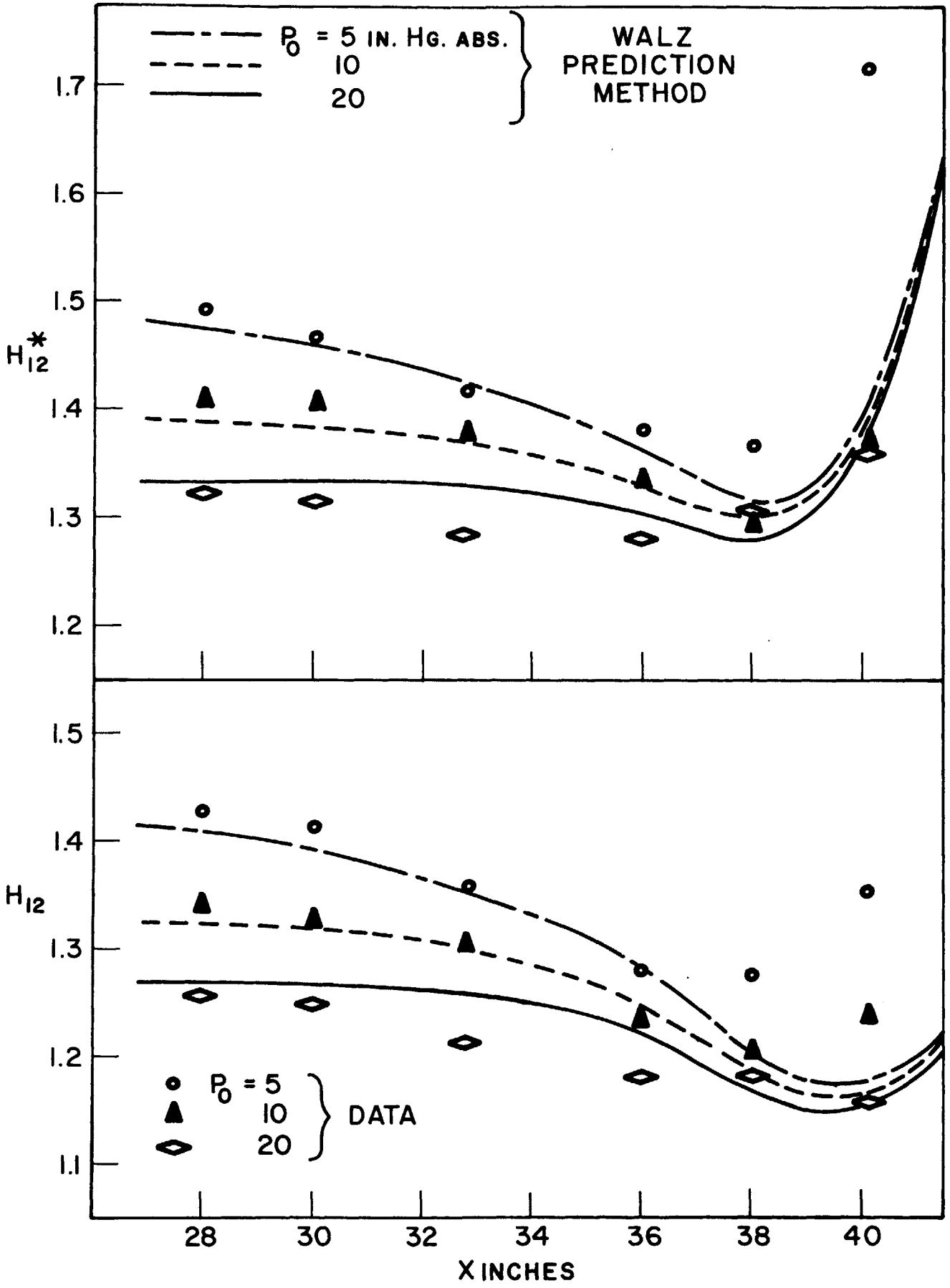

FIG. 19 SHAPE FACTORS DEVELOPMENT — NOZZLE B

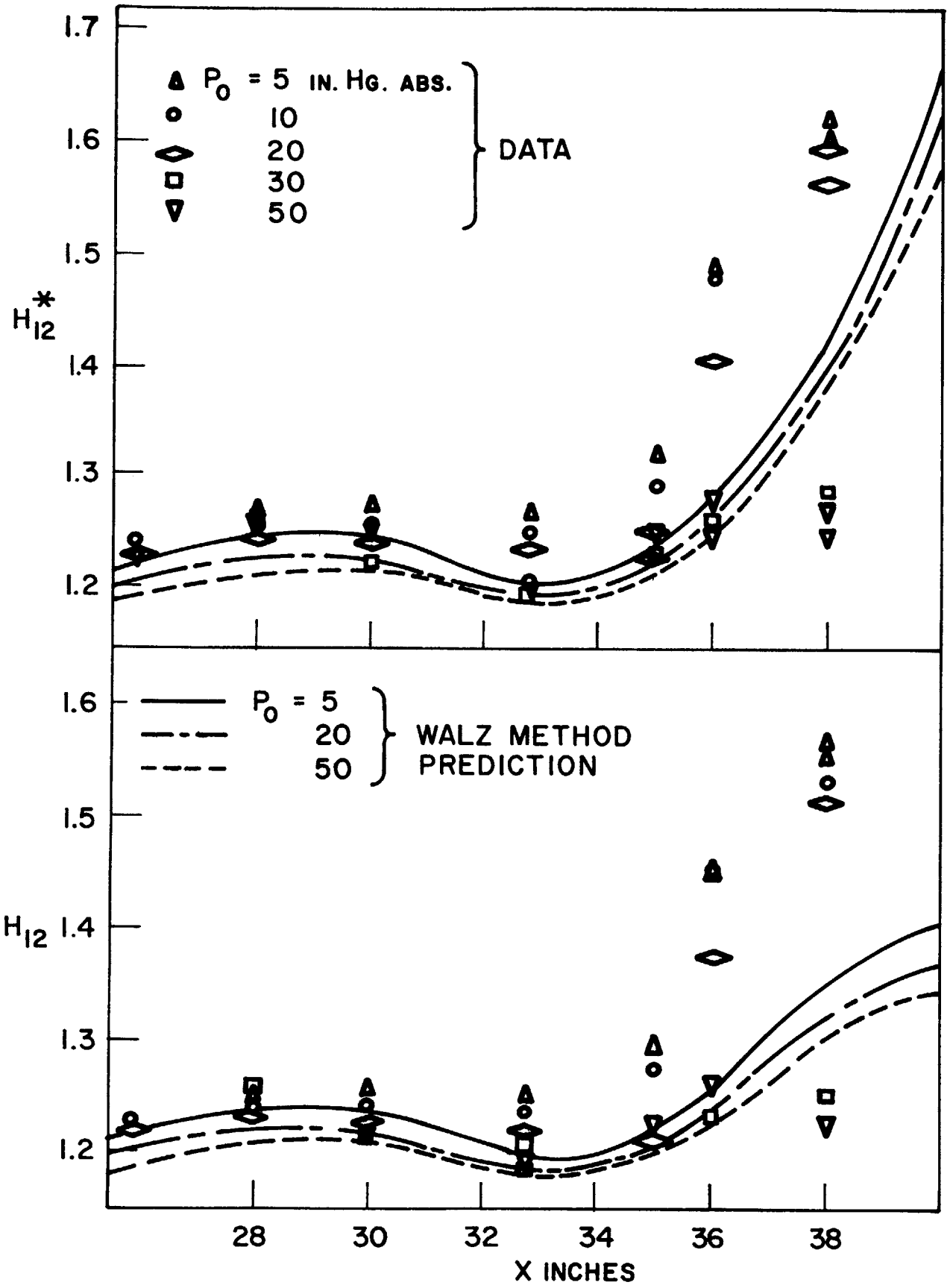

FIG. 20 SHAPE FACTORS DEVELOPMENT NOZZLE C

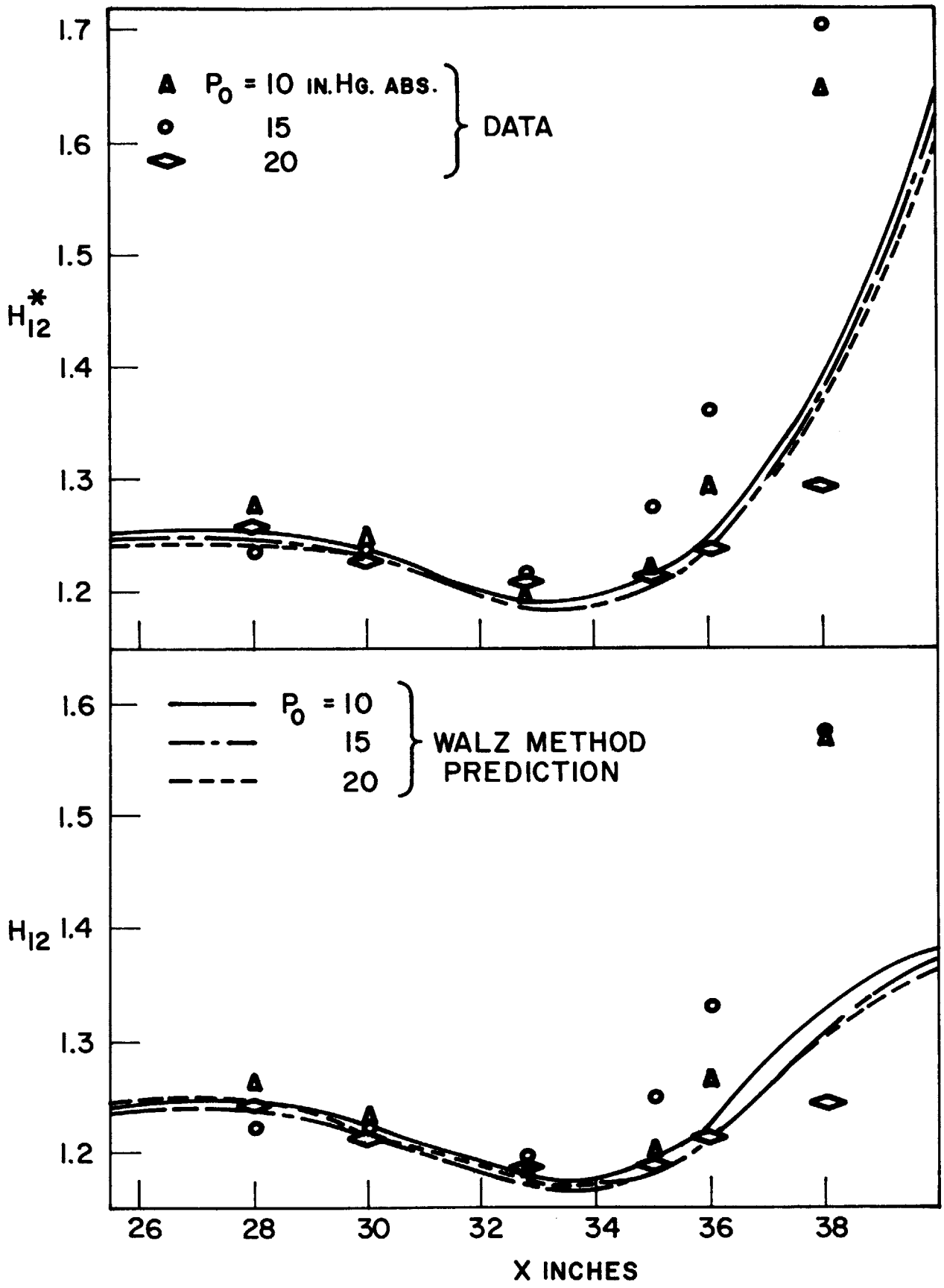

FIG. 21 SHAPE FACTORS DEVELOPMENT
NOZZLE C WITH SPOILER

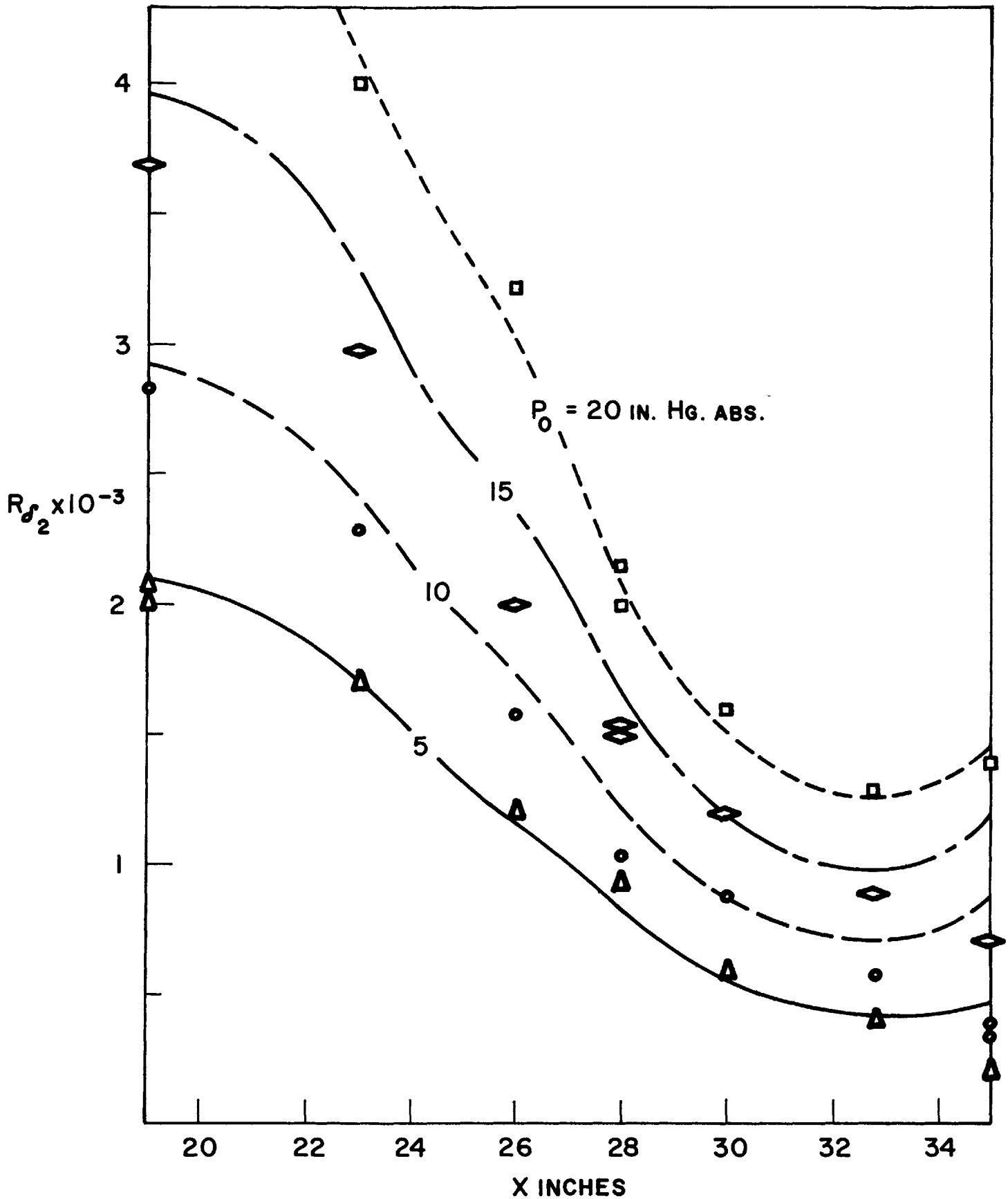

FIG. 22 COMPARISON OF MEASURED AND COMPUTED R_{δ_2} NOZZLE A

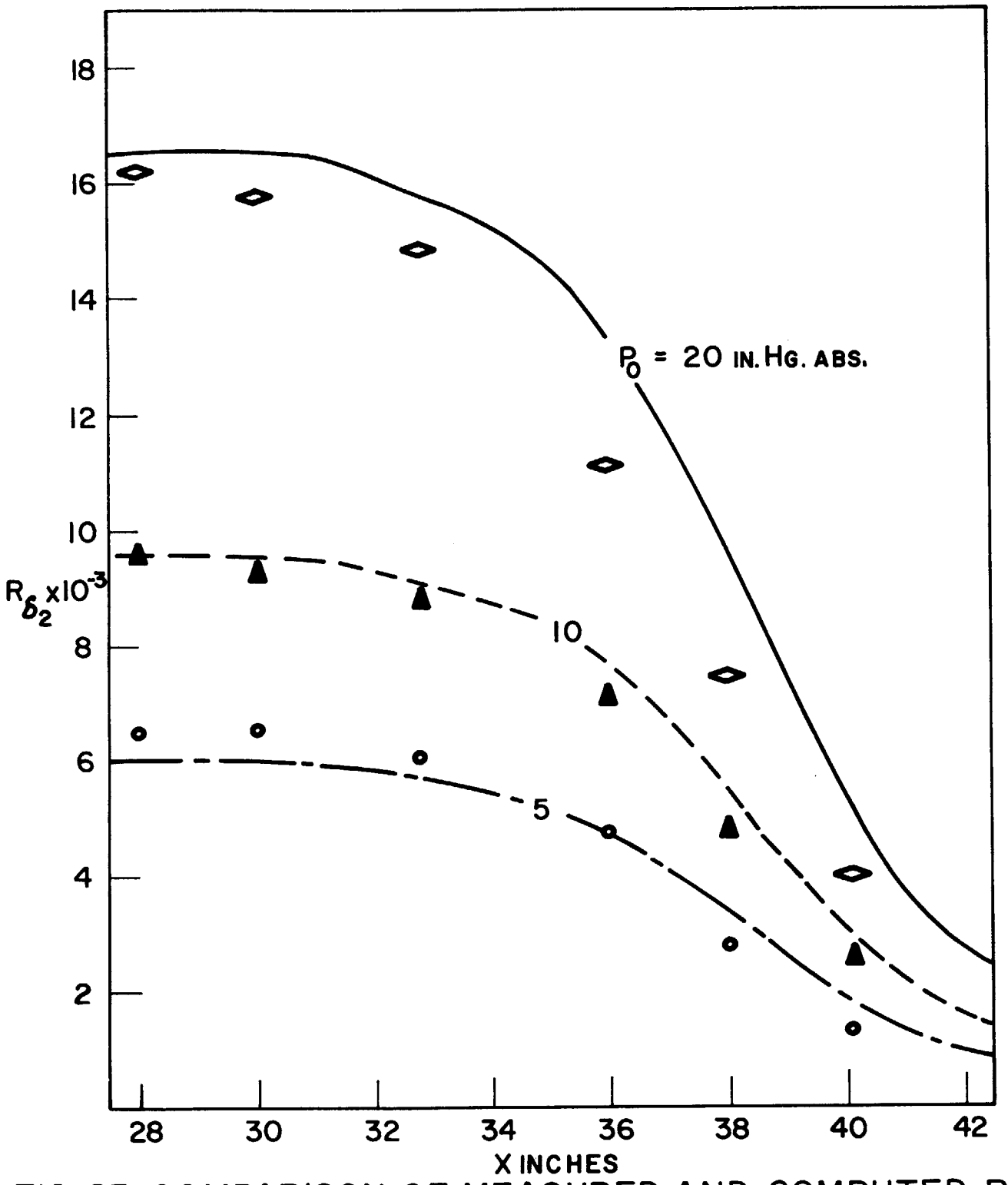

FIG. 23 COMPARISON OF MEASURED AND COMPUTED R_{δ_2}
NOZZLE B

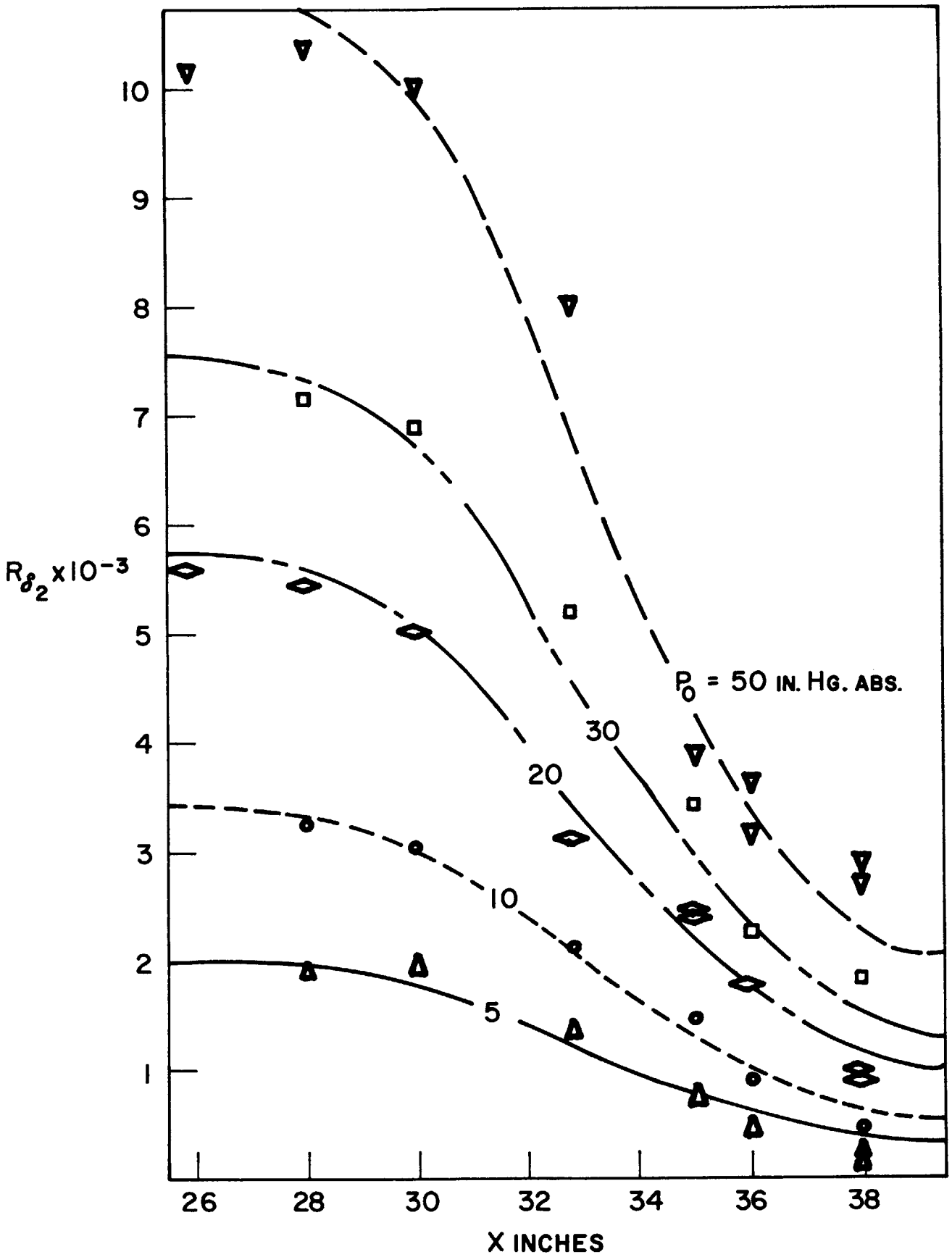

FIG. 24 COMPARISON OF MEASURED AND COMPUTED R_{δ_2}
NOZZLE C

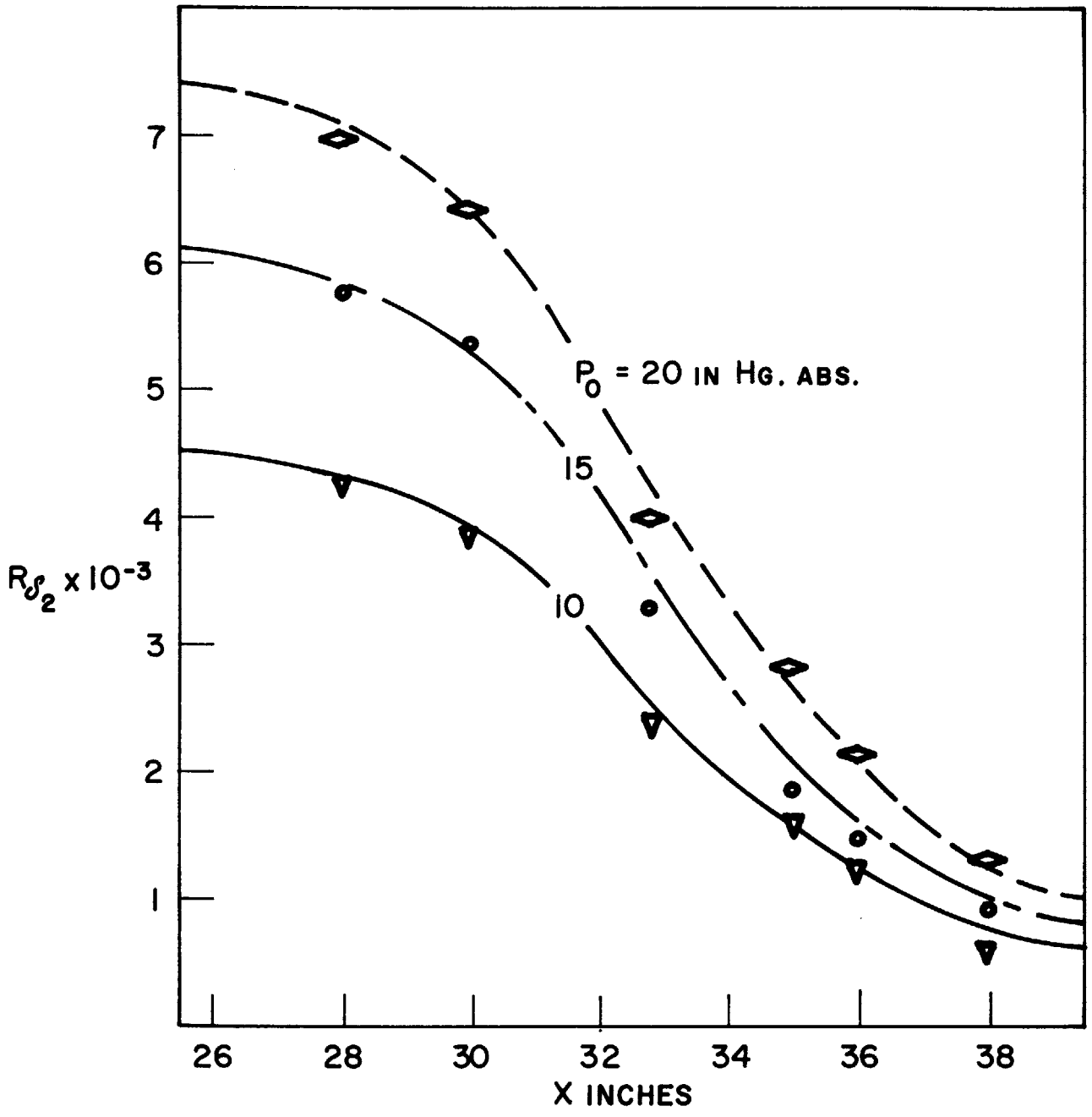

FIG. 25 COMPARISON OF MEASURED AND COMPUTED R_{δ_2} NOZZLE C WITH SPOILER

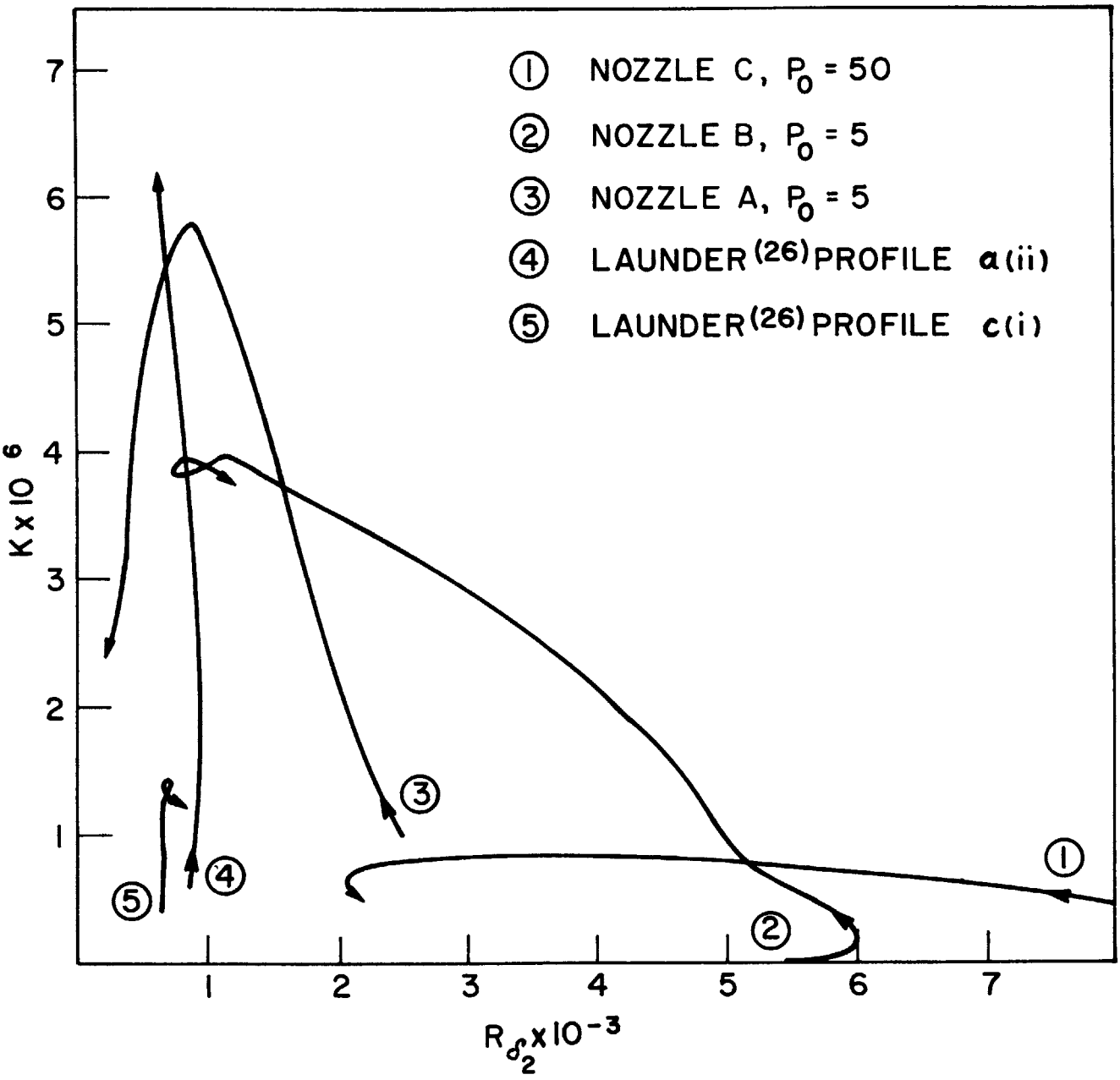

FIG. 26 TYPICAL TRAJECTORIES ON K– R_{δ_2} PLOT

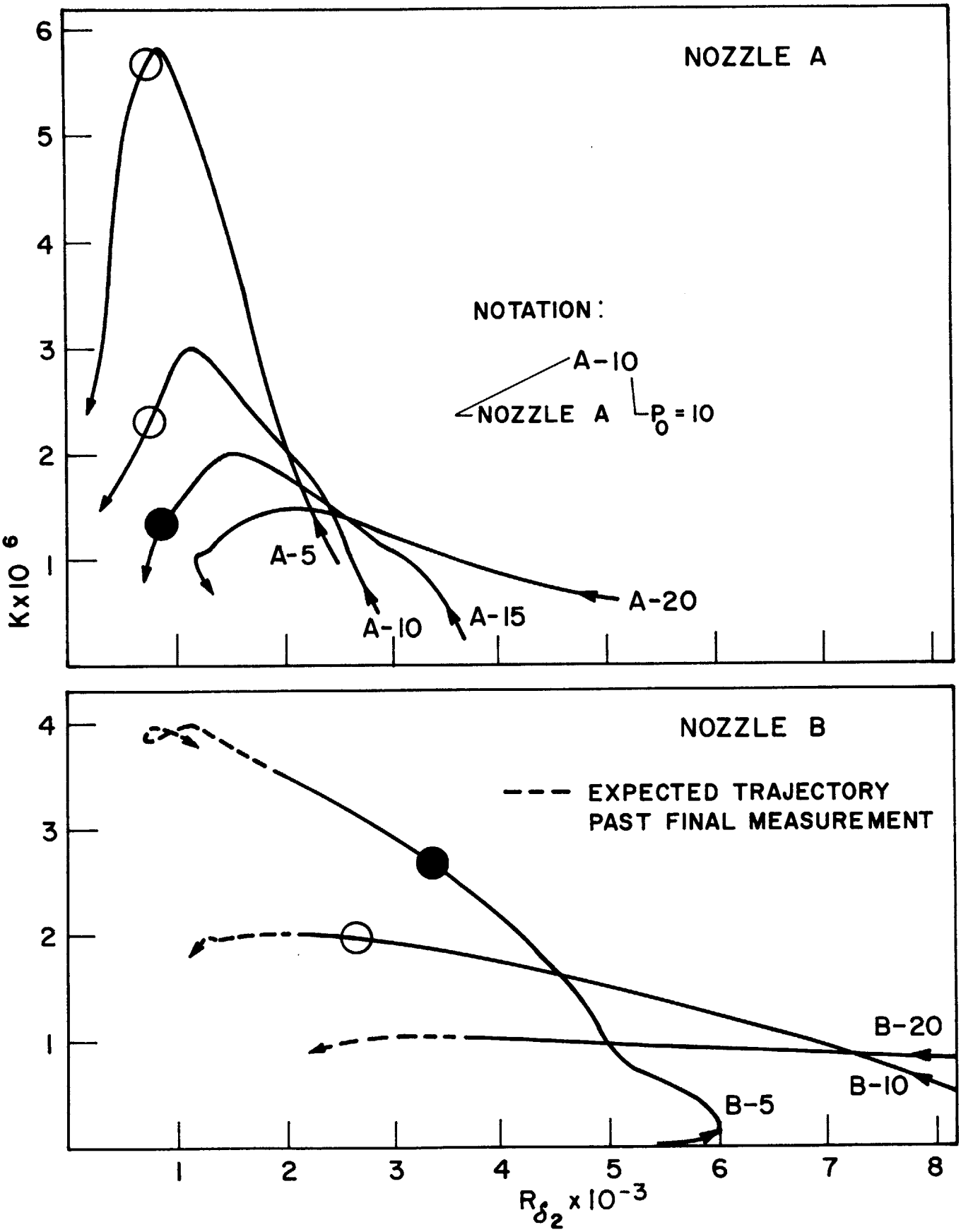

FIG. 27 CONSTRUCTION OF BOUNDARY POINTS FOR THE LAMINARISING REGION

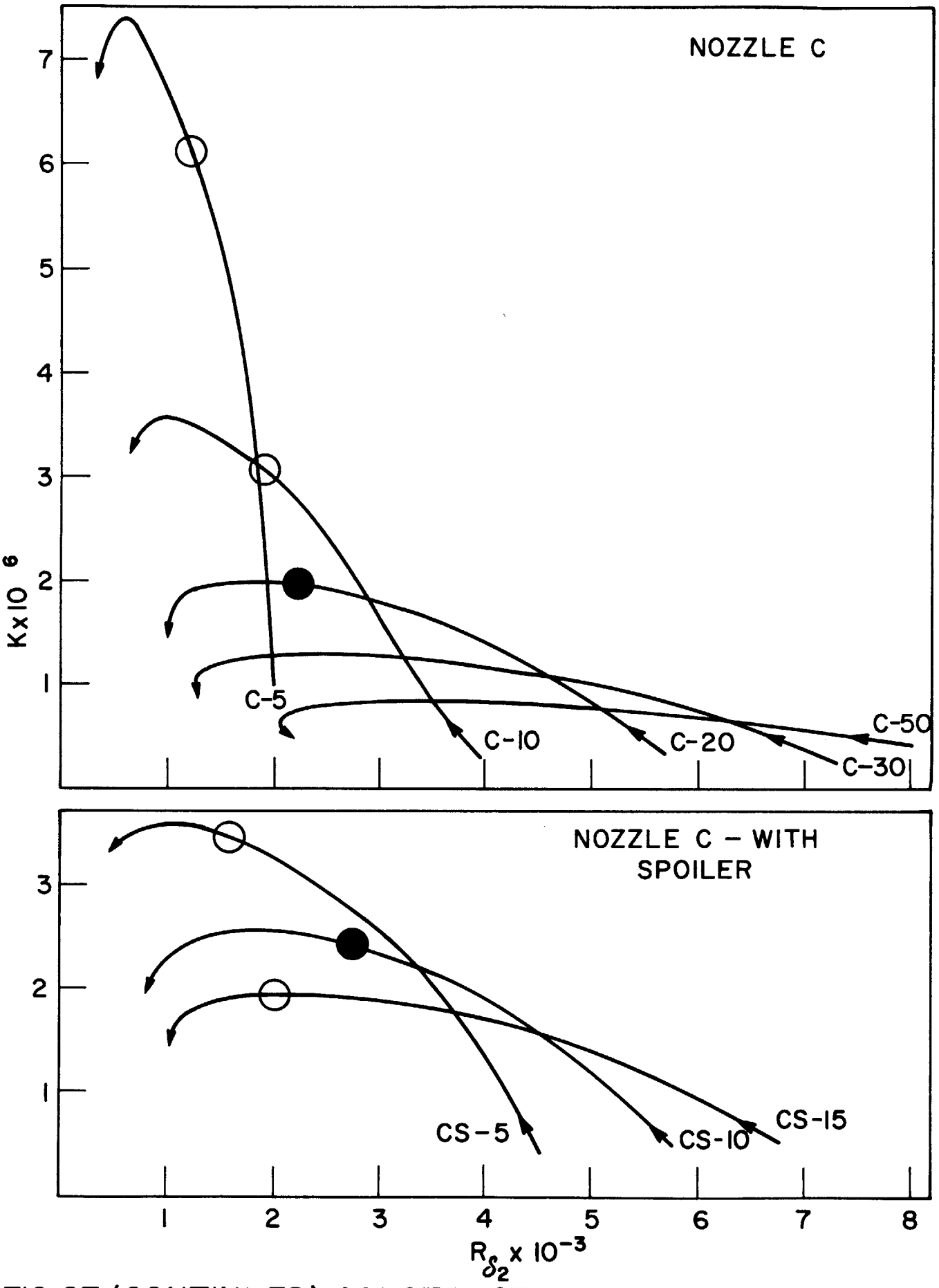

FIG. 27 (CONTINUED) CONSTRUCTION OF BOUNDARY POINTS FOR THE LAMINARISING REGION

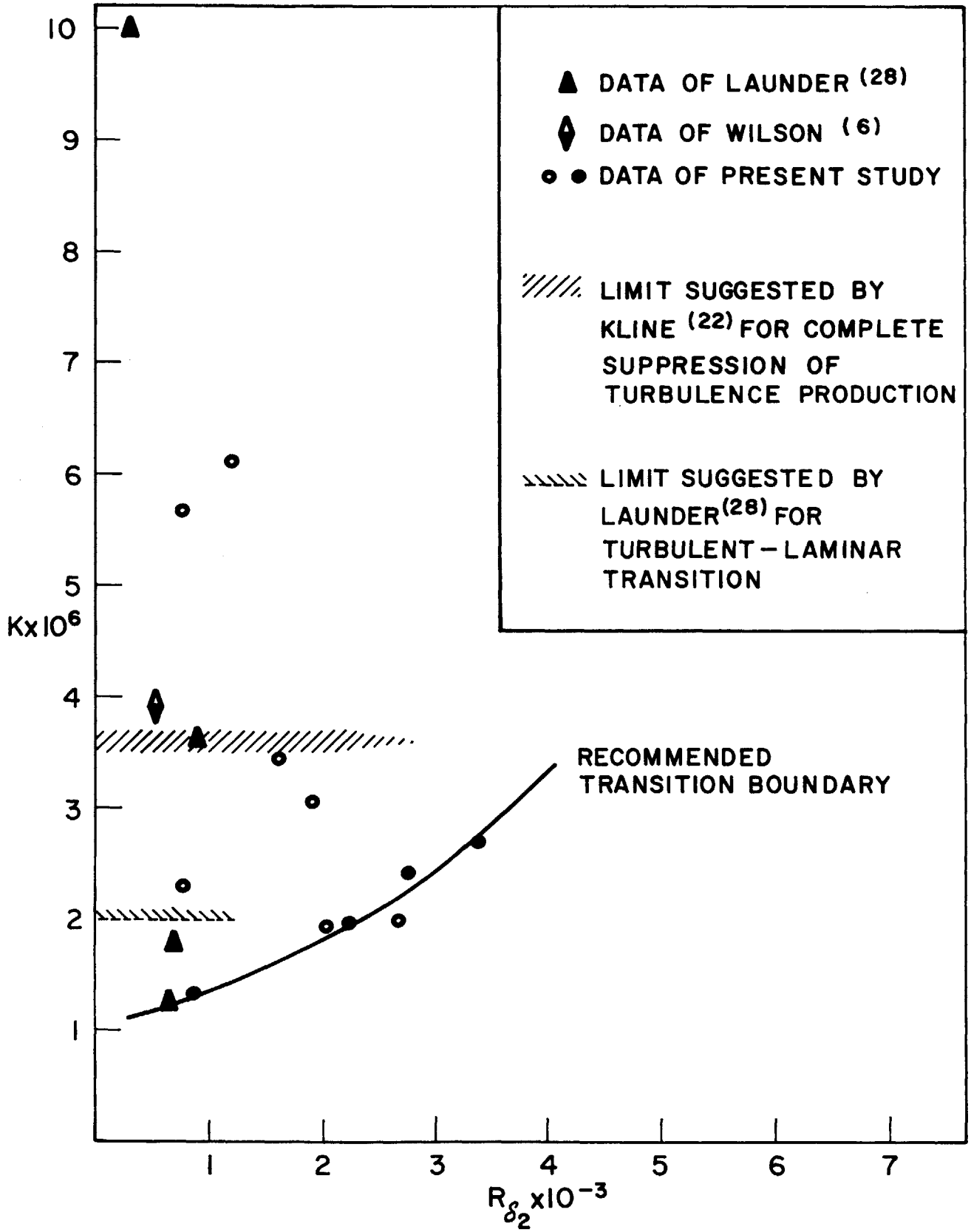

FIG. 28 TURBULENT-LAMINAR TRANSITION BOUNDARY FOR AN ADIABATIC WALL SHEAR LAYER

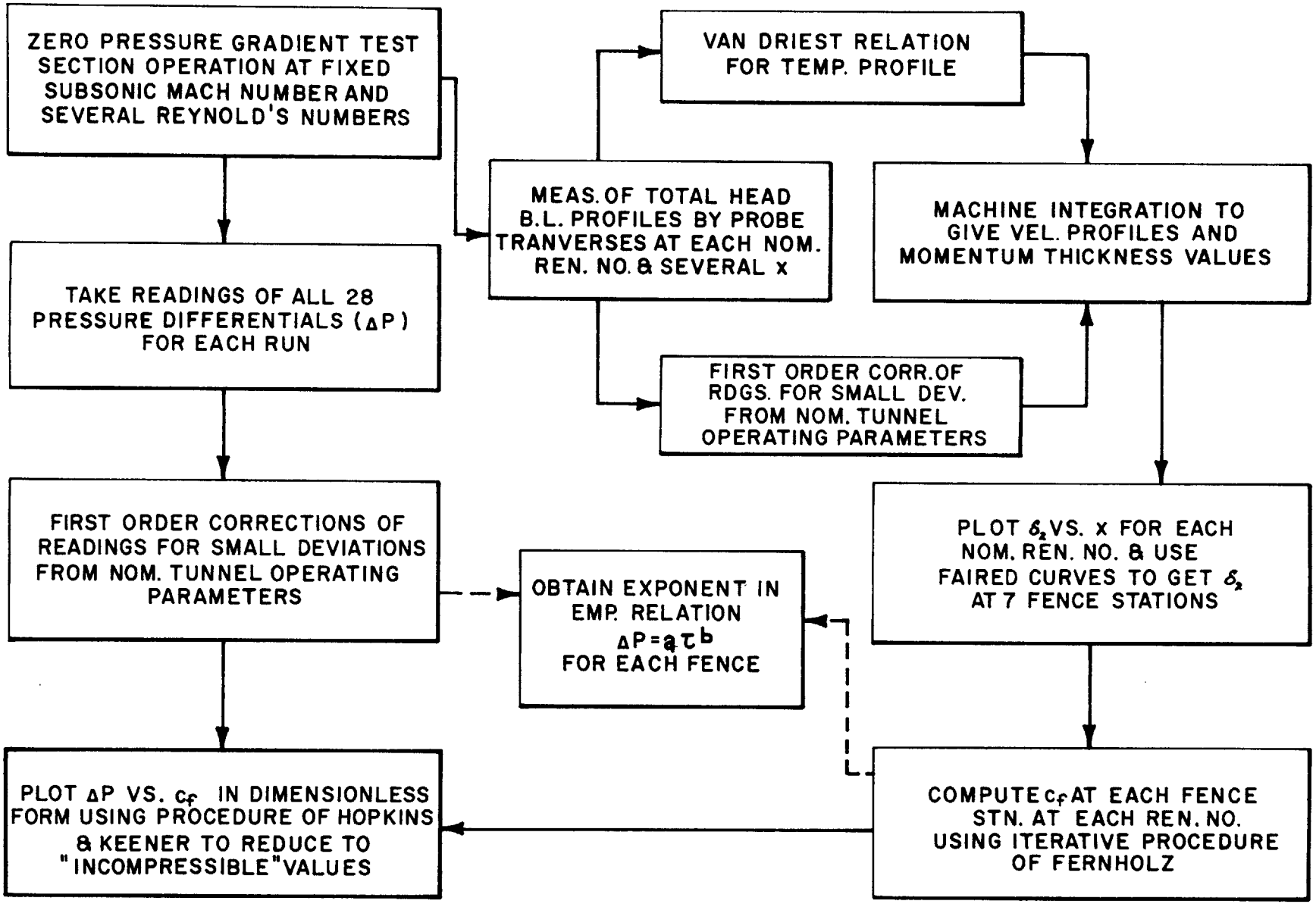

FIG. 29 SUBLAYER FENCE CALIBRATION PROCEDURE

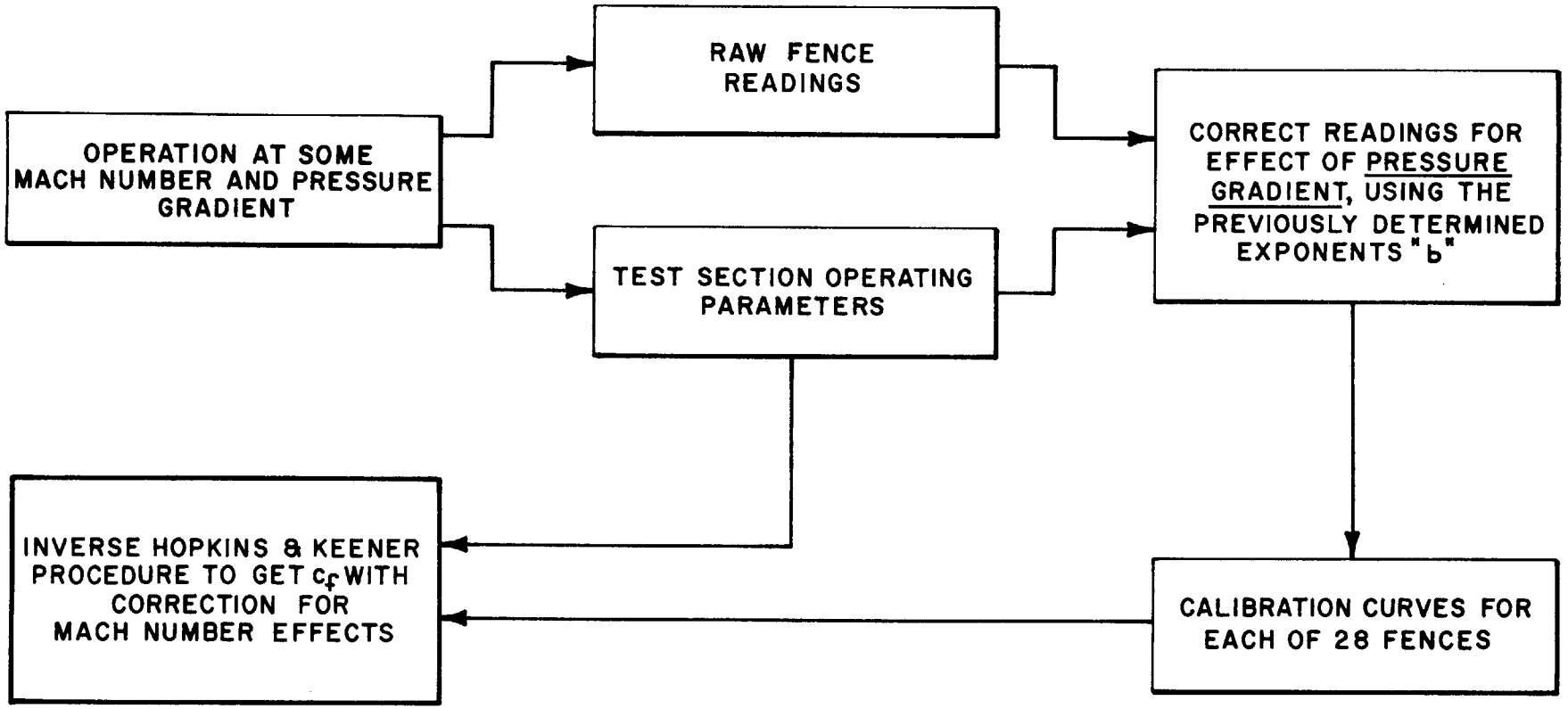

FIG. 30 INTERPRETATION OF SUBLAYER FENCE READINGS FOR FLOW WITH ARBITRARY MACH NUMBER AND PRESSURE GRADIENT

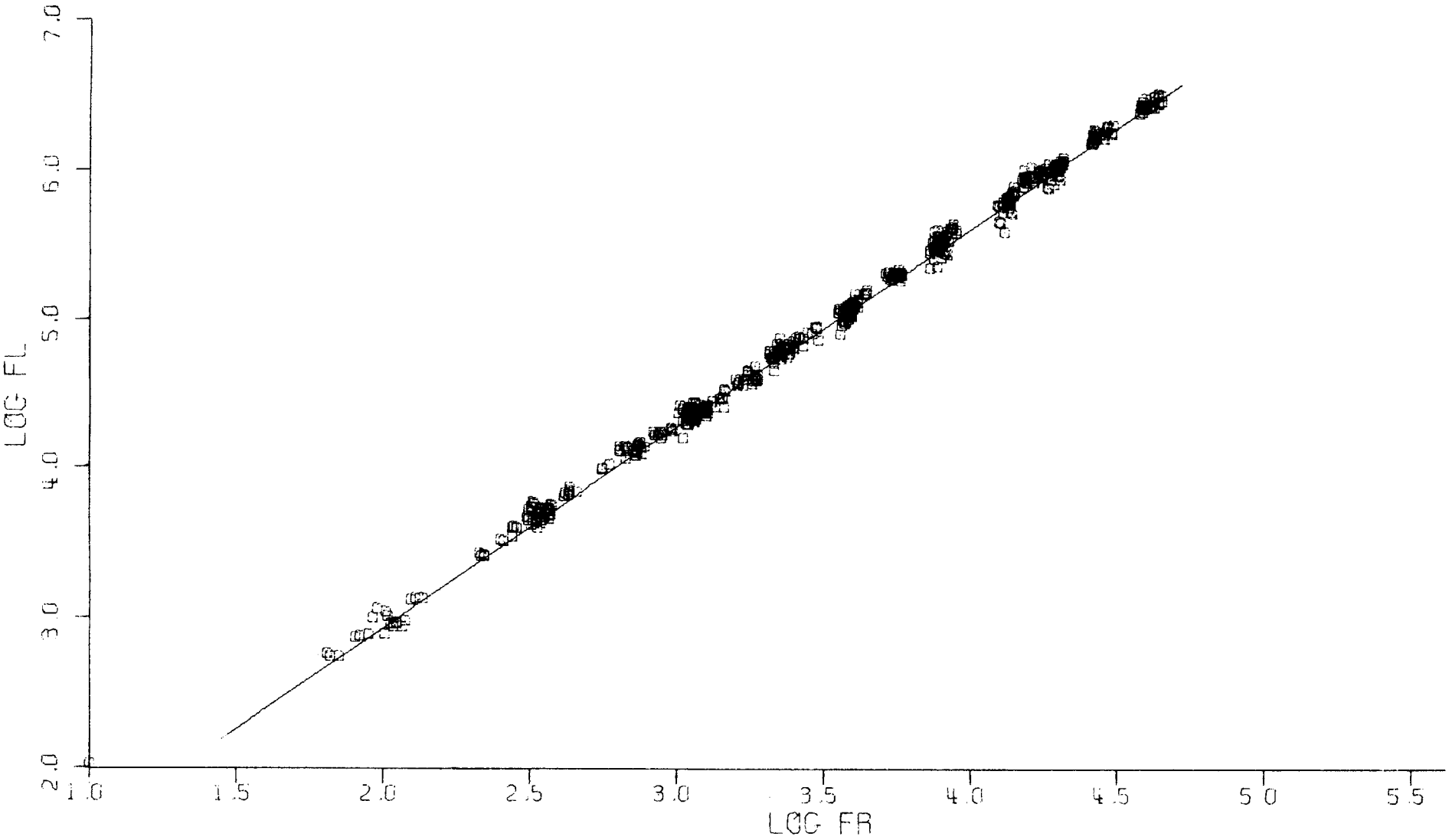

FIG. 31 COMBINED CALIBRATION DATA POINTS FOR ALL FENCES AND RUNS AND BEST-FIT LINE THROUGH 532 POINTS

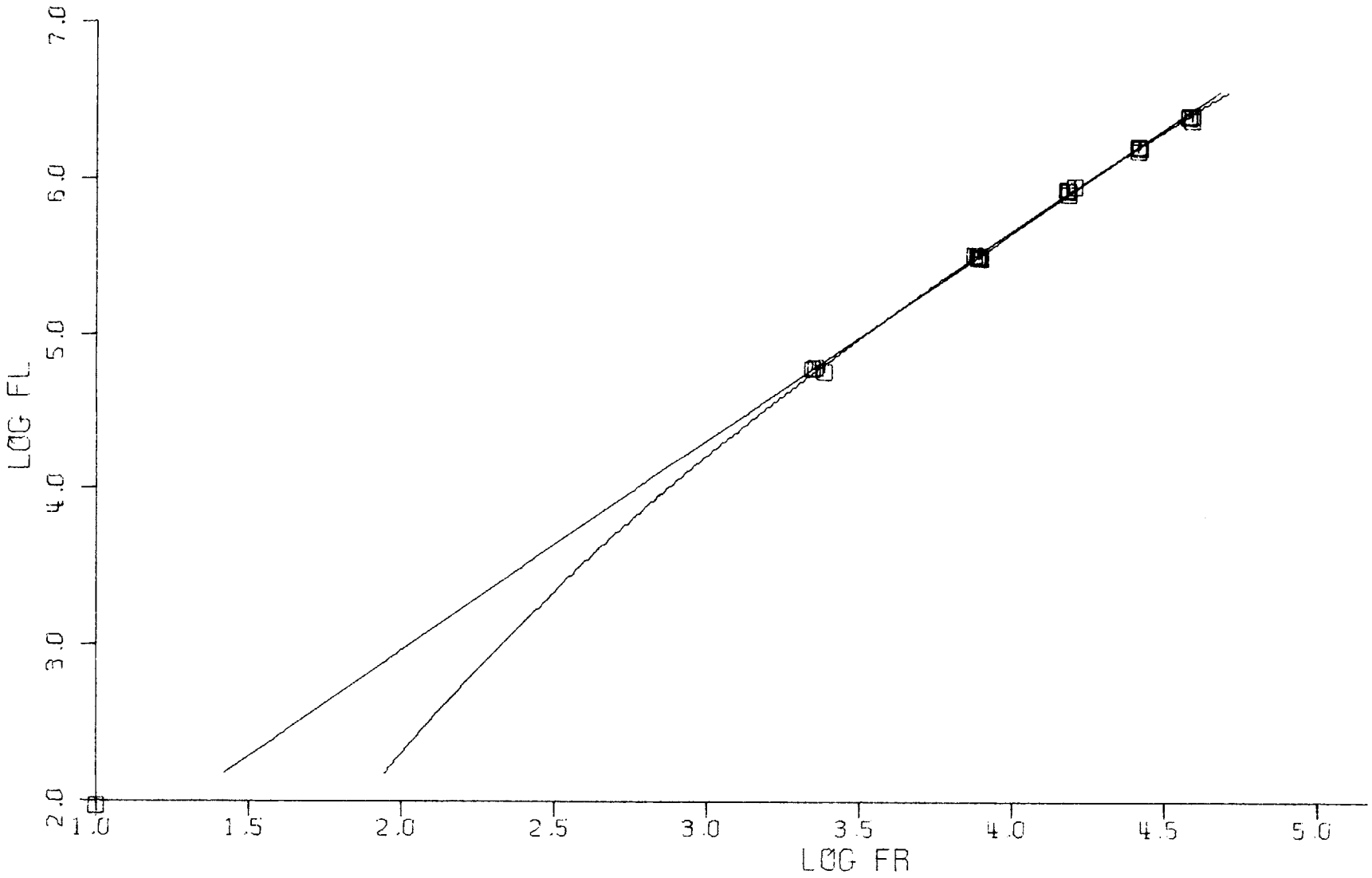

FIG. 32 MACHINE PLOT OF CALIBRATION DATA POINTS AND BEST-FIT LINES FOR FENCE 28